NUREG/CR-5901
SAND92-1422
CO, C4, R3, R5, R7,
1M, 1S, 1V, 9L, 9R

A Simplified Model of Aerosol Scrubbing by a Water Pool Overlying Core Debris Interacting With Concrete

Final Report

Manuscript Completed: October 1993
Date Published: November 1993

Prepared by
D. A. Powers, J. L. Sprung

Sandia National Laboratories
Albuquerque, NM 87185

Prepared for
Division of Safety Issue Resolution
Office of Nuclear Regulatory Research
U.S. Nuclear Regulatory Commission
Washington, DC 20555-0001
NRC FIN L2035

ABSTRACT

A classic model of aerosol scrubbing from bubbles rising through water is applied to the decontamination of gases produced during core debris interactions with concrete. The model, originally developed by Fuchs, describes aerosol capture by diffusion, sedimentation, and inertial impaction. This original model for spherical bubbles is modified to account for ellipsoidal distortion of the bubbles. Eighteen uncertain variables are identified in the application of the model to the decontamination of aerosols produced during core debris interactions with concrete by a water pool of specified depth and subcooling. These uncertain variables include properties of the aerosols, the bubbles, the water and the ambient pressure. Ranges for the values of the uncertain variables are defined based on the literature and experience. Probability density functions for values of these uncertain variables are hypothesized. The model of decontamination is applied in a Monte Carlo sampling of the decontamination by pools of specified depth and subcooling. Results are analyzed using a nonparametric, order statistical analysis that allows quantitative differentiation of stochastic and phenomenological uncertainty. The sampled values of the decontamination factors are used to construct estimated probability density functions for the decontamination factor at confidence levels of 50%, 90% and 95%. The decontamination factors for pools 30, 50, 100, 200, 300, and 500 cm deep and subcooling levels of 0, 2, 5, 10, 20, 30, 50, and 70°C are correlated by simple polynomial regression. These polynomial equations can be used to estimate decontamination factors at prescribed confidence levels.

TABLE OF CONTENTS

LIST OF ILLUSTRATIONS

LIST OF ILLUSTRATIONS (continued)

LIST OF TABLES

FOREWORD

The U.S. Nuclear Regulatory Commission (NRC) has released a Draft Report for Comment, "Accident Source Terms for Light-Water Nuclear Power Plants," NUREG-1465. The information in NUREG-1465 will be considered by the NRC staff in the formulation of updated accident source terms for light water reactors to replace those given in TID-14844, "Calculations of Distance Factors for Power and Test Reactor Sites." These source terms are used in the licensing of nuclear power plants to ensure adequate protection of the public health and safety.

The revised source term report (NUREG-1465) outlines the rates at which various groups of fission products are expected to emerge from the degrading core into the containment atmosphere as a postulated severe accident advances in time. Simultaneously, the action of certain intentionally installed safety systems, together with certain natural fission-product removal processes, will tend to reduce the airborne radioactive inventory in the containment atmosphere.

If, during the accident, the reactor vessel fails and molten core debris comes into contact with structural concrete, highly refractory fission products may be released from the fuel. If a pool of water is present above the core debris, the amount of radioactivity released to containment will be reduced, thus lowering the radiological source term. This final report, "A Simplified Model of Aerosol Scrubbing by a Water Pool Overlying Core Debris Interacting with Concrete" (NUREG/CR-5901) supports the revised source-term document (NUREG-1465) by providing a detailed analysis of aerosol decontamination by overlying water pools. In addition the report presents simplified mathematical expressions that may be used to approximate the degree of aerosol scrubbing.

This final report has benefitted from the comments provided by several reviewers on an earlier draft. The authors thank those who took the time to read and comment on the draft version of the report.

I. BACKGROUND

The uninterrupted progression of a severe nuclear reactor accident will eventually lead to the expulsion of core debris from the reactor coolant system and interaction of this core debris with the structural concrete of the reactor containment building. Analyses of the interaction of core debris with concrete [1] have shown that the interactions pose a threat of long-term overpressurization of the containment and contribute to the threats posed by hydrogen combustion to containment integrity. It has also been shown by both experiment and analysis [2-6] that core-debris interactions with concrete contribute to the inventory of radioactive material that would escape from a nuclear plant in the event of the loss of containment integrity.

Assessments of core debris interactions with concrete in severe nuclear reactor accidents have not routinely considered the effects water might have on these interactions. Overlying pools of water may be present during core debris interactions with concrete either as a natural consequence of accident events or as a result of deliberate measures taken to mitigate the effects of core debris interactions with concrete [7,8].

There has been a significant debate on what effects overlying water pools might have on core debris-concrete interactions.* Most of the debate has focused on whether the water will augment hydrogen production [9] or will quench the core debris and terminate the attack on concrete. The one well-recognized and universally accepted effect water will have is to sharply attenuate the magnitude of aerosol production and radionuclide release to the reactor containment atmosphere during core debris interactions with concrete. This effect has been demonstrated experimentally [10] and sophisticated models of the physical phenomena responsible for the attenuation process are available [6]. The reduction in radionuclide release occurs whether or not the overlying water is able to quench the core debris.

Aerosol production is affected by water because aerosol-laden gases produced by the core-debris attack on concrete must sparge through the water. Aerosols within gas bubbles can diffuse, sediment or inertially impact the gas-water interface. Surface tension and van der Waals forces assure that when an aerosol particle reaches the gas-water interface, it will be trapped in the aqueous phase. This trapping is somewhat similar to the aerosol trapping that occurs when aerosol-laden gases sparge through steam suppression pools in boiling water reactor accidents [11-13]. There are, however, significant differences in the two situations particularly with regard to the composition of the carrier gas, its temperature and the mode of injection into the water pool. Some eleboration on these differences is provided in the discussion of scrubbing phenomena presented in Chapter II of this report.

Computer models of the detailed processes involved in aerosol trapping by water pools have become familiar. The effects of water on aerosol production predicted by these computer models are profound. It would be useful, then, to have a simplified description of the effects of water on aerosol production during core debris-concrete interactions for engineering

* E. R. Copus and D. A. Powers, "A Study of the Limits of Core Debris Coolability During Interactions with Concrete," Sandia National Laboratories, Albuquerque, NM, unpublished.

evaluations or bounding analyses. This document describes such a simplified representation of water effects on aerosol generation during core-debris interactions with concrete.

The approach adopted here to prepare the simplified representation is to fit a polynomial to the results obtained with a detailed model of the processes. The physical phenomena considered in the detailed, mechanistic model of the aerosol trapping process are described in Chapter II of this report. The detailed model is used to calculate aerosol trapping by water pools of various depths and temperatures. Aerosol trapping is reported in terms of the decontamination factor (DF):

$$DF = \frac{\textit{Mass of aerosol entering the water pool}}{\textit{Mass of aerosol escaping the water pool}}$$

Many of the models and parameters used to calculate decontamination factors are uncertain. A variety of techniques have been advanced in the nuclear safety community to address phenomenological uncertainties and uncertainties propagated from analyses of earlier phases of severe reactor accidents. A quantitative analysis of uncertainty is an essential step in preparing a simplified model of decontamination by water pools. It is difficult to anticipate how a simplified model will be used. Bounding or conservative analyses for one situation may not be bounding or conservative for other situations. A quantitative uncertainty analysis using the mechanistic model of decontamination by an overlying water pool is presented in Chapter III of this report. The uncertainty analysis is done using a Monte Carlo method that produces detailed probability distribution functions for the decontamination achieved by water pools. Medians of the distributions and other quantiles of the distributions are fit to polynomial expressions in Chapter IV to produce simple expressions that can be used to estimate the decontamination by water pools.

II. DESCRIPTION OF THE PHYSICAL PHENOMENA

In this chapter, the physical phenomena that result in trapping of aerosols by an overlying water pool during core debris interactions with concrete are described. These phenomena are modeled in the POOL subroutine of the VANESA model of aerosol generation and radionuclide release during the interactions of core debris with concrete [6].

A. Models of Deposition Processes

In a gas bubble containing aerosols that is thermally and chemically equilibrated with a water pool, the aerosols will:

(1) inertially impact the bubble walls,
(2) diffuse to the bubble walls, and
(3) sediment to the bubble walls.

Inertial impaction of aerosol particles with the bubble walls occurs because gases within a rising bubble circulate. The nature of the gas circulation depends on the bubble size and the purity of the system. When gas circulation does occur, excessively large aerosol particles cannot follow the stream lines of the gas flow. Because of inertia, these particles will cross the streamlines and impact the bubble walls. Particles larger than about 0.5 μm are most affected by inertial impaction.

Diffusion of aerosol particles within the bubbles is, of course, the result of Brownian motion brought on by the stochastic nature of gas molecule collisions with the particles. Diffusion significantly affects only very small particles--particles with sizes less than about 0.1 μm. There has been little experimental validation of diffusion models for the situations of interest here. Powers [14] has criticized the available models.

Sedimentation is the gravitational settling of particles within the bubbles. Typically, sedimentation is important only for particles larger than 1 μm.

Fuchs [15] articulated quantitative models for aerosol deposition processes within spherical bubbles. Moody and coworkers [16] have published expressions for the deposition rates in ellipsoidal bubbles. Powers has derived and discussed these models for non-spherical bubbles [14].

Aerosols within rising bubbles will also coagulate. Growth of the aerosol particles within the bubbles will, in principle, affect the deposition of aerosols. But, for aerosols of interest here, aerosol growth by coagulation is expected to be slow in comparison to the time it takes a bubble to rise through a water pool. Consequently, aerosol coagulation within bubbles is neglected here.

Other mechanisms of aerosol deposition can be imagined. For instance, in the analysis of aerosol trapping in steam suppression pools thermophoresis and diffusiophoresis are thought to be important mechanisms of deposition. Interest in these mechanisms in the analysis of

scrubbing by suppression pools comes about because the gases expelled to the pool can be quite hot and have very high partial pressures of steam. Further, gas flow to the suppression pool can be quite high under reactor accident conditions.

The carrier gas flow to the water pool during core debris concrete interactions is thought to be quite different. Gases evolved during the high temperature melt attack on concrete cool as they pass through a solidified crust of debris that separates the molten core debris from the water. Gas production rates associated with the attack of melt on concrete are expected to be low in comparison to the rates of steam production at the water crust interface. The gases produced by attack on the concrete are expected to have low partial pressures of steam because of the chemical reactions of steam with core debris to form hydrogen. Consequently, gas bubbles formed at the water crust interface will be undersaturated in steam and essentially isothermal with the surroundings. It is expected that diffusiophoresis and thermophoresis during formation of bubbles are negligible. (But, note that diffusiophoresis is not negligible once a bubble detaches and begins to rise through a subcooled pool.)

The dynamic events of bubble formation, collapse, and coalescence associated with high velocity gas injection into steam suppression pools are not expected to be important during core debris concrete interactions with an overlying water pool. Gas injection into the pool in the case of core debris/concrete interactions is dominated by steam formation and there are no engineered orifices for injection. Bubble formation is expected to be limited by hydrodynamic forces of the pool rather than gas flow.

Hydrodynamic phenomena in the pool are expected to be simplified since gas injection is expected to take place over the entire bottom of the pool. Complicated plume effects that arise around local gas injection sites in steam suppression pools do not need to be considered.

Aerosol trapping by water pools is described, then, by the deposition of aerosols within bubbles. The deposition rate models consider the mass of particles having diameters d_p. The mass removed per unit rise of a bubble through a water pool is given by:

$$\frac{dM(d_p,x)}{dx} = -[\alpha(D,d_p,D_b) + \alpha(S,d_p,D_b) + \alpha(I,d_p,D_b)]\ M(d_p,x)$$

where

$M(d_p,x)$ = *mass of aerosol particles in the bubble at a distance x above the point of bubble generation*
$\alpha(D,d_p,D_b)$ = *coefficient for particle diffusion*
$\alpha(S,d_p,D_b)$ = *coefficient for particle sedimentation*
$\alpha(I,d_p,D_b)$ = *coefficient for inertial impaction of particles*
D_b = *diameter of the spherical bubble having the same volume as the bubble in question*

The additive treatment of the three deposition processes follows a tradition in aerosol science to treat deposition processes as independent. The processes are certainly not actually independent and there have been some attempts made to examine the interrelationships [18]. It will be shown below that most aerosol particles are affected significantly by only one of the three processes considered here. Only in very narrow size ranges will the interactions among two or more of the processes affect the magnitude of the decontamination factor. Any error in assuming additivity is probably small.

Note that, as written, the bubble rise is assumed to be steady. Transient effects during bubble formation are not considered, nor are secondary motions of larger bubbles considered [17]. More quantitative discussions of these phenomena will be presented below.

The coefficient for particle diffusion in an ellipsoidal bubble of eccentricity E is given by [14]:

$$\alpha(D,d_p,D_b) = 6\sqrt{\frac{8\theta}{\pi U_T D_b^3}}\left[\frac{(E^2-1)\,f(E)}{1+\sqrt{4+2(E^2-1)}}\right]$$

where:

$$\theta = kT\bar{c}/3\pi\mu_g d_p$$

k = *Boltzmann's constant*

$$= 1.3807 \times 10^{-16} \textit{ergs/molecule-K}$$

T = *absolute temperature*

$\bar{c}$ = *Cunningham slip correction* =

$$= 1 + \left(\frac{2\lambda}{d_p}\right)[1.257 + 0.4\ \exp.\ (-0.55 d_p/\lambda)]$$

λ = *mean free path of a gas molecule* =

$$= [\sqrt{(2)}\ \pi\ d_g^2\ N_A\ P/82.06T]^{-1} \qquad (cm)$$

d_g = *effective diameter of a gas molecule (cm)*

N_A = *Avogadro's number* = 6.022×10^{23}

P = *absolute pressure (atms)*

μ_g = *gas viscosity (Poises)*

E = *bubble eccentricity (see discussion below)*

$$f(E) = \left[\frac{1.76E^2}{E^2 - 1} - \sqrt{(2)}\right]^{1/2} \left[\frac{E^2 \tan^{-1}(\sqrt{E^2 - 1})}{\sqrt{(E^2 - 1)}} - 1\right]^{-1/2}$$

Note that $f(E)$ approaches $1.625/(E^2-1)$ as E approaches 1.

The coefficient for deposition by sedimentation of particles within a bubble is given by:

$$\alpha(S,d_p,D_b) = 1.5E^{2/3}J/D_bU_T$$

where

$J = g\rho_p d_p^2 \bar{c}/18\mu_g$
ρ_p = *material density of the aerosol particles*
U_T = *terminal rise velocity of the bubbles*

The coefficient for aerosol deposition by inertial impaction is given by:

$$\alpha(I,d_p,D_b) = \frac{6U_T \tau g(E)}{D_b^2}$$

where

$$\tau = \rho_p d_p^2 \bar{c}/18\mu_g$$

$$g(E) = \frac{E^{4/3}[(E^2 - 1)^2 + (E^2 - 1)^{3/2}(E^2 - 2)\tan^{-1}(\sqrt{E^2 - 1})]}{[\sqrt{(E^2 - 1)} - E^2 \tan^{-1}(\sqrt{E^2 - 1})]^2}$$

$$g(E=1) = 3$$

For spherical bubbles *(E=1)* these equations become:

$$\alpha(D,d_p,D_b) = 1.8[8\theta/U_T D_b^3]^{1/2}$$

$$\alpha(S,d_p,D_b) = 1.5g\tau/D_b U_T$$

$$\alpha(I,d_p,D_b) = 18U_T\tau/D_b^2$$

The reduction of the complex formulas for eccentric bubbles to these simple expressions for spherical bubbles is easily seen by expanding $tan^{-1}(x)$ as $x - x^3/3$ for $x < 1$.

From these equations, it is evident that the aerosol trapping is a strong function of the depth of the water pool. Pool depth is treated here as an independent variable as is the temperature of the water. The equations also show that the trapping is quite dependent on:

- the size of the gas bubbles,
- the shape of the gas bubbles,
- the sizes of the aerosol particles,
- the properties of the liquid phase, and
- the properties of the gas phase.

These and other factors that affect aerosol trapping are discussed in the balance of this chapter.

B. Bubble Shapes

The formulae for the coefficients of the major deposition processes all include as a variable the eccentricity of the bubble, E. A general bubble is considered to have an envelope well approximated by an oblate ellipsoid:

$$\frac{v^2}{a^2} + \frac{u^2}{a^2} + \frac{y^2}{b^2} = 1$$

where

v,u,y = *Cartesian coordinates*
a = *major axis of the ellipsoid*
b = *minor axis of the ellipsoid*

By recognizing axi-symmetry, this equation for the envelope can be rewritten as:

$$\frac{x^2}{a^2} + \frac{y^2}{b^2} = 1$$

where a and b are the lengths of the major and minor axes of an ellipse, respectively. Then,

$$E = a/b$$

The diameter of the spherical bubble ha ing the same volume as the ellipsoidal bubble in question is:

$$D_b = 2a/E^{1/3}$$

Eccentricities of gas bubbles rising in water are correlated by [19]:

$$1/E = \begin{cases} 1 & \text{for } Ta \leq 1 \\ \{0.81 + 0.206 \tanh[2(0.8 - \log_{10} Ta)]\}^3 & \text{for } 1 < Ta \leq 39.8 \\ 0.24 & \text{for } Ta > 39.8 \end{cases}$$

where

Ta = *Tadaki number* = $ReM^{0.23}$
M = *Morton number*
= $g\mu_l^4/\rho_l\sigma_l^3$
Re = *Reynolds number*
= $U_T\rho_l D_b/\mu_l$
σ_l = *surface tension of the liquid*
μ_l = *liquid viscosity*
ρ_l = *liquid density*
g = *gravitational acceleration* = 980 cm/s^2

C. Terminal Velocities of Bubbles

The terminal velocity of a rising bubble depends on the nature of the bubble and the medium. For very clean water, the terminal velocity can be found from [20]:

$$E_o^{1.5}/M^{1/2} = Re^2 C_D = U_T^2 \rho_l^2 D_b^2 C_D/\mu_l^2$$

where

E_o = *Eotvos number* = $g\rho_l D_b^2/\sigma_l$

C_D = *the drag coefficient which is given by*:

$C_D = 576M^{1.2}/E_o^{1.5}$ *for spherical bubbles in which gas does not circulate*

$C_D = 83.8M^{0.3033}/E_o^{0.959}$ *for spherical bubbles in which gas does circulate*

$C_D = E_o/(2.14 + 0.505E_o)$ *for ellipsoidal bubbles* ($E > 1$)

$C_D = 8/3$ *for spherical-cap bubbles* ($E \geq 4.1$)

For bubbles in contaminated water [21]:

$$U_T = \frac{\mu_l}{\rho_l D_b} M^{-0.149} (J_o + 0.857)$$

where

$$J_o = 0.94\left[\frac{4}{3}E_o M^{-0.149}(\mu_l/\mu_w)^{-0.14}\right]^{0.757} \quad \text{for } 2 < H_o \leq 59.3$$

$$J_o = 3.42\left[\frac{4}{3}E_o M^{-0.149}(\mu_l/\mu_w)^{-0.14}\right]^{0.441} \quad \text{for } H_o > 59.3$$

$$H_o = 4/3E_o M^{-0.149}(\mu_l/\mu_w)^{-0.14}$$

μ_w = 0.009 *Poises*

D. Bubble Size

The diameter of the bubble that forms at the interface between core-debris and an overlying water pool depends on the superficial gas velocity and the nature of the surface. At very low gas production rates, the crust of frozen core debris resembles a porous plate. The size of bubbles produced on a porous plate can be derived from the Fritz equation [22]:

$$D_b = 0.0105\,\Psi[\sigma_l/g(\rho_l - \rho_g)]^{1/2}$$

where Ψ is the contact angle (in degrees) between the liquid and the crust of frozen core debris. It is usually thought that water will wet the crusts poorly so $\Psi = 120°$.

With increasing gas generation rates the initial bubble diameter grows as described by the low viscosity form of the Davidson-Schuler equation [24]:

$$D_b = 1.11\left(\frac{6}{\pi}\right)^{1/3}\frac{V_S^{0.4}}{g^{0.2}} \qquad (cm)$$

where V_S is the superficial gas velocity in cm/s.

At very high gas velocities the size of the bubbles is dictated by the Rayleigh-Taylor instability of a gas-liquid interface [23]:

$$D_b = 2C\sigma_l/(\rho_l - \rho_g)^{1/2}$$

where C can have values between 1.9 and 4.

For the analyses presented below, the Davidson-Schuler equation is used to calculate the bubble size. The smallest bubble diameter is limited by what would be predicted by the Fritz equation. The largest bubble size is limited by the prediction obtained from the Taylor instability model.

As bubbles rise through the water pool they will grow as a result of the loss of hydrostatic head from the water pool. Again, considering conditions in which the gas in the bubble does not dissolve in the liquid or liquid does not vaporize into the bubble, the variation in the volume-equivalent spherical bubble diameter as the bubble rises through the liquid is given by:

$$\frac{D_b^3(0)}{D_b^3(x)} = \frac{P_{atm} + g\rho_l(H-x)/1033.3}{P_{atm} + g\rho_l H/1033.3}$$

where

$D_b(0)$ = *initial bubble diameter*

$D_b(x)$ = *bubble diameter a distance x<H above the point of bubble formation*

H = *depth of the liquid pool (cm)*

P_{atm} = *atmospheric pressure*

Bubbles cannot, however, grow to unlimited sizes. The envelope defining a bubble is unstable. Disturbances continually develop, grow and are swept away as the bubble rises. If a bubble grows too large, a disturbance in the gas-liquid interface can grow to be of bubble dimensions before it is swept away as the bubble rises. When this happens, the bubble will split. A simple criterion for the maximum, stable, bubble size is given by Levich [25]:

$$D_b^c = 1.8\sigma_l / U_T^2[\rho_g \rho_l^2]^{1/3}$$

where D_b^c is the critical diameter of the volume equivalent spherical bubble. Levich used intuitive arguments to develop this criterion for the largest stable bubble. Analyses using stability theory yield somewhat smaller values for D_b^c [6].

E. Gas Properties

The evaluation of the aerosol deposition models requires data on the density and the viscosity of the gas phase in the bubble. The gas phase, as is discussed further below, is composed mostly of H_2O, H_2, CO, and CO_2. Pressures in the bubble are low, typically (< 10 atmospheres). The density of the gas phase is fairly well described by the ideal gas law:

$$\rho_g = \frac{P(H_2)2.016}{RT} + \frac{P(H_2O)18.015}{RT} + \frac{P(CO)28.00}{RT} + \frac{P(CO_2)44.001}{RT}$$

where

ρ_g = *density of the gas* (g/cm^3)

$P(i)$ = *partial pressure of the species in the gas phase (atmospheres)*

R = *gas constant* (82.06 cm^3-*atms/mole-K*)

T = *absolute temperature (K)*

Powers et al. [6] utilize the Herning-Zipperer correlation [26] to derive gas viscosity values for mixtures from data for the pure, constituent gases:

$$\mu_g\ (mixture) = \frac{\sum_{i=1}^{N} P(i)\mu_g(i)M(i)^{1/2}}{\sum_{i=1}^{N} P(i)M(i)^{1/2}}$$

where

$\mu_g(mixture)$ = *viscosity of the gas mixture*

$\mu_g(i)$ = *viscosity of the i^{th} constituent gas in the mixture*

$P(i)$ = *partial pressure of the i^{th} constituent gas in the mixture*

$M(i)$ = *moleculear weight of the i^{th} constituent gas in the mixture*

N = *number of gases in the mixture*

For gases of interest here [6]:

$$\mu(CO) = \frac{14.151x10^{-6}T^{0.502012}}{(1 + 117.178/T)} \quad (Poises)$$

$$\mu(CO_2) = \frac{15.957x10^{-6}T^{0.497212}}{(1 + 246.744/T)} \quad (Poises)$$

$$\mu(H_2) = \frac{1.5769x10^{-6}T^{0.705712}}{(1 - 3.378/T)} \quad (Poises)$$

$$\mu(H_2O) = \frac{0.950x10^{-6}T^{0.892912}}{(1 + 207.219/T)} \quad (Poises)$$

Predictions of the Herning-Zipperer correlation agree with measurements for CO-H_2 mixtures at 298 K to within 2% [6].

F. Liquid Properties

Properties of the liquid phase are also needed to evaluate aerosol trapping by a water pool. The liquid phase is considered to be a continuum and its properties are found considering the effects of both dissolved and suspended solids. The properties of interest are:

- liquid density
- liquid surface tension
- liquid viscosity.

These properties are, of course, well-known for pure water. Uncertainty in the properties of the liquid phase are caused by the presence of dissolved and suspended materials. Experimental evidence from tests of combined core debris-concrete-coolant interactions [10] show that a water pool quickly becomes heavily contaminated with suspended solids. Only a small fraction of the suspended material comes from trapped aerosols. Much of the material is the result of actions of the hot water on concrete and solidified core debris. Suspended solids concentrations of 0.2 to 0.05 g/kg water were observed in the SWISS tests [10]. Some of the chemical species found in the water are listed in Table 1.

Table 1 Solids Found Suspended in Water Overlying the Melt Interacting with Concrete in Test SWISS 2
ZrO_2
SiO_2
$MgCa(CO_3)_2$
$NaAlSiO_4$
$Al_2Si_2O_5OH$
$CaCO_3$

Note that because solid carbonates are found in the water pool it is apparent that the pool is saturated in carbon dioxide. Transport of carbon dioxide within bubbles to the bubble surface and the consequent effect on aerosol trapping can obviously be neglected.

The properties of pure water are shown in Table 2. Dissolution and suspension of materials in water will affect these properties. The density of water with dissolved and suspended solids can be estimated from:

$$\rho_l = \left[\rho(w) + \frac{S}{v(f)}\right](1 - \phi_s) + \rho(s)\phi_s$$

where

ρ_l = *density of the liquid*
$\rho(w)$ = *density of pure water*
$S/v(f)$ = *mass of solute per unit volume of water*
ϕ_s = *volume fraction of suspended solids*
$\rho(s)$ = *density of the suspended solid material.*

The surface tension of the liquid phase ought not be affected much by suspended solids. Materials likely to dissolve in water during core debris interactions with concrete are not especially powerful surface active agents. Changes in the surface tension of water caused by various inorganic solutes [29] are shown in Figure 1. The results shown in this figure are

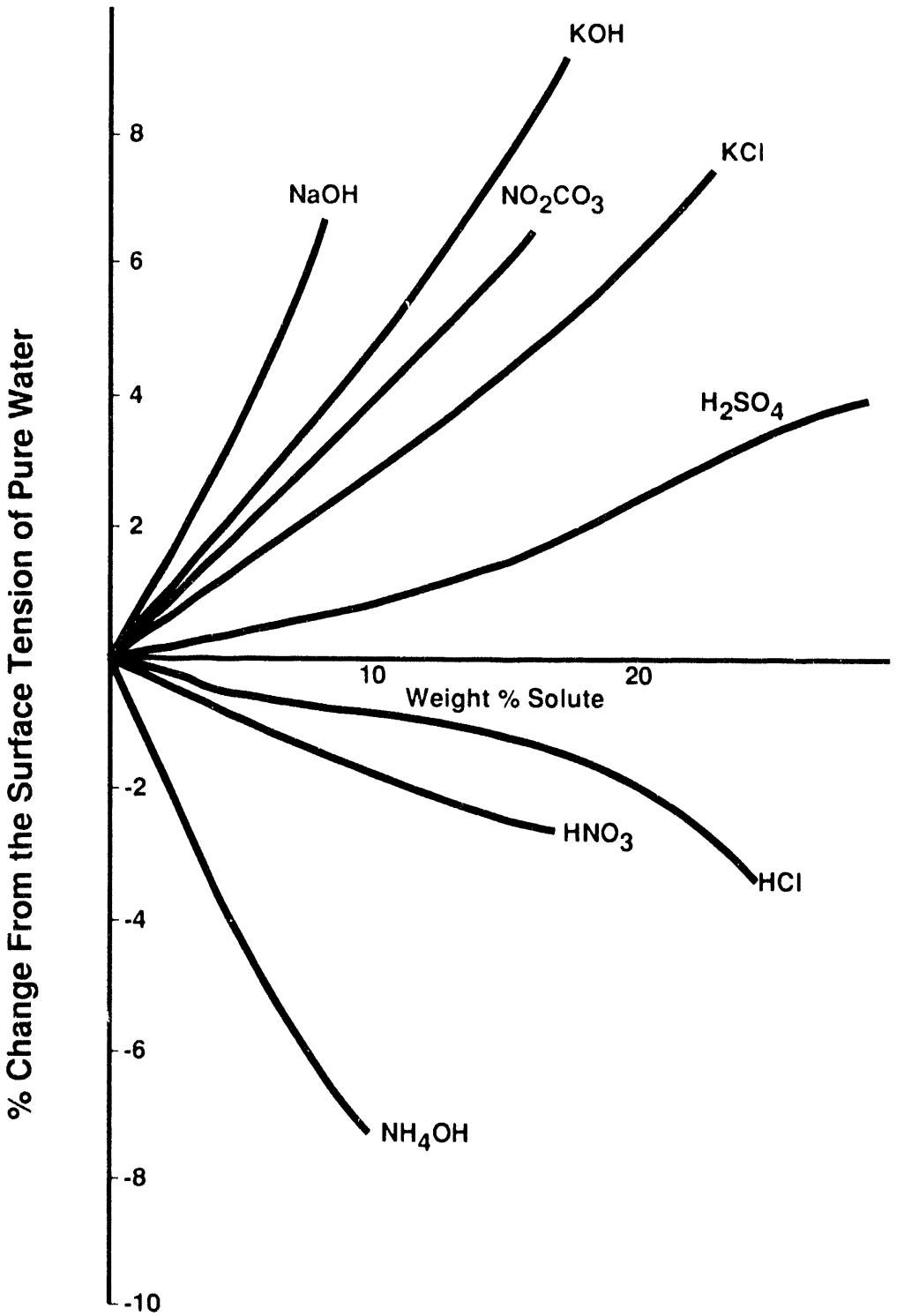

Figure 1. Effects of Inorganic Solutes on the Surface Tension of Water

intended merely to be illustrative of the changes in surface tension that can be caused by inorganic solutes. The solutes can either increase or decrease the surface tension. There are no data for the effects on surface tension likely to be caused by solutes produced during core debris interactions with concrete. For concentrations of solutes expected to develop during core debris interactions with concrete, changes in the surface tension of water will be less than +/-10%.

Table 2
Properties of Pure Water

Density (g/cm^3):

$$\rho(w) = 0.849397 + 1.29812x10^{-3}T - 2.69223x10^{-6}T^2$$

Viscosity (Poises):

$$\log_{10}\mu(l) = \log_{10}(0.01002) + [1.3272(293-T) - 1.52x10^{-3}(T-293)^2] / (T-168)$$

Surface Tension (dyne/cm):

$$\sigma_l = 34.6(T / 704)^{-0.8373}$$

The viscosity of water will be affected by both the dissolved and the suspended solids. The effect of low concentrations of dissolved materials can be estimated from the Einstein equation:

$$\frac{\mu(solution)}{\mu(pure)} = 1 + 2.5\phi$$

where

$\mu(solution)$ = *viscosity of the solution*

$\mu(pure)$ = *viscosity of pure water*

ϕ = *ratio of ions and neutral molecules to the molecules of water*

Thus, for 1 molal concentrations of dissolved, neutral molecules ϕ = 1/55.5 moles H_2O/KgH_2O = 0.018. For one molal concentrations of a strong electrolyte that produces one cation and one anion upon dissolution, such as NaOH, ϕ = 2/55.5 = 0.036. As shown by data in Figure 2, at higher concentrations, the effect of solutes on viscosity is more dramatic.

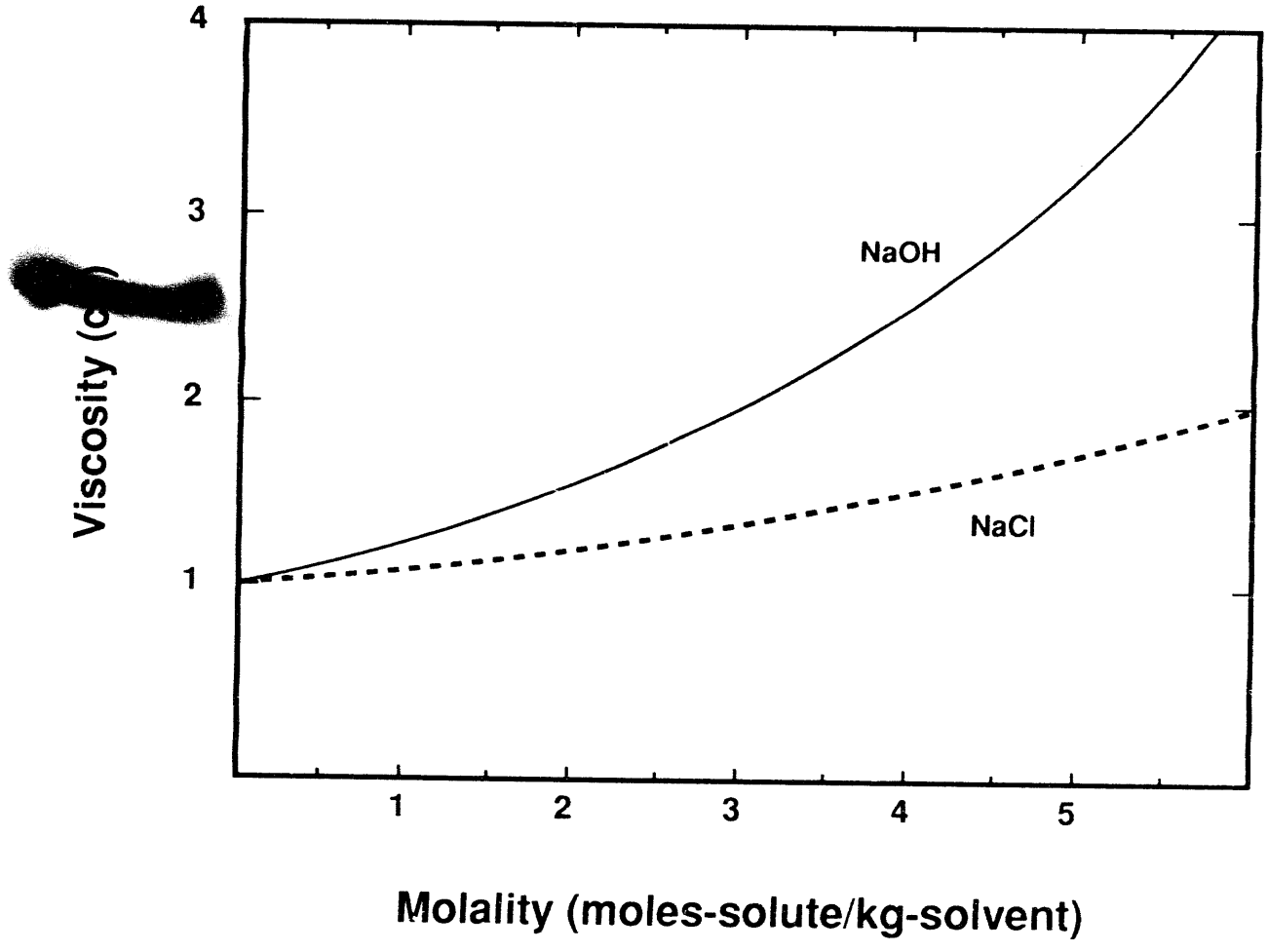

Figure 2. Effects of NaOH and NaCl on the Viscosity of Water. The unit of viscosity in this figure is centiPoises = 10^{-3}Pa-S.

A variety of models appear in the chemical engineering literature on the effects of suspended solids on the viscosity of liquids. These models all yield similar results for conditions in which the solids constitute less than 30 volume percent of the liquid phase. The model adopted here is [28]:

$$\frac{\mu(slurry)}{\mu(solution)} = \frac{0.403}{0.403 - \phi_s}$$

where

$\mu(slurry)$ = *viscosity of the liquid with suspended solids*

$\mu(solution)$ = *viscosity of the liquid including the effects of dissolved solids*

ϕ_s = *volume fraction of suspended solids*

This model is useful for conditions in which $\phi_s < 0.1$. The model fails if ϕ_s exceeds 0.403. Volume fractions of solids in excess of 0.1 can, in principle, arise if overlying water pools evaporate to near dryness during core debris/concrete interactions. A variety of other issues arise if such extensive evaporation takes place. Consequently, the discussions here are restricted to conditions for which $\phi_s < 0.1$.

G. Gas Generation Rates and Superficial Gas Velocities

The gas generation of interest for the analysis of aerosol scrubbing by an overlying water pool comes from two processes:

- gas production by core debris attacking concrete, and
- boiling of water at the interface with the core debris.

Gases produced by the thermal attack of core debris on concrete are steam and carbon dioxide. Steam comes primarily from water in the cementitious phase of concrete. The water contents of concretes depend, then, on the cement in the concretes and these cements are nearly the same in all reactors. The water content does, however, depend on the ambient, relative humidity that the concrete is exposed to prior to interaction with the core debris [30]. Typically, concretes are found to have between 5 and 8 weight percent water.

Carbon dioxide evolved from concrete is the product of thermal decomposition of carbonates in the concrete. All concretes contain a certain amount of carbonate. Carbon dioxide in the atmosphere will react with $Ca(OH)_2$ in the cement phase of concrete to form carbonates:

$$Ca(OH)_2(s) + CO_2(g) \rightarrow CaCO_3(s) + H_2O(g)$$

Because of this type of reaction, which starts when the concrete is first placed and continues slowly throughout the existence of the concrete, the concrete will have at least 1 weight percent

carbon dioxide. Much more carbon dioxide will be present in the concrete if carbonates such as limestone ($CaCO_3$) or dolomite ($CaMg(CO_3)_2$) are used as aggregates. Up to 36 weight percent of the concrete can be carbon dioxide trapped as carbonates. Typically, however, a carbonate-rich concrete will have about 22 weight percent carbon dioxide.

The carbon dioxide and steam evolved from concrete as it is attacked by core debris react especially with metals in the core debris to form carbon monoxide and hydrogen:

$$2H_2O + Zr \rightarrow ZrO_2 + 2H_2$$
$$2CO_2 + Zr \rightarrow ZrO_2 + 2CO$$
$$H_2O + Fe \rightarrow FeO + H_2$$
$$CO_2 + Fe \rightarrow FeO + CO$$

There is thermodynamic evidence that CO_2 can be reduced completely to carbon by zirconium (and perhaps by chromium):

$$CO_2 + Zr \rightarrow ZrO_2 + [C]_{solution}$$

where $[C]_{solution}$ denotes carbon dissolved in core debris. Experimental evidence for this complete reduction of carbon dioxide is, however, not strong and the complete reduction is discounted here.

The extent to which steam and carbon dioxide are reduced to hydrogen and carbon monoxide depends on the composition of the core debris. Early in the attack on concrete when highly reducing metals such as Zr and U can be present, nearly complete reduction can take place. That is, water vapor evolved from the concrete is nearly all reduced to hydrogen and CO_2 is nearly completely reduced to CO if not to carbon. The equilibrium hydrogen-to-steam partial pressure ratio in gases escaping from the core debris is [6]:

$$\frac{P(H_2)}{P(H_2O)} \approx 10^5$$

If the reactive metals are completely oxidized, as they would be late in the course of core debris attack on concrete so that the metal phase is essentially iron, the reduction of evolved gases is much less. The equilibrium hydrogen-to-steam partial pressure ratio is [6]:

$$\frac{P(H_2)}{P(H_2O)} \approx 2$$

The situation is complicated if core debris is replenished by fresh material draining from the reactor coolant system. Detailed scenarios are needed then to predict the amount of reduction that occurs when debris is replenished.

The reduction of steam and carbon dioxide is not independently variable. Repeated experimental evidence shows that the so-called "shift gas" equilibrium prevails in gases produced by core debris attack on concrete [32-33]:

$$CO_2 + H_2 \rightleftarrows CO + H_2O$$

Experimental evidence indicates that this equilibrium is maintained until gas temperatures fall below about 1300-1100 K. The equilibrium constant,, K(T), for the above reaction can be calculated from readily available thermodynamic data for the four gas species [27]. Thus, the partial pressures of the four constituent gases are related by:

$$K(T) = \frac{P(CO)P(H_2O)}{P(CO_2)P(H_2)} = \exp\left[\frac{-4078.3}{T} + 3.705\right]$$

at least until these gases produced by attack on the concrete mix with steam produced by the boiling of water.

The gases produced by core debris attack on concrete are the result of thermal decomposition processes that take place in the concrete at temperatures much less than the ablation temperature of concrete [31]. "Gel" water within the pore structure of concrete begins to evaporate rapidly at temperatures above 378 K. Water coordinated with metal ions in the concrete vaporizes rapidly at about 400 K. Chemically constituted water such as water in $Ca(OH)_2$ is vaporized at about 673 K. Carbon dioxide begins to evolve from carbonates at about 900 K. Ablation temperatures of concrete vary from about 1350 to over 1800 K [31]. It has, however, been repeatedly shown by experiments [see for example reference 10] that thermal fronts marking the onset of these various rapid gas generation processes will propagate into the concrete at rates that are equal to the ablation rate at least as long as the core debris is molten. When the core debris solidifies, the conduction of heat into the concrete progresses faster than ablation.

The period of greatest interest in evaluating the decontaminating potential of water pools is when core debris is molten and radionuclide releases from the core debris can be extensive. During this period, the rates of gas production from the concrete can be taken as proportional to the rate of concrete ablation. These ablation rates vary from about 3 cm/hr when the core debris is just starting to solidify to about 35 cm/hr when the core debris is very hot [3]. The constant of proportionality between ablation rates and gas generation rates is determined by the concrete composition. Thus, from the concrete composition, the shift gas equilibrium and the total pressure (including the hydrodynamic heads provided by core debris and water) the composition of the gas evolved from the concrete can be calculated.

Gas production as a result of water being in contact with core debris is controversial. Early in the discussion of the effects of water on core debris-concrete interactions it was hypothesized by workers at Brookhaven National Laboratory [9] that water pools overlying core debris might lead to enhanced hydrogen production. Experiments seem to show that this will not happen [10,33,34]. As long as a crust of frozen core debris separates the water from molten core debris, temperatures are too low to promote reaction of steam with constituents of core debris to produce any substantial amount of hydrogen.

Gas production due to the water pool is then just steam production as a result of boiling. The nature of the boiling process is, however, controversial. At first examination, it might be thought that the boiling rate would be determined by film-boiling heat fluxes. Depending on the surface temperatures of the crust, film boiling heat fluxes can vary from very low values associated with the minimum film boiling heat flux [5]:

$$\dot{q}_L = 1.88\ P^{0.894}/[1+0.00758P^{0.956}] \quad W/cm^2$$

where P is the local pressure in atmospheres to values given by:

$$\dot{q} = q_c^{4/3}/\dot{q}^{1/3} + q_r$$

where

$$\dot{q} = \textit{heat flux}$$

$$q_c = q_L\{[T_{crust} - T_{water}]/\Delta T_L\}^{3/4}$$

$$\Delta T_L = 85.6P^{0.848}/[1+0.138P^{0.075}]$$

$$q_r = \sigma_B[T_{crust}^4 \quad T_{water}^4]$$

$$T_{crust} = \textit{crust surface temperature}$$

$$T_{water} = \textit{saturation temperature of water at the local pressure}$$

$$\sigma_B = \textit{Stefan-Boltzmann constant}$$

$$= 5.67 \times 10^{-12} \quad (W/cm^2\text{-}K^4)$$

The "barbotage" effect of gases produced from the concrete and subcooling of the water can further affect the film-boiling heat flux.*

Others have argued that water on a frozen crust of core debris will be in nucleate boiling [35]. It has been suggested, in fact, that film boiling will be unstable on solidified core debris. Nucleate boiling produces much higher heat fluxes and consequently much higher steam generation rates than does film boiling.

Experimental evidence obtained to date suggests that very high heat fluxes consistent with nucleate boiling can be obtained only for a short period of time when water first contacts core debris. In the SWISS tests [10] of combined core debris-concrete-coolant interactions, heat fluxes with subcooled water were 70 to 80 W/cm^2. In the MACE scoping test [37] similar heat fluxes were obtained though periodic bursts of heat transfer up to perhaps 160 W/cm^2 were recorded. A recent criterion for the design of advanced light water reactors suggests a heat flux of 50 W/cm^2 [36].

* D. R. Bradley, "Modifications to the Coolant Heat Transfer Models in CORCON," Sandia National Laboratories, Albuquerque, NM, unpublished.

H. The Effect of Subcooling

The conceptual model adopted here for the behavior of aerosols involves complete mixing of the aerosol-laden gas, produced during core debris interactions with concrete, and steam, produced by the boiling of water in contact with the core debris. Whether the mixing occurs in a gas film separating the water pool from a crust of solidified core debris or occurs during vaporization of water into a bubble of gas developing on a crust is not described by the model. It is, however, assumed that water adjacent to the crust is at the saturation temperature whether or not the bulk water is at this temperature.

A gas bubble formed at the interface with the water pool detaches, enters the water pool and begins to thermally equilibrate with the pool. If the bulk water pool is subcooled, there will be a higher than equilibrium partial pressure of steam in the bubble initially. Condensation of this steam will sweep aerosols out of the bubble into the water pool. This diffusiophoretic deposition of particles from the bubble into the pool will have an efficiency that is independent of the aerosol particle size. That is, the decontamination caused by condensation of excess steam is given approximately by considering the volume of the bubble before and after equilibration with the pool.

The diffusiophoretic deposition of aerosols into the water pool is not especially large. What is significant is that the bubble that remains after condensation is smaller. Inspection of the coefficients for aerosol deposition by sedimentation, diffusion and inertial impaction shows that the efficiencies of the deposition processes increase with decreasing bubble size. The equilibration of the bubble with the subcooled pool, then, has two effects. It removes some fraction of the particles as the bubble shrinks. It also increases the efficiency of the other deposition processes as the shrunken bubble rises through the water pool.

The virtue of this model is that it can be used to successfully predict aerosol decontamination observed in the SWISS-II test of core debris-concrete-coolant interactions [10]. (See Figure 3.) These data are sparse. Alternate models can be invoked that will also describe the test results. It might, for instance, be argued that the decontamination observed in the SWISS test was caused by the crust of solidified core debris and that bubbles rising through the pool were equilibrated with the pool from the time of formation. Such a model would predict an initial decontamination but would not predict enhanced removal of aerosols as the bubbles rise through the pool.

For bubbles of the size that is of interest here (see Levich criterion above), the condensation of steam and the equilibration of the bubble with the pool is rapid. Pigford et al. indicate that the molar mass transfer rate associated with the change of phase is given by [as cited in 13]:

$$\frac{dN}{dt} = \frac{P(H_2O)}{RT} A\, k_m \ln\left\{\frac{1 - P_{eq}(H_2O)/P}{1 - P(H_2O)/P}\right\}$$

where

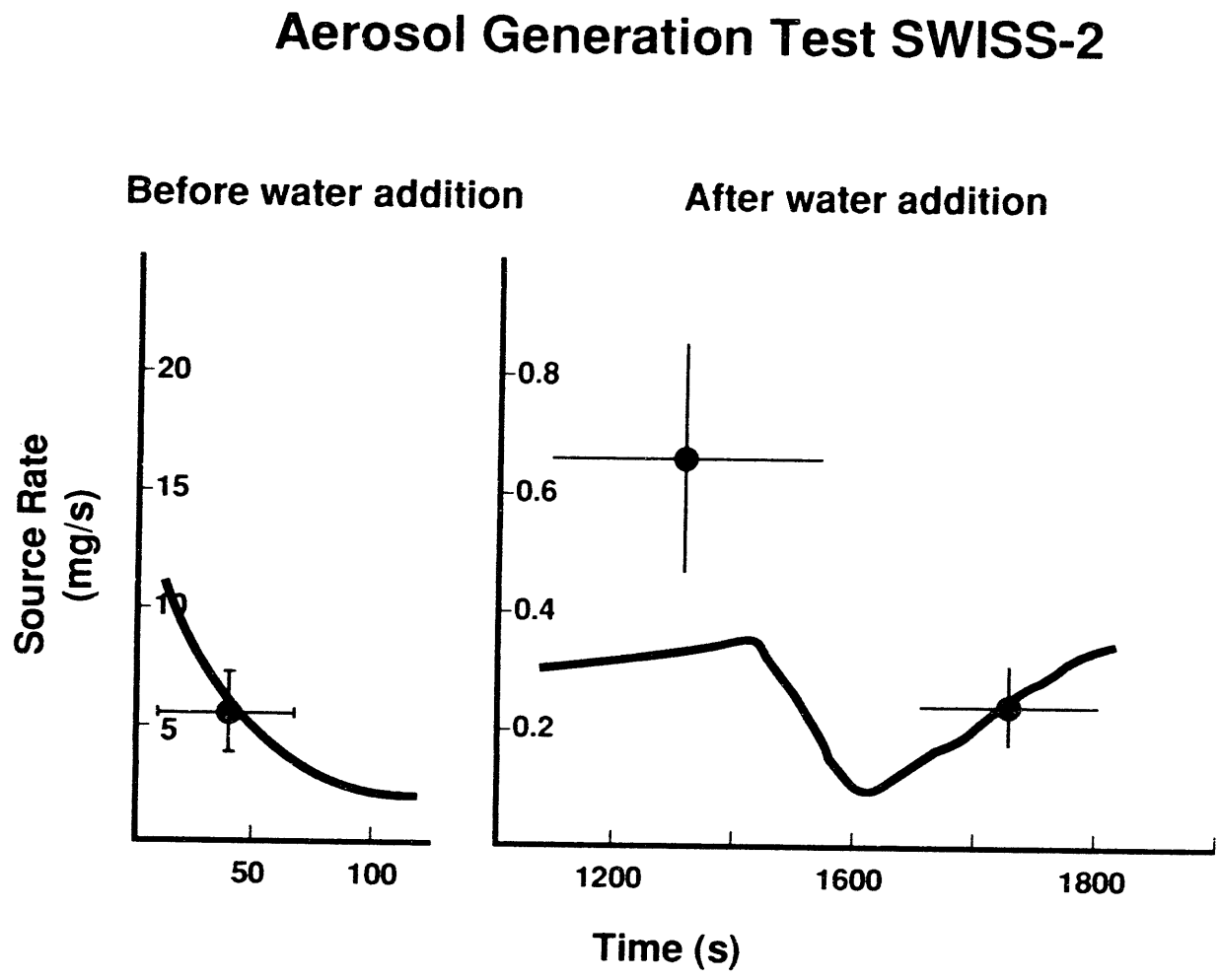

Figure 3. Aerosol Source Rates in the SWISS-II Test Before and After Water Addition. Note change in the vertical scale after water addition. Solid lines were calculated with the VANESA model.

$\frac{dN}{dt}$ = *mass transfer rate*

R = *gas constant*

A = *surface area of the bubble*

$P_{eq}(H_2O)$ = *equilibrium partial pressure of steam at the water pool temperature*

$P(H_2O)$ = *actual partial pressure of steam in the bubble*

k_m = *mass transfer rate in the gas bubble*

Mass transfer coefficients within the bubble are difficult to estimate. A lower bound on this mass transfer rate used in the VANESA model [6]:

$$k_m = \frac{2}{D_b} \varphi$$

where φ is the diffusion coefficient of the condensing species. Theoretical estimates for the mass transport rate for bubbles under creeping flow conditions are [20]:

$$k_m = \frac{17.66}{D_b} \varphi \qquad \textit{for bubbles with internal gas circulation}$$

$$k_m = \frac{6.58}{D_b} \varphi \qquad \textit{for bubbles without internal gas circulation}$$

Numerical values show that bubbles of the size of interest here will reach about 90% equilibration in less than a second. For pool depths greater than a few tens of centimeters this is essentially instantaneous equilibration. Kinetics of condensation can be neglected.

Apparently for much larger bubbles the kinetics of steam condensation is important [13]. Such large bubbles are, however, unstable and will tend to disintegrate. Disintegration will rapidly accelerate equilibration of the bubbles with the subcooled pool.

Steam within the bubble could, in principle, condense on the bubble walls, condense on particles or homogeneously nucleate. Condensation of excess steam on particles is of concern because it will make the particles larger. Inspection of the deposition formulae presented above shows that deposition rates are strong and complicated functions of particle size.

Water can condense in the concave interstices of particle agglomerates. This will cause aerosol particles to behave more as spheres and might reduce the effective material density of the particle but will not greatly alter the deposition characteristics of the particle. In the early stages

of core debris interactions with concrete, the aerosol mass evolved is predominantly constituents of concrete. Experiments by Adams [45] have shown that the aerosols, produced by vaporization of concrete are not greatly affected by condensing steam. Apparently such aerosols are not sufficiently hygroscopic to grow significantly by water condensation on their external surfaces.

Water condensation on aerosol particles is neglected in the analyses presented here except insofar as internal condensation affects shape factors.

I. Aerosol Size Distribution and Aerosol Properties

The size distribution of aerosols produced during core debris interactions with concrete have only been measured in cases where there was no overlying water pool. The data for the mean aerodynamic diameter of the aerosol are correlated in the VANESA model by [6]:

$$d_p(mean) = 0.266\left[\frac{A}{\rho_p}\right]^{1/3} \quad (\mu m)$$

where

A = *mass concentration of aerosol in the gas* (g/m^3)
ρ_p = *aerosol material density* (g/cm^3)

The VANESA model was constructed assuming the aerosol size distributions to be lognormal with a mean given by the above equation and a geometric standard deviation of 2.3. It is difficult to predict the spread of aerosol size distributions produced during large-scale core debris interactions with concrete. The spreads in the distributions usually arise from heterogeneity in the precise details of condensation and coagulation processes throughout the area involved in the generation of condensible vapors. The geometric standard deviation of aerosols was selected in the VANESA model as a weighted average of reported values from 1.6 to 3.2 [38].

There is no reason to believe that the size distributions for aerosols observed in experiments without a water pool present are indicative of the size distributions of aerosol particles that are formed in cases when a water pool is present. An argument can be advanced that when a water pool is present, the vapors that condense to form aerosols pass through a much sharper thermal gradient and have less time to grow than in cases without a water pool present. Consequently, aerosols formed initially would have smaller mean sizes and narrower distributions than have aerosols observed in experiments without water present.

On the other hand, it can equally well be argued that aerosols form from vapors produced during core debris interactions with concrete before the vapors are affected by the presence of the water pool. Growth of the particles might be complete before the water pool can affect the nucleation and growth processes. If such an argument were accurate, aerosol size distributions observed in tests without water present would be quite similar to aerosol size distributions in bubbles just forming in a water pool.

III. UNCERTAINTY ANALYSIS

A. Approach and the Uncertain Quantities

There are several types of uncertainty that arise in the phenomenological description of aerosol scrubbing from bubbles in water pools. An obvious type of possible uncertainty is, of course, the uncertainty in the material properties and model parameters which are known with limited accuracy. Another type of uncertainty that arises is the uncertainty created when alternate models can be used to describe the same observation. Finally, for the purposes of this work there are uncertainties in the decontamination caused by uncertainties in the precise nature of the reactor accident such as the type of concrete and the rates of concrete erosion.

To assess the effects of all of these uncertainties on the overall uncertainty in aerosol decontamination, a Monte Carlo uncertainty analysis was undertaken. This type of uncertainty analysis has proven useful in the analysis of other severe reactor accident source term issues [39-42]. Major steps in the uncertainty analysis are:

- selection of uncertain parameters, properties and models,
- definition of ranges for the uncertain parameters and properties,
- definition of probability density functions for the uncertain parameters and properties,
- multiple executions of the model while randomly selecting parameter values according to their respective probability density functions, and
- accumulation of model predictions to define probability density functions for the predictions.

The discussions of the phenomena involved in aerosol scrubbing presented in Chapter II of this report identified many of the uncertain features of the model. The uncertainties considered in the uncertainty analysis are summarized in Table 3. Ranges for parametric values are also shown in this table. These values are discussed in greater detail below.

The Monte Carlo approach can treat uncertainties in the appropriate model as well as uncertainties in parametric values. For this work, model uncertainty is handled in two ways. When there are two similar models of a particular phenomenon that yield different results, $\pi(A)$ and $\pi(B)$, the value, π, used in the Monte Carlo sampling is obtained from:

$$\pi = \pi(A)\epsilon + \pi(B)(\epsilon - 1)$$

Table 3
Uncertain Parameters and Properties

Parameter or Property	Range	Probability Density
(1) Ambient Pressure	1-9 atms.	uniform
(2) Concrete Erosion Rate	3-35 cm/hr	log-uniform
(3) Carbon Dioxide Content of Concrete (wt. frac.)	0.01-0.36	log-uniform
(4) Water Content of Concrete (wt. frac.)	0.05-0.08	uniform
(5a) Hydrogen-to-Steam Partial Pressure Ratio	$2\text{-}10^5$	log-uniform
(5b) CO/CO_2 Quench Temperature	1000-1300 K	uniform
(6) Solute Mass	0.05-100 g/kg H_2O	log-uniform
7 Volume Fraction Suspended Solids	0-0.1	uniform
8 Density of Suspended Solids	1-6 g/cm^3	uniform
9 Sign Indicator for Uncertainty in Water Surface Tension	0-1	uniform
10 Mean Aerosol Particle Size	0.25-2.5 μm	log-uniform
11 Geometric Standard Deviation of Particle Size Distribution	1.6-3.2	uniform
12 Aerosol Material Density	1.5-10.0 g/cm^3	uniform
13a Coefficient in Davidson-Schular Model for Initial Bubble Size	1-1.54	uniform
13b Contact Angle in Fritz Formula	20-120°	uniform
13c Coefficient in the Taylor Instability Model for Bubble Size	1.9-4	uniform
14 Multiplier for Inertial Impaction	0-1	uniform
15 Boiling Heat Flux	0.16-1.6 MW/m^2	lognormal $\mu = 0.5$ = mean $\sigma = 1.645$ = std. dev.

where

$$\pi = \textit{value used in the calculation}$$
$$\pi(A) = \textit{value predicted by model A}$$
$$\pi(B) = \textit{value predicted by model B}$$

and ϵ is a random variable with values uniformly distributed over the range of 0 to 1.

When there are two distinctly different models, A and B, to describe the same phenomenon, the value, π, used in the Monte Carlo system is given by

$$\pi = \begin{cases} \pi(A) & \textit{for} \quad \epsilon < 0.5 \\ \pi(B) & \textit{for} \quad \epsilon \geq 0.5 \end{cases}$$

where, again, ϵ is a parameter whose values are uniformly distributed over the interval between 0 and 1 and π(A) and π(B) are predictions of the two models.

The definition of probability density functions for uncertain quantities appears to be an entirely subjective process. Though some "rules" and guidance for the definitions of these ranges have been advanced [43], there does not seem to be any uncontestable or mechanical method to do this. The rules for selecting probability density functions used here are as follows:

- in the absence of a strong data base providing indications to the contrary, a uniform probability density function was assumed for parameters whose range of values did not span more than one order of magnitude.

- again, barring evidence to the contrary, the natural logarithm of the value of a parameter was assumed uniformly distributed when the possible range of parametric values exceeded one order of magnitude.

- a lognormal probability density function was assumed for positive definite values that were not uniformly distributed.

When lognormal probability density functions are assumed, the parameter value ranges listed in Table 3 were assumed to correspond to the 1 and 99 percentiles.

Correlations among uncertainties are the most difficult aspects of quantitative uncertainty analyses. Some care has been taken here to define phenomenological uncertainties so that they are uncorrelated. One can only attest that this has been done to the best of the analysts' abilities within the time constraints of this work.

The uncertain parameters considered in the analysis are discussed below. Many of the bases used to select ranges for the uncertain parameters were discussed in Chapter II of this report.

(1) Ambient Pressure. The atmospheric pressure over a water pool can vary from approximately 1 atmosphere to the pressure at which the reactor containment fails. Failure pressures of reactor containments depend very much on the design. Ice condenser containments are quite vulnerable to overpressurization with typical failure pressures of about 5 atmospheres gauge. Large dry containments are thought to have failure pressures of 7-8 atmospheres gauge. Mark I boiling water reactor containments are quite strong though the volumes of these containments are small so they pressurize quickly. Failure pressures can exceed 10 atmospheres gauge. All estimates of containment failure pressure are quite uncertain. The estimates are necessarily the results of fairly global analyses of the designs. Experimental studies show, however, that containment failure occurs at local points of unusual stress. It seems likely, then, that failure pressures quoted above for reactor containments are upper bounds.

For the purposes of this uncertainty analysis, the ambient pressure was assumed to be uniformly distributed over the range of 1 to 9 atmospheres absolute.

(2) Concrete Erosion Rate. The rate at which concrete erodes depends on the temperature of the core debris and the enthalpy of ablation of the concrete. Thus, the erosion rates vary throughout the interaction with concrete. For the purposes of this work, the concrete erosion rate is taken as an uncertain quantity. It is assumed that the natural logarithm of the erosion rate is uniformly distributed over the range of ln (3 cm/hr) = 1.10 to ln (35 cm/hr) = 3.56. The density of the concrete is taken to be 2.35 g/cm^3.

(3) Carbon Dioxide Content of the Concrete. As discussed above, all concretes will contain some carbon dioxide in the form of carbonates and this carbon dioxide is thermally released as core debris attacks the concrete. It is assumed here that the natural logarithm of the weight fraction of carbon dioxide in concrete is uniformly distributed over the range of ln (0.01) = -4.61 to ln (0.36) = -1.02.

(4) Water Content of the Concrete. The weight fraction of water in concrete is assumed here to be uniformly distributed over the range of 0.05 to 0.08.

(5) Equilibrium Hydrogen-to-Steam Partial Pressure Ratio. Carbon dioxide and steam vaporized from the concrete will react with the metallic phases of core debris to form carbon monoxide and hydrogen. When the metal phase of the core debris is rich in zirconium the reduction of carbon dioxide and steam is nearly complete. Hydrogen-to-steam partial pressure ratios are expected to be on the order of 10^5. As zirconium is depleted, the most reactive remaining elements in the metallic phase of core debris are silicon (produced by Zr reactions with SiO_2) and chromium from stainless steel. The equilibrium hydrogen-to-steam partial pressure ratio is expected to be between 10^3 and 10^2. Once the chromium has been oxidized, the hydrogen-to-steam partial pressure ratio is controlled by the oxidation of iron to be about 2.

For the purposes of this uncertainty study, the natural logarithm of the hydrogen-to-steam partial pressure ratio is assumed to be uniformly distributed over the range of ln (2) = 0.69 to ln (10^5) = 11.51. The carbon monoxide-to-carbon dioxide partial pressure ratio is assumed here to be perfectly correlated with the hydrogen-to-steam partial pressure ration through the "shift gas" equilibrium. The correlation depends on temperature. An equilibrium constant can be calculated from known thermodynamic properties of the gases until the gases cool to below the

so-called "quench" temperature. At temperatures below this quench temperature the kinetics of gas phase reactions among CO, CO_2, H_2, and H_2O are too slow to maintain chemical equilibrium on useful time scales. In the sharp temperature drop created by the water pool, very hot gases produced by the core debris are suddenly cooled to temperatures such that the gas composition is effectively "frozen" at the equilibrium composition for the "quench" temperature. Experimental evidence suggest that the "quench" temperature is 1300 to 1000 K. The value of the quench temperature was assumed to be uniformly distributed over this temperature range for the calculations done here.

(6) Solute Mass. The mass of solutes in water pools overlying core debris attacking concrete has not been examined carefully in the experiments done to date. It is assumed here that the logarithm of the solute mass is uniformly distributed over the range of ln(0.05 g/kilogram H_2O) = -3.00 to ln(100 g/kilogram H_2O) = 4.61.

(7) Volume Fraction Suspended Solids. The volume fraction of suspended solids in the water pool will increase with time. Depending on the available facilities for replenishing the water, this volume fraction could become quite large. Models available for this study are, however, limited to volume fractions of 0.1. Consequently, the volume fraction of suspended solids is taken to be uniformly distributed over the range of 0 to 0.1.

(8) Density of Suspended Solids. Among the materials that are expected to make up the suspended solids are $Ca(OH)_2$ (ρ = 2.2 g/cm^3) or SiO_2 (ρ = 2.2 g/cm^3) from the concrete and UO_2(ρ = 10 g/cm^3) or ZrO_2 (ρ = 5.9 g/cm^3) from the core debris or any of a variety of aerosol materials. It is assumed here that the material density of the suspended solids is uniformly distributed over the range of 2 to 6 g/cm^3. The upper limit is chosen based on the assumption that suspended UO_2 will hydrate, thus reducing its effective density. Otherwise, gas sparging will not keep such a dense material suspended.

(9) Surface Tension of Water. The surface tension of the water can be increased or decreased by dissolved materials. The magnitude of the change is taken here to be $S\sigma(w)$ where S is the weight fraction of dissolved solids. The sign of the change is taken to be minus or plus depending on whether a random variable ϵ is less than 0.5 or greater than or equal to 0.5. Thus, the surface tension of the liquid is:

$$\sigma_l = \left\{ \begin{array}{ll} \sigma(w)\ (1-S) & for\ \epsilon < 0.5 \\ \sigma(w)\ (1+S) & for\ \epsilon \geq 0.5 \end{array} \right\}$$

where σ(w) is the surface tension of pure water.

(10) Mean Aerosol Particle Size. The mass mean particle size for aerosols produced during melt/concrete interactions is known only for situations in which no water is present. There is reason to believe smaller particles will be produced if a water pool is present. Examination of aerosols produced during melt/concrete interactions shows that the primary particles are about 0.1 μm in diameter. Even with a water pool present, smaller particles would not be expected.

Consequently, the natural logarithm of the mean particle size is taken here to be uniformly distributed over the range from ln (0.25 μm) = -1.39 to ln (2.5 μm) = 0.92.

(11) Geometric Standard Deviation of the Particle Size Distribution. The aerosols produced during core debris-concrete interactions are assumed to have lognormal size distributions. Experimentally determined geometric standard deviations for the distributions in cases with no water present vary between 1.6 and 3.2. An argument can be made that the geometric standard deviation is positively correlated with the mean size of the aerosol. Proof of this correlation is difficult to marshall because of the sparse data base. It can also be argued that smaller geometric standard deviations will be produced in situations with water present. It is unlikely that data will ever be available to demonstrate this contention. The geometric standard deviation of the size distribution is assumed to be uniformly distributed over the range of 1.6 to 3.2. Any correlation of the geometric standard deviation with the mean size of the aerosol is neglected.

(12) Aerosol Material Density. Early in the course of core debris interactions with concrete, UO_2 with a solid density of around 10 g/cm^3 is the predominant aerosol material. As the interaction progresses, oxides of iron, manganese and chromium with densities of about 5.5 g/cm^3 and condensed products of concrete decomposition such as Na_2O, K_2O, Al_2O_3 SiO_2, and CaO with densities of 1.3 to 4 g/cm^3 become the dominant aerosol species. Condensation and reaction of water with the species may alter the apparent material densities. Coagglomeration of aerosolized materials also complicates the prediction of the densities of materials that make up the aerosol. As a result the material density of the aerosol is considered uncertain. The material density used in the calculation of aerosol trapping is taken to be an uncertain parameter uniformly distributed over the range of 1.5 to 10.0 g/cm^3.

Note that the mean aerosol particle size predicted by the VANESA code [6] is correlated with the particle material density to the -1/3 power. This correlation of aerosol particle size with particle material density was taken to be too weak and insufficiently supported by experimental evidence to be considered in the uncertainty analyses done here.

(13) Initial Bubble Size. The initial bubble size is calculated from the Davidson-Schular equation:

$$D_b = \epsilon\left(\frac{6}{\pi}\right)^{1/3} \frac{V_S^{0.4}}{g^{0.2}} \; cm$$

where ϵ is assumed to be uniformly distributed over the range of 1 to 1.54. The minimum bubble size is limited by the Fritz formula to be:

$$D_b = 0.0105 \; \Psi[\sigma_l / g(\rho_l - \rho_g)]^{1/2}$$

where the contact angle is assumed to be uniformly distributed over the range of 20 to 120°. The maximum bubble size is limited by the Taylor instability model to be:

$$D_b = 2C\sigma_l/(\rho_l-\rho_g)^{1/2}$$

where C is uniformly distributed over the range of 1.9 to 4. The maximum bubble size is also limited by the Levich criterion:

$$D_b(\text{max}) = 1.8\sigma_l/U_T^2(\rho_g\rho_l^2)^{1/3}$$

When a bubble is calculated to exceed this critical size, the bubble is assumed to instantaneously divide into two, equal-volume, bubbles.

(14) Bubble Circulation and Inertial Impaction. The interface between the gas in a bubble and the water is an energetic surface that will accumulate suspended solids. It is thought that these suspended solids will retard internal circulation of gases and consequently the efficiency of inertial impaction of aerosol particles. Consequently, inertial impaction of aerosols within bubbles is uncertain. This uncertainty is considered here by multiplying the coefficient for inertial impaction by a parameter uniformly distributed over the range from 0 to 1.

(15) Boiling Heat Flux. The heat flux involved in boiling is quite controversial. The data base that is developing suggests fluxes are in the neighborhood of 0.5 MW/m^2. Values as low as 0.3 MW/m^2 have been suggested. However, periodic eruptions as large as 1.6 MW/m^2 have been observed in steady state melt/concrete interaction tests. It is assumed here that the boiling heat flux is lognormally distributed. The mean heat flux is taken to be 0.5 MW/m^2 and the geometric standard deviation is taken to be 1.645. The range developed here from experimental data implicitly accounts for accentuation of the boiling heat flux by subcooling and barbotage effects.

B. Results of the Monte Carlo Uncertainty Analysis

The POOL model from the VANESA code [6] was modified to conduct the uncertainty analyses. This model is based on a fourth-order Runge-Kutta solver of the differential equation for aerosol deposition in rising bubbles. Aerosols size distributions were divided into 20 size ranges such that each size range contained 5% of the initial mass of aerosol. Aerosols within each bin were characterized by the mass median diameter of particles classed in the bin. The Runge-Kutta solver was applied then to each of these representative particles. Results for each bin were accumulated to determine the overall decontamination factor. Step sizes in the Runge-Kutta solution method were controlled so that in any one step no more than 10% of the aerosol mass in the bubble deposited.

Uncertain quantities used in the analyses were selected according to their respective probability density functions. The selection of values was done with a random number generator. Random numbers were obtained with a congruent sequential generator algorithm. These numbers were then "shuffled" to avoid the cyclical behavior of the random number generator [44].

Because of all the uncertainties, the decontamination factor calculated with the model described above is uncertain. Values of the decontamination factor are distributed over a range. The

range and the probable distribution of values in the range are not known a priori. A single calculation of the decontamination factor with a prescribed pool depth, a prescribed pool temperature and sampled values of the uncertain parameters constitutes a sample of the unknown distribution for the decontamination factor. By collecting enough samples of the distribution an approximate description of the distribution can be constructed using the statistical methods described in Appendix A. The approximation can be carried to any desired level of accuracy simply by increasing the number of samples. For the purposes of this work, samples were taken until it was at least 95% certain that 95% of the range of values for the decontamination factor produced by a pool of given depth and subcooling had been sampled. In general, more than 300 samples were taken for any one case. For some cases more than 1400 samples were taken. The samples obtained in the calculations were ordered and analyzed by non-parametric statistics as described in Appendix A. These analyses yield cumulative probability distributions for the natural logarithm of the decontamination factor. Though the sample sizes used in these analyses are large, they are still quite finite. Consequently, there is some uncertainty in the distribution functions derived from the samples. These uncertainties were characterized again using non-parametric statistics as described in Appendix A.

1. Saturated Pool Results

For the cases involving a saturated pool, it was assumed that the depth of the water pool was known exactly. Analyses were done for pool depths of 30, 50, 100, 200, 300, and 500 cm. The results of the calculations are summarized in Tables 4 to 9. Note that the natural logarithms of the calculated decontamination factors are listed in these tables. The samples are characterized in terms of a mean and a standard deviation:

$$\textit{Mean} = \sum_{i=1}^{N} x(i)/N = \bar{x}$$

$$\textit{Standard Deviation} = \left[\sum_{i=1}^{N} (x(i)-\bar{x})^2/(N-1) \right]^{1/2}$$

where

$x(i)$ = i^{th} *sample value of* $\ln(DF)$
N = *sample size*

Table 4
Summary of Results for a Saturated Pool 30 cm Deep

Pool Depth (cm)	Pool Temp (K)	Quan-tile (%)	Range for ln DF at a Confidence Level (%) of			
			50	80	90	95
30	sat'd	5	0.2264-0.2354	0.2164-0.2432	0.2144-0.2482	0.2123-0.2539
		10	0.3032-0.3217	0.2949-0.3292	0.2915-0.3348	0.2890-0.3361
mean =		15	0.3668-0.3891	0.3539-0.3928	0.3516-0.3966	0.3474-0.3995
0.928		20	0.4201-0.4465	0.4140-0.4519	0.4070-0.4583	0.4043-0.4603
		25	0.4830-0.5169	0.4732-0.5266	0.4628-0.5332	0.4589-0.5370
std. dev.		30	0.5518-0.5781	0.5414-0.5890	0.5368-0.5929	0.5307-0.5990
=0.586		35	0.6110-0.6280	0.5997-0.6391	0.5948-0.6416	0.5902-0.6485
		40	0.6596-0.6861	0.6502-0.6999	0.6409-0.7079	0.6391-0.7166
		45	0.7229-0.7478	0.7154-0.7620	0.7044-0.7673	0.6997-0.7732
		50	0.7854-0.8158	0.7705-0.8228	0.7645-0.8295	0.7600-0.8382
sample		55	0.8504-0.8805	0.8366-0.9056	0.8267-0.9119	0.8225-0.9255
size =		60	0.9329-0.9689	0.9234-0.9837	0.9100-0.9927	0.9051-1.0066
1000		65	1.0203-1.0476	1.0093-1.0574	0.9918-1.0661	0.9843-1.0727
		70	1.0891-1.1254	1.0775-1.1382	1.0685-1.1575	1.0617-1.1642
		75	1.1928-1.2400	1.1731-1.2578	1.1615-1.2659	1.1555-1.2685
		80	1.3188-1.3741	1.2980-1.4022	1.2702-1.4104	1.2666-1.4138
		85	1.4738-1.5207	1.4382-1.5340	1.4322-1.5449	1.4202-1.5628
		90	1.7042-1.7496	1.6539-1.8067	1.6267-1.8245	1.6159-1.8534
		95	1.9797-2.0714	1.9612-2.0956	1.9566-2.1116	1.9486-2.1177

Table 5
Summary of Results for a Saturated Pool 50 cm Deep

Pool Depth (cm)	Pool Temp. (K)	Quan-tile (%)	Range for ln DF at a Confidence Level (%) of			
			50	80	90	95
	sat'd	5	0.3525-0.3712	0.3437-0.3752	0.3402-0.3805	0.3393-0.3823
50		10	0.4629-0.4754	0.4467-0.4842	0.4419-0.4885	0.4362-0.4909
		15	0.5382-0.5614	0.5298-0.5674	0.5223-0.5749	0.5177-0.5815
		20	0.6141-0.6416	0.6063-0.6487	0.6031-0.6587	0.6004-0.6623
mean =		25	0.7012-0.7202	0.6878-0.7303	0.6767-0.7348	0.6707-0.7440
1.262						
		30	0.7699-0.7928	0.7618-0.8009	0.7537-0.8086	0.7484-0.8143
std.		35	0.8361-0.8626	0.8266-0.8762	0.8203-0.8804	0.8176-0.8855
dev. =		40	0.9068-0.9270	0.8975-0.9386	0.8932-0.9437	0.8855-0.9536
0.689		45	0.9802-1.0038	0.9660-1.0164	0.9578-1.0227	0.9508-1.0316
		50	1.0511-1.0763	1.0419-1.0891	1.0365-1.0925	1.0302-1.0979
sample						
size =		55	1.1281-1.1636	1.1150-1.1762	1.0994-1.1850	1.0974-1.2030
1455		60	1.2318-1.2660	1.2189-1.2768	1.2071-1.2921	1.2002-1.2990
		65	1.3272-1.3633	1.3164-1.3745	1.3052-1.3810	1.2991-1.3906
		70	1.4194-1.4552	1.4081-1.4680	1.3987-1.4769	1.3918-1.4863
		75	1.5328-1.5750	1.5171-1.5907	1.5035-1.6030	1.4934-1.6063
		80	1.7091-1.7659	1.6685-1.7863	1.6507-1.7918	1.6482-1.8010
		85	1.8747-1.9569	1.8534-1.9749	1.8427-1.9975	1.8306-2.0150
		90	2.1647-2.2469	2.1216-2.3118	2.1050-2.3269	2.0951-2.3399
		95	2.5977-2.7028	2.5404-2.7312	2.5281-2.7375	2.5156-2.7529

Table 6
Summary of Results for a Saturated Pool 100 cm Deep

Pool Depth (cm)	Pool Temp. (K)	Quan-tile (%)	Range for ln DF at a Confidence Level (%) of			
			50	80	90	95
100	sat'd	5	0.6049-0.6482	0.5949-0.6575	0.5909-0.6631	0.5827-0.6732
		10	0.7259-0.7960	0.7497-0.8039	0.7454-0.8135	0.7341-0.8267
mean =		15	0.8920-0.9472	0.8731-0.9668	0.8645-0.9810	0.8478-0.9886
1.826		20	1.0228-1.0635	1.0073-1.0885	0.9956-1.0998	0.9858-1.1072
		25	1.1382-1.1990	1.1255-1.2080	1.1049-1.2110	1.0994-1.2152
std. dev.						
= 0.947		30	1.2350-1.2890	1.2154-1.3017	1.2109-1,3058	1.2080-1.3115
		35	1.3318-1.3718	1.3107-1.3883	1.3052-1.3915	1.2999-1.4068
sample		40	1.4173-1.4504	1.3922-1.4717	1.3888-1.4810	1.3815-1.4965
size =		45	1.5043-1.5592	1.4814-1.5690	1.4718-1.5810	1.4570-1.5858
838		50	1.5948-1.6251	1.5808-1.6577	1.5685-1.6680	1.5631-1.6742
		55	1.6870-1.7634	1.6674-1.7870	1.6573-1.8077	1.6482-1.8263
		60	1.8383-1.9027	1.8078-1.9392	1.7872-1.9537	1.7781-1.9628
		65	1.9815-2.0527	1.9549-2.0771	1.9396-2.0883	1.9260-2.1038
		70	2.1174-2.1901	2.0951-2.2110	2.0824-2.2265	2.0737-2.2387
		75	2.2564-2.3399	2.2385-2.3932	2.2238-2.4089	2.2115-2.4280
		80	2.4872-2.5605	2.4306-2.6005	2.4241-2.6292	2.4073-2.6387
		85	2.7340-2.8233	2.6879-2.8750	2.6636-2.9149	2.6458-2.9588
		90	3.0832-3.1937	3.0274-3.2636	2.9863-3.2813	2.9770-3.2974
		95	3.5186-3.6444	3.4664-3.7427	3.4338-3.7745	3.4139-3.8078

Table 7
Summary of Results for a Saturated Pool 200 cm Deep

Pool Depth (cm)	Pool Temp (K)	Quan-tile (%)	Range for ln DF at a Confidence Level (%) of			
			50	80	90	95
200	sat'd	5	1.0174-1.0802	0.9958-1.1196	0.9887-1.1394	0.9808-1.1493
		10	1.2552-1.3074	1.2273-1.3350	1.2214-1.3413	1.1830-1.3438
		15	1.4174-1.4704	1.3570-1.4966	1.3459-1.5108	1.3426-1.5274
mean		20	1.5519-1.6513	1.5286-1.6735	1.5123-1.7012	1.4985-1.7083
= 2.696		25	1.7379-1.7881	1.7047-1.8350	1.6847-1.8405	1.6611-1.8485
std. dev.		30	1.8755-1.9257	1.8401-1.9600	1.8191-1.9711	1.7980-1.9761
= 1.453		35	1.9786-2.0540	1.9651-2.0909	1.9386-2.1046	1.9276-2.1109
		40	2.1096-2.1705	2.0918-2.2103	2.0731-2.2202	2.0527-2.2383
sample		45	2.2235-2.2946	2.2093-2.3237	2.1743-2.3372	2.1673-2.3572
size=626		50	2.3532-2.4236	2.3229-2.4676	2.3057-2.4976	2.2812-2.5070
		55	2.5001-2.5888	2.4667-2.6427	2.4370-2.6619	2.4158-2.6770
		60	2.6671-2.7536	2.6425-2.7821	2.5971-2.8071	2.5842-2.8213
		65	2.8185-2.9152	2.7823-2.9688	2.7724-2.9872	2.7492-3.0043
		70	3.0054-3.0925	2.9706-3.1275	2.9626-3.1481	2.9190-3.1845
		75	3.2215-3.3226	3.1412-3.3724	3.1158-3.3831	3.0984-3.4222
		80	3.4533-3.5749	3.3894-3.6368	3.3760-3.7005	3.3472-3.7377
		85	3.7687-3.9238	3.7416-3.9653	3.7006-3.9905	3.6578-4.0159
		90	4.2515-4.3681	4.1133-4.4475	4.0325-4.4659	3.9971-4.4921
		95	5.1455-5.4756	5.0488-5.7198	4.9747-5.7888	4.8134-5.8896

Table 8
Summary of Results for a Saturated Pool 300 cm Deep

Pool Depth (cm)	Pool Temp. (K)	Quan-tile (%)	Range for ln DF at a Confidence Level (%) of			
			50	80	90	95
300	sat'd	5	1.4561-1.5365	1.3207-1.5769	1.3081-1.6027	1.3021-1.6165
		10	1.7294-1.8223	1.6656-1.8436	1.6174-1.8495	1.6025-1.8544
		15	1.8555-1.9050	1.8488-1.9786	1.8373-1.9975	1.8280-2.0415
		20	2.0180-2.1206	1.9786-2.1517	1.9204-2.1931	1.8944-2.2423
mean = 3.545		25	2.1920-2.2956	2.1290-2.3410	2.1143-2.3657	2.0948-2.3884
		30	2.3459-2.4540	2.3054-2.5282	2.2932-2.5460	2.2647-2.5978
std. dev.		35	2.5298-2.6808	2.4658-2.7504	2.4105-2.7652	2.3893-2.7744
= 2.132		40	2.7503-2.7942	2.6795-2.8747	2.6342-2.9005	2.6057-2.9012
		45	2.8729-2.9210	2.7924-2.9744	2.7801-3.0095	2.7696-3.0534
sample size=351		50	2.9651-3.1248	2.9197-3.1615	2.9113-3.2035	2.9082-3.2145
		55	3.1612-3.2511	3.1223-3.3864	3.0810-3.3964	3.0161-3.4098
		60	3.3807-3.4723	3.2506-3.5032	3.2361-3.5757	3.2265-3.5896
		65	3.5017-3.6545	3.4722-3.6892	3.4385-3.7368	3.3989-3.8269
		70	3.6913-3.9590	3.6596-4.0264	3.6479-4.0472	3.5912-4.0618
		75	4.0282-4.1220	3.9769-4.2851	3.9023-4.3521	3.8637-4.3703
		80	4.3372-4.5201	4.2143-4.6660	4.1157-4.7664	4.0963-4.4987
		85	4.7865-4.9344	4.6484-5.1521	4.5475-5.1661	4.4945-5.3428
		90	5.4210-5.9354	5.1630-6.2323	5.1449-6.3903	4.9749-6.7622
		95	7.1595-8.2965	6.8295-9.3387	6.1621-9.3885	5.3965-9.4600

Table 9
Summary of Results for a Saturated Pool 500 cm Deep

Pool Depth (cm)	Pool Temp. (K)	Quan-tile (%)	Range for ln DF at a Confidence Level (%) of			
			50	80	90	95
500	sat'd	5	2.1395-2.2673	2.0833-2.3210	2.0599-2.3560	2.0204-2.4051
		10	2.5731-2.6106	2.4574-2.6380	2.4456-2.6467	2.4391-2.6507
		15	2.7328-2.8345	2.6869-2.8984	2.6467-2.9065	2.6380-2.9096
		20	2.9174-3.004	2.9064-3.0395	2.8974-3.0845	2.8765-3.1348
mean = 5.086		25	3.1348-3.2601	3.0441-3.3965	3.0279-3.4173	3.0031-3.4297
		30	3.4251-3.5594	3.3756-3.6051	3.3195-3.6374	3.2430-3.6834
std. dev. = 3.185		35	3.6384-3.8268	3.6040-3.8682	3.5611-3.8932	3.5447-3.8990
		40	3.8808-3.9942	3.8527-4.0280	3.8268-4.0785	3.7984-4.1016
		45	4.0608-4.2350	4.009 -4.2832	3.9924-4.3214	3.9690-4.3404
sample size = 483		50	4.3187-4.4998	4.2693-4.5328	4.2097-4.5649	4.1856-4.5936
		55	4.5408-4.7216	4.5103-4.7661	4.4554-4.7915	4.4340-4.7970
		60	4.7742-4.8849	4.7488-4.9324	4.7180-4.9543	4.6936-4.9929
		65	4.9512-5.2122	4.9037-5.3576	4.8849-5.3718	4.8633-5.3866
		70	5.3719-5.5122	5.2494-5.5863	5.2185-5.6406	5.1056-5.6551
		75	5.6481-5.8440	5.5629-5.9537	5.5219-5.9756	5.5046-6.0331
		80	6.0245-6.3781	5.9554-6.3870	5.8722-6.4057	5.8457-6.4158
		85	6.4754-6.8767	6.4039-7.1308	6.3867-7.1974	6.3841-7.3955
		90	7.8250-8.0354	7.3955-8.7341	7.2146-8.8799	7.1400-9.2984
		95	10.0329-11.8123	9.7581-12.8553	9.5838-13.6204	9.4155-13.8318

Because the probability distribution functions are not classical normal distribution functions, the mean and the standard deviation are not especially good descriptors of the distributions. The best characterization of the probability distribution function is provided by the ranges for quantile points shown in Tables 4 to 9. Let ξ_p be the point in the real cumulative probability distribution for ln(DF) in a given case. That is, 100p percent of the values obtained for ln(DF) will be less than or equal to ξ_p. ξ_p marks the 100p percent quantile of the real distribution. Thus, the median or 50% quantile of the distribution is given by $\xi_{0.5}$. The value of ξ_p can be bracketed at a prescribed confidence level by values obtained in the finite sample. The bracketing values define an uncertainty range for values of ξ_p. In Tables 4 to 9 ranges are given for p equal 0.05 to 0.95 in steps of 0.05.

Distributions for ln(DF) for saturated pool depths of 30, 50, 100, 200, 300, and 500 cm are shown in Figures 4 to 9. Solid lines and vertical bars in the figures define the 50% confidence levels for these distributions. Dashed lines define the 90% confidence intervals for the distributions. In all cases, the distributions are sufficiently narrowly defined for most reactor safety analyses. That is, the stochastic uncertainty that arises from the finite sample size is small in comparison to the phenomenological uncertainty in the decontamination factor.

The distributions for ln(DF) at all pool depths have similar shapes. The distribution rises sharply to a linear regime between about the 20% and 80% quantiles. Over this linear region, the probability density function is sensibly a constant. Often it is found that in the linear region of a cumulative distribution one uncertain input parameter is a dominant contributor to the uncertainty in a computed result. No attempt has been made to ascertain if only one of the uncertain parameters identified above is responsible for variations in ln(DF) in the cases examined here.

For quantiles greater than about 80% there is a long decreasing tail in the probability density function of ln(DF). Large uncertainties in the locations of quantile points in this region could be reduced by using large samples from the Monte Carlo analyses. Unfortunately the uncertainty ranges decrease with the square root of the sample size so that a great deal of work is required to reduce the uncertainties in the larger quantiles.

The median (50% quantile) of ln(DF) is plotted in Figure 10 against pool depth. For pool depths up to about 100 cm, the ln(DF) increases rapidly with pool depth. For depths greater than 100 cm, the median ln(DF) increases linearly, but slowly with pool depth. This behavior of the median ln(DF) is also seen at least qualitatively in the variations with pool depth of the other quantiles of the distribution of ln(DF). The behavior can be understood as follows:

- inertial impaction and diffusion are responsible for most of the decontamination (see Figure 11).

- very large and very small aerosol particles are quickly removed from the bubble; results of the analyses suggest essentially all of the large and small particles are removed during bubble rise through a 100 cm deep saturated pool.

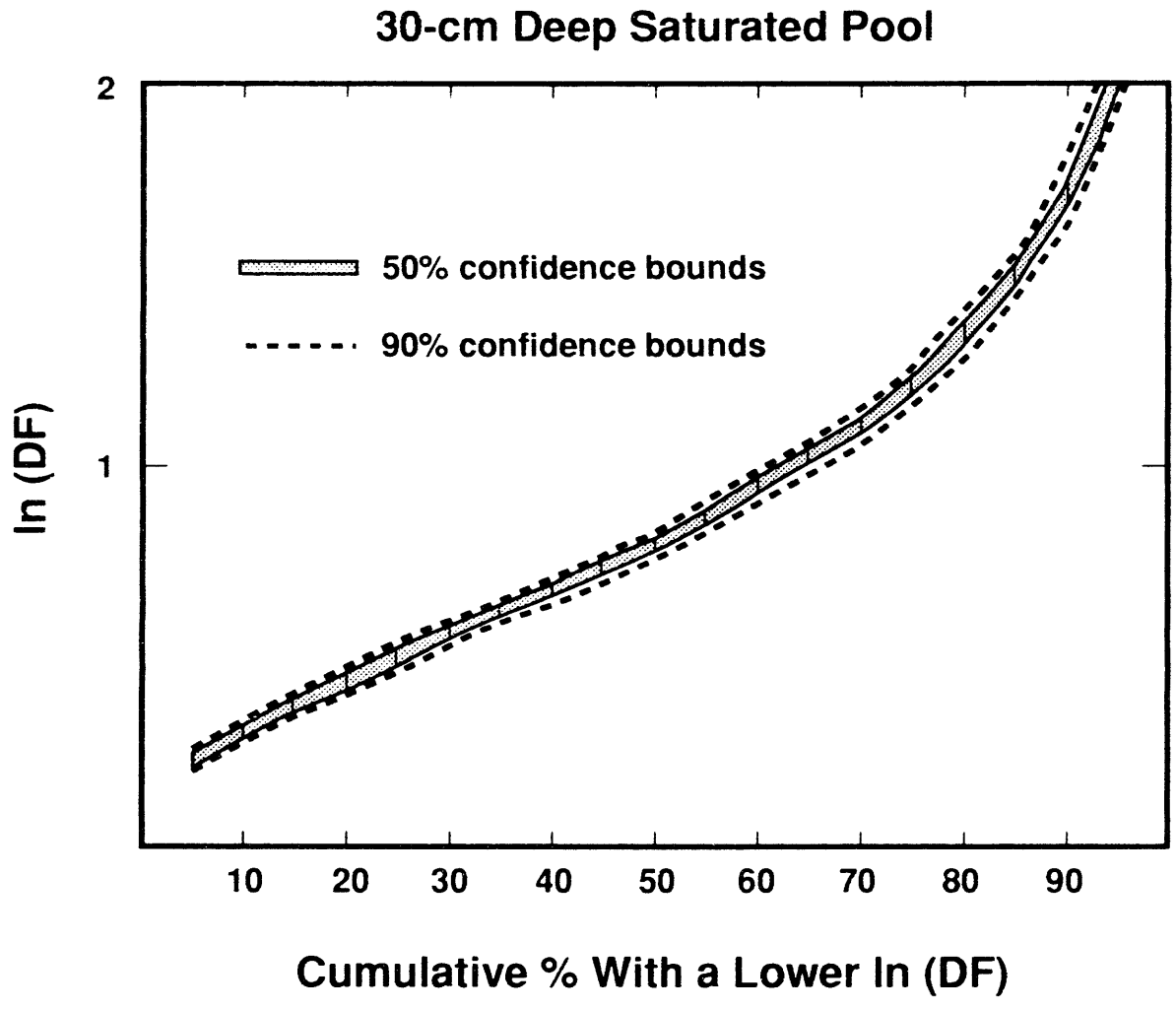

Figure 4. Cumulative Probability Distribution for ln(DF) Produced by a Saturated Water Pool 30 cm Deep

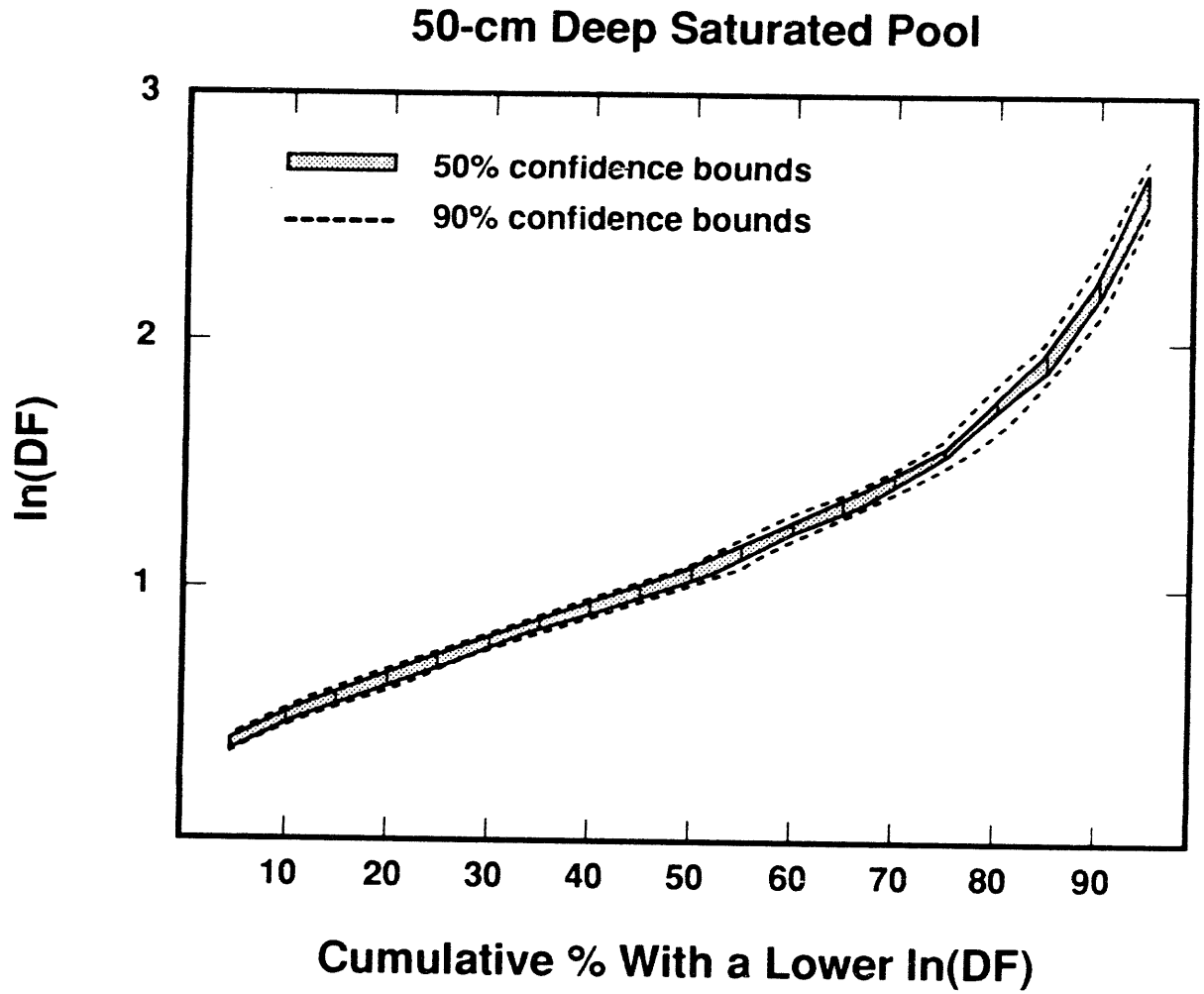

Figure 5. Cumulative Probability Distribution for ln(DF) Produced by a Saturated Water Pool 50 cm Deep

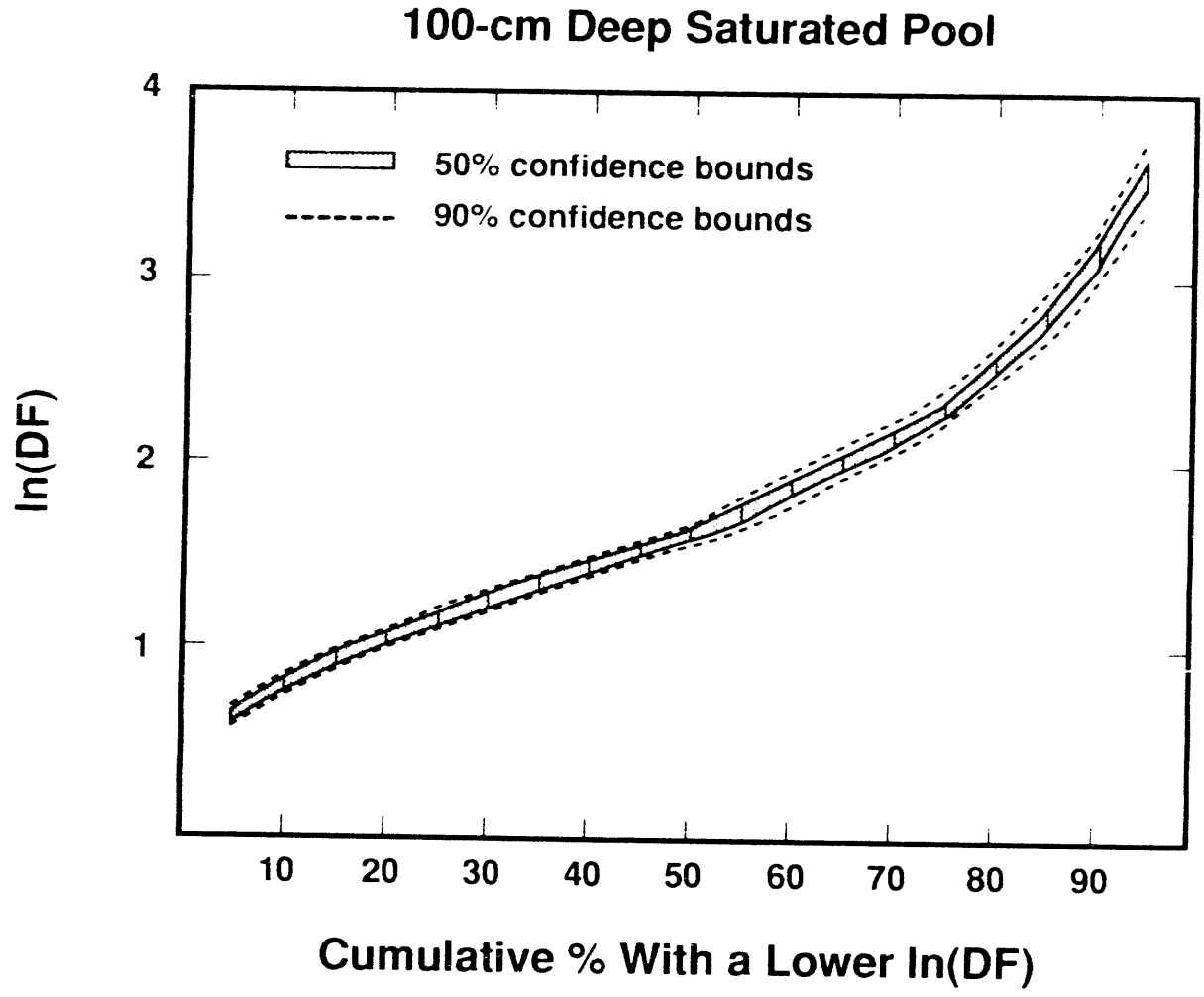

Figure 6. Cumulative Probability Distribution for ln(DF) Produced by a Saturated Water Pool 100 cm Deep

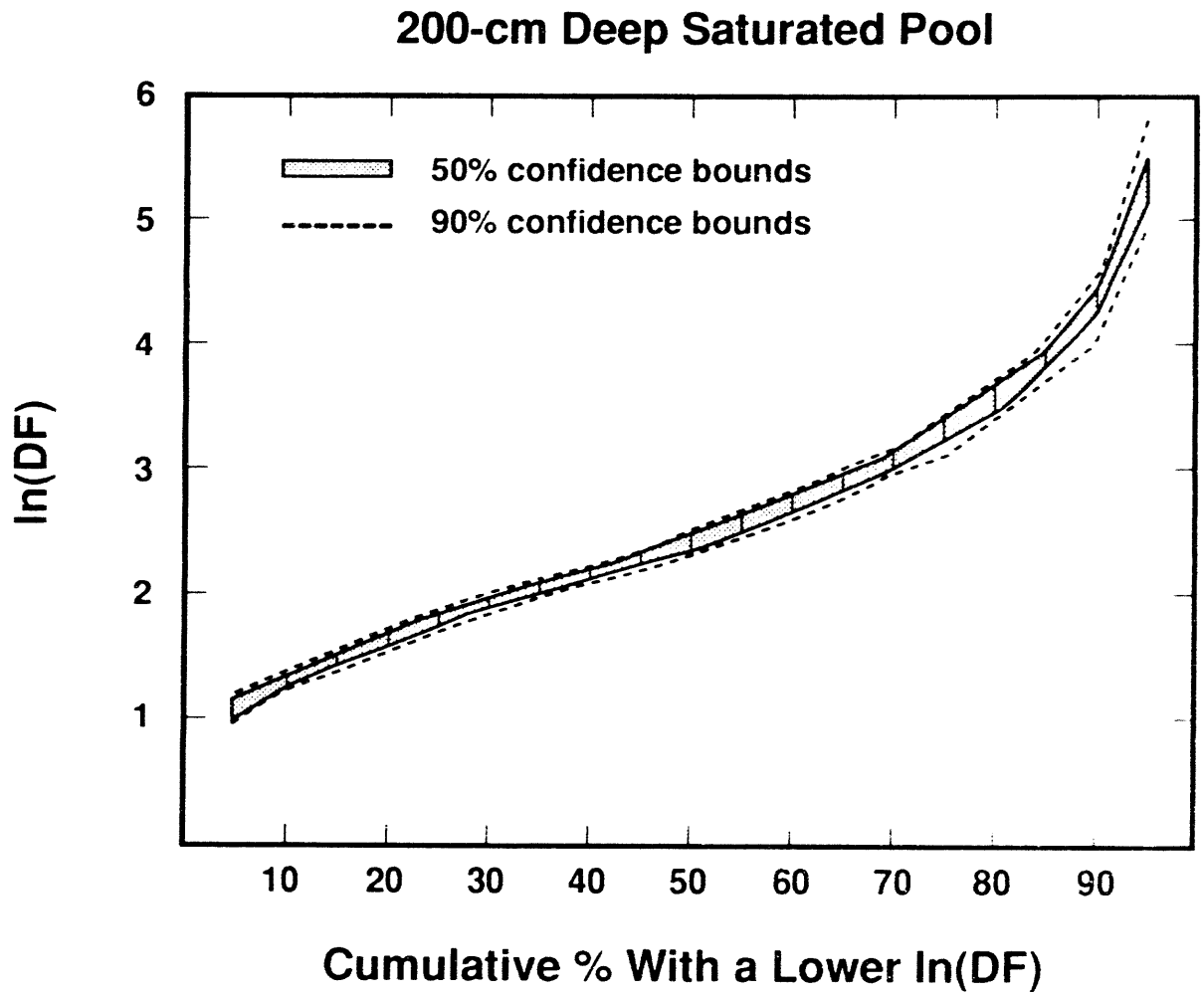

Figure 7. Cumulative Probability Distribution for ln(DF) Produced by a Saturated Water Pool 200 cm Deep

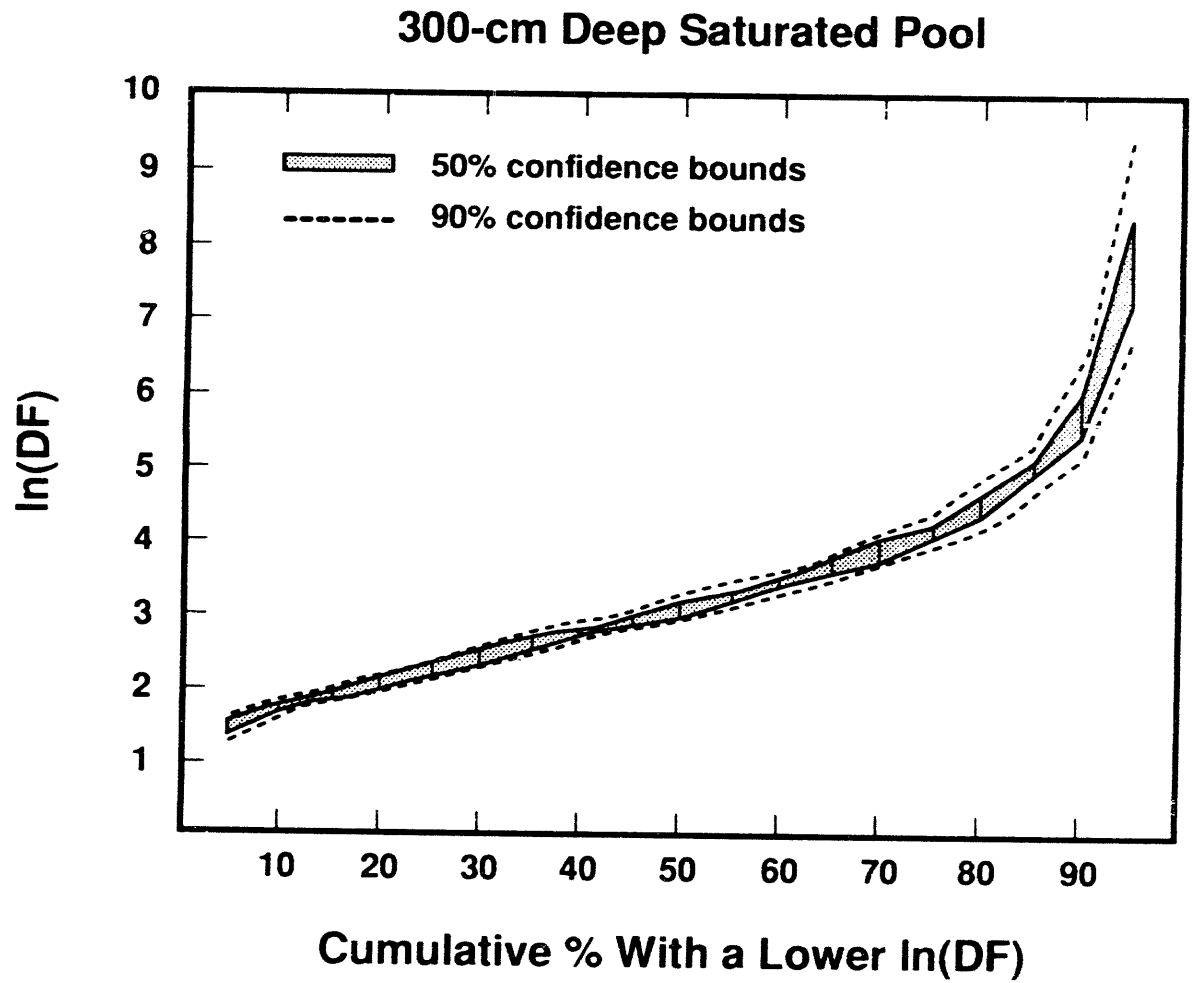

Figure 8. Cumulative Probability Distribution for ln(DF) Produced by a Saturated Water Pool 300 cm Deep

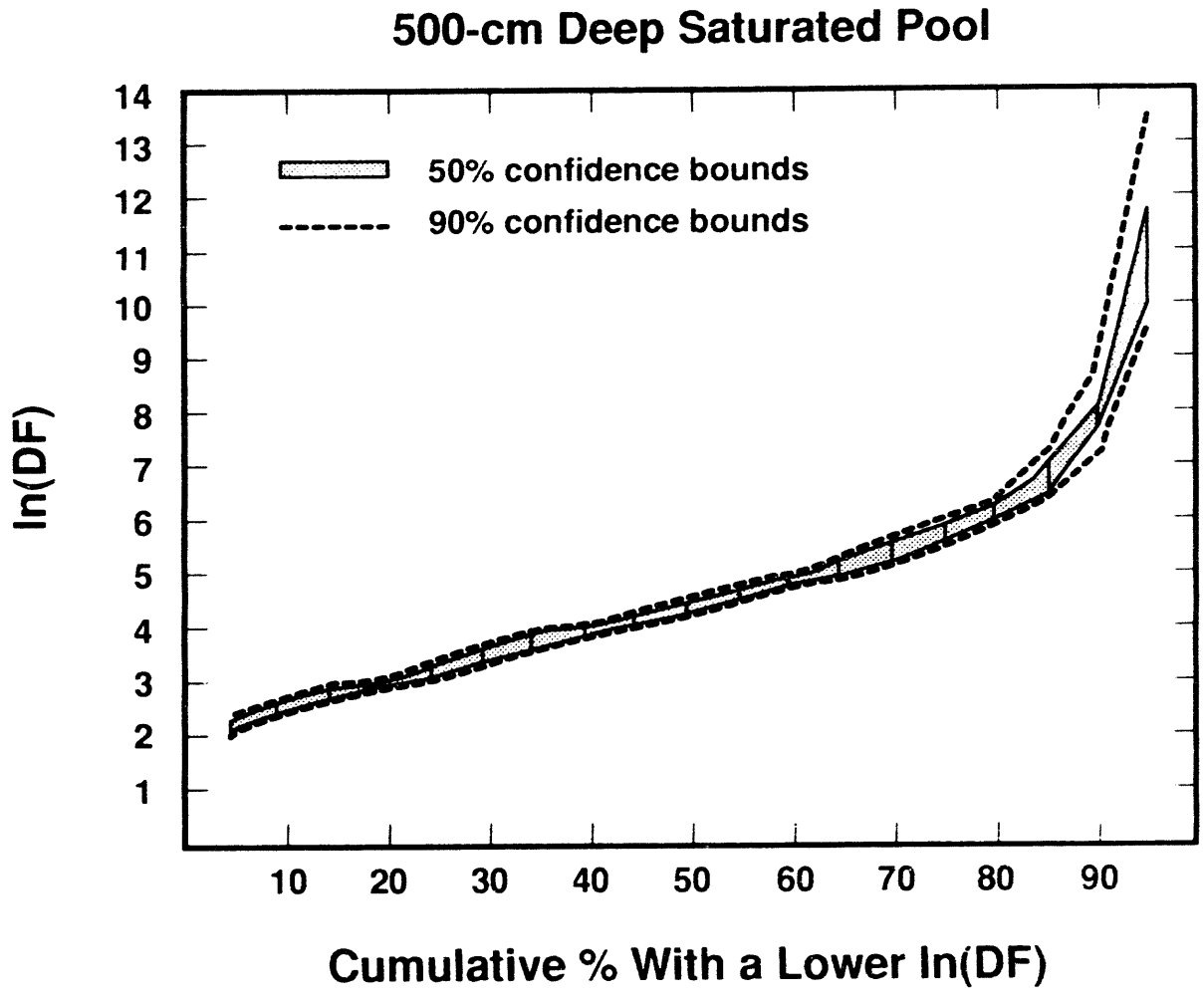

Figure 9. Cumulative Probability Distribution for ln(DF) Produced by a Saturated Water Pool 500 cm Deep

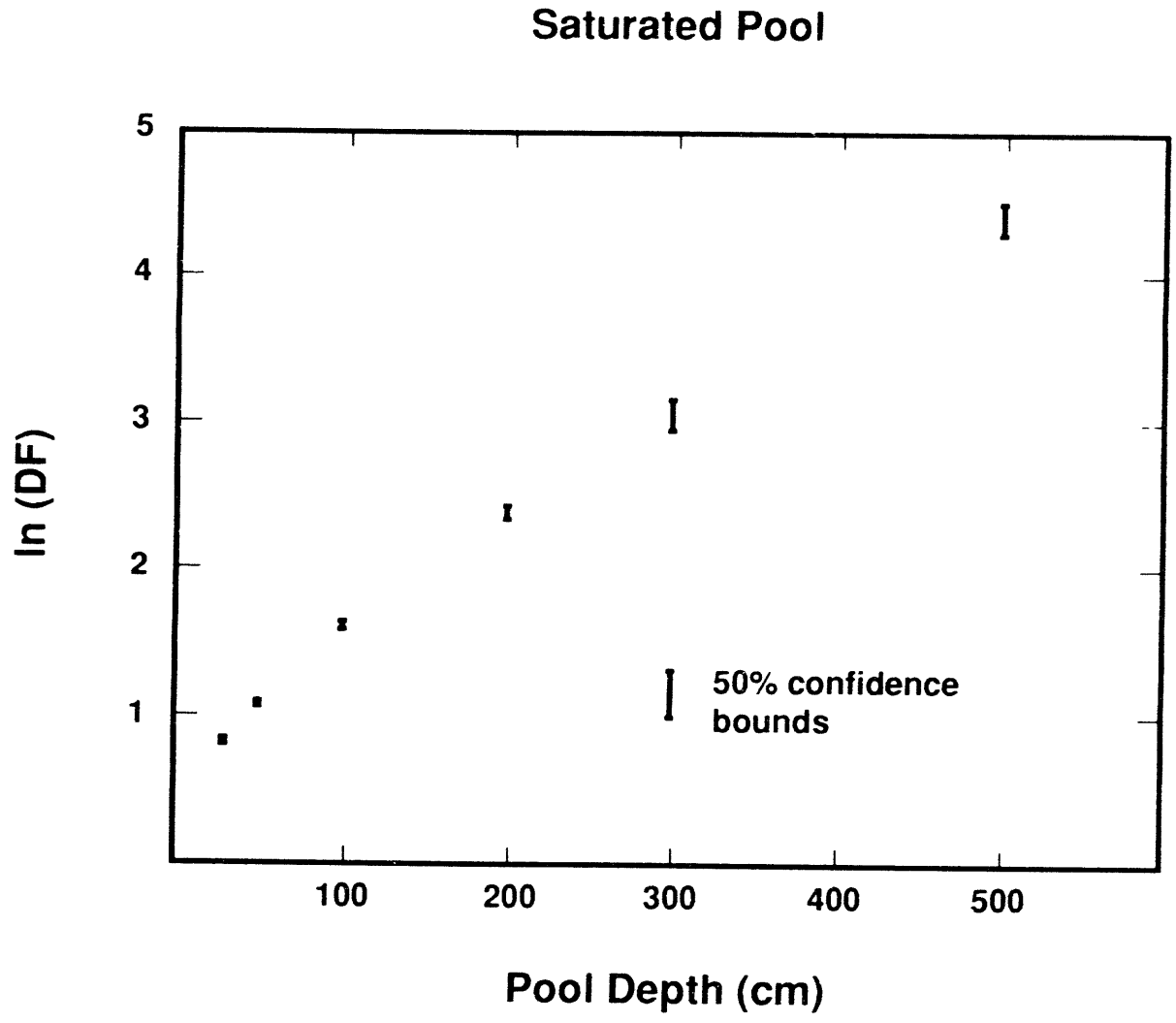

Figure 10. Median Values of ln(DF) for Various Saturated Water Pool Depths. Bars indicate 50% confidence intervals for the medians.

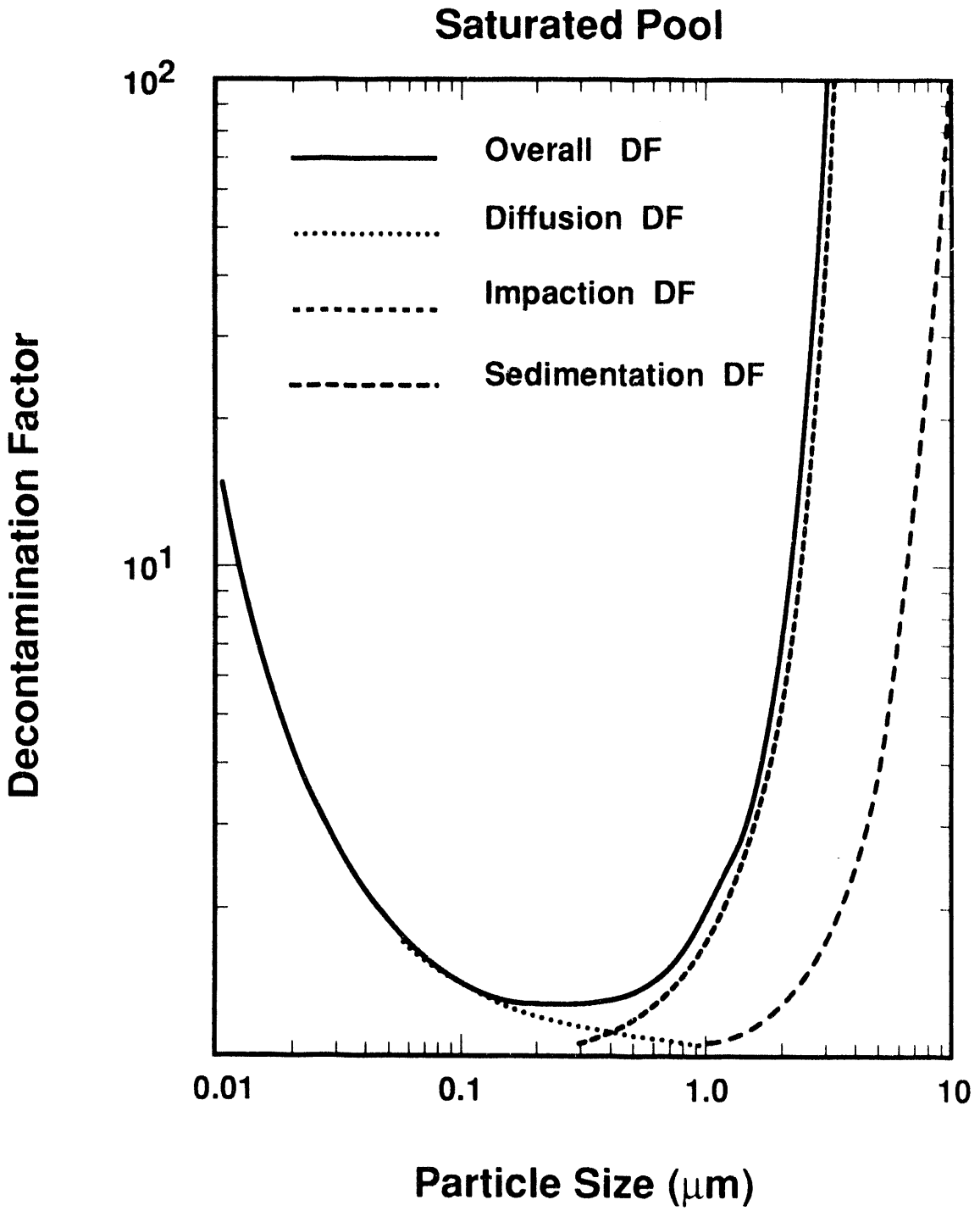

Figure 11. Decontamination Factors Produced by Diffusion, Inertial Impaction and Sedimentation in a 100 cm Deep, Saturated Water Pool as Functions of Aerosol Particle Size

- pools deeper than 100 cm achieve higher decontamination factors by removing aerosol particles in an intermediate size regime that is not strongly affected by either diffusion or inertial impaction (see Figure 12).

- because particles in the intermediate size regime are not strongly affected by either diffusion or inertial impaction, the rate of decontamination after the bubble has risen about 100 cm slows significantly.

This qualitative behavior raises a significant point about decontamination factors produced by water pools overlying core debris interacting with concrete. The water pools not only attenuate the magnitude of aerosol released to the containment, they also alter the size distribution of the aerosol. Aerosols that emerge from the water pool are distributed in size relatively narrowly around the maximum pool penetration size regardless of the size distribution of aerosols that entered the water pool. For most of the cases considered here, the mass median size of particles emerging from the water pool is 0.3 ± 0.15 μm.

One consequence of the changes in the particle size distribution caused by water pools is that decontamination factors for water pools cannot simply be multiplied by decontamination factors for subsequent processes to obtain overall decontamination factors. Decontamination factors for subsequent processes such as containment sprays must recognize the narrowed distribution of aerosol particles that do emerge from the water pools.

2. Subcooled Pool Results

In most reactor accidents, it is likely that the water pool overlying core debris interacting with concrete will quickly become saturated. There are some reactors for which so much water can be applied to core debris in the reactor cavity that subcooled water pools can be maintained for protracted periods. As increased attention is focused on accident management, it is often found that providing water to the reactor containment to cool core debris is one of the least expensive plant modifications that can be made [7,8]. It is, therefore, likely that there will be more need to consider subcooling of the water pool overlying core debris. Accordingly analyses were done of the effects of subcooling on the decontamination factors that can be achieved by water pools.

As discussed briefly in Chapter II of this report, subcooling can:

- increase removal of aerosol particles from gases in bubbles by diffusiophoresis as steam condenses on the bubble walls, and

- accentuate deposition of particles by diffusion, inertial impaction and sedimentation because the bubbles in the water pool are smaller once the bubble has equilibrated with the pool.

The kinetics of steam condensation were neglected in the analyses of the effects of subcooling. Bubbles expected to form during combined core debris-concrete-coolant interactions are small enough that condensation of the steam is expected to be rapid in comparison to the time-scales of interest here. Neglect of steam condensation kinetics does, however, make it important that the correlations of results presented here not be extrapolated to pools shallower than about

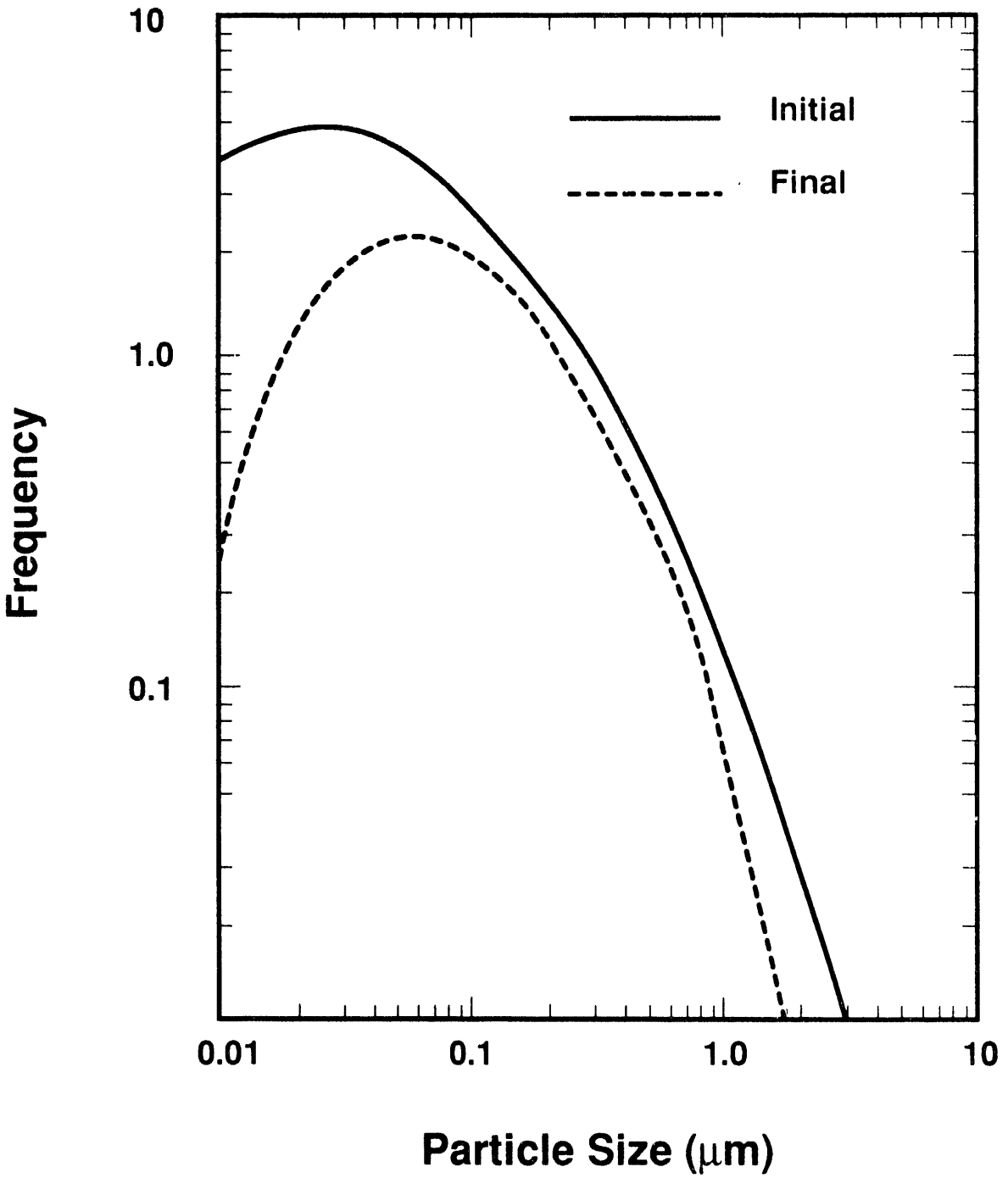

Figure 12. Aerosol Particle Size Distribution Before and After Passing Through a 100 cm Deep, Saturated Water Pool

30 cm. Steam condensation kinetics may well limit the diffusiophoretic decontamination that can be achieved before the bubbles burst through the surface of a very shallow water pool.

As bubbles rise through the subcooled water pool, there is a weak mass flux of water vapor into the bubble. This mass flux was considered to be too small to affect the diffusion, inertial impaction and sedimentation processes that produce decontamination after the bubble has equilibrated with the pool.

Results of the analyses of subcooling effects are summarized in Table 10. Detailed probability distributions for decontamination by pools of depths from 30 to 300 cm with subcooling of 2 to 70 K are collected in Appendix B. The decontamination by a water pool is plotted against pool depth for various levels of subcooling in Figure 13. Decontamination factor is plotted against subcooling for various pool depths in Figure 14. The plotted values in these figures are the medians (50% quantiles) of the distributions at 50% confidence level. The solid curves in the figures were calculated from the regression equation described below.

Note that the logarithm of the decontamination factor increases sharply from the values obtained for saturated conditions as the subcooling increases from 2 to about 10 degrees. The effects of subcooling greater than about 10 K are less dramatic. These results parallel in a sense the shrinkage of the bubble that accompanies condensation of steam in the subcooled pool. There is significant shrinkage for even small amounts of subcooling. Further subcooling does not produce proportional reductions in the bubble size. The general dependence of the logarithm of the decontamination factor on pool depth at constant subcooling is rather similar to that seen for saturated cases. This dependence is determined by the particles with sizes of about 0.3 μm that resist decontamination by diffusion, sedimentation, and inertial impaction.

Table 10
Summary of Results for the Subcooled Cases

Pool Depth (cm)	Sub-Cooling (K)	50% Quantile of ln(DF) at 50% Confidence	σ^*	90% Quantile of ln(DF) at 90% Confidence	σ^*	10% Quantile of ln(DF) at 90% Confidence	σ^*
30	0	0.7854-0.8158	1	1.6267-1.8245	2	0.2915-0.3348	1
30	2	2.3629-2.4250	2	3.6861-3.9945	3	1.2111-1.3854	1
30	5	3.0708-3.1175	3	4.7041-5.1801	2	1.7941-2.0150	1
30	10	3.7884-3.8978	2	5.5885-5.9541	3	2.2236-2.4091	2
30	20	4.5743-4.6779	2	6.6050-7.1592	3	2.9425-3.1907	2
30	30	5.0977-5.2478	2	7.2795-7.9798	2	3.3269-3.5749	2
30	50	5.7907-5.8814	3	8.3760-8.7992	4	3.8181-4.0992	2
30	70	5.7892-5.9429	2	8.5337-9.3989	2	3.5725-3.9342	2
50	0	1.0511-1.0763	2	2.1050-2.3269	2	0.4419-0.4885	2
50	2	2.7048-2.7805	2	4.2535-4.5795	3	1.4652-1.6618	1
50	5	3.5281-3.6559	1	5.4022-5.8733	3	1.9907-2.2740	1
50	10	4.3825-4.4949	2	6.4373-6.9502	3	2.6093-2.9217	2
50	20	5.0951-5.2448	2	7.7528-8.2354	4	3.0929-3.4076	2
50	30	5.6469-5.7914	2	8.0362-8.5868	3	3.4996-3.9106	2
50	50	6.4307-6.5659	3	9.3374-10.4523	2	3.9620-4.2385	2
50	70	7.1014-7.2417	3	10.0721-12.4243	1	4.3884-4.9852	1
100	0	1.5948-1.6251	3	2.9863-3.2813	2	0.7454-0.8135	2
100	2	3.4795-3.5774	3	5.4399-5.9751	2	2.0625-2.2355	2
100	5	4.4869-4.5630	2	6.6838-7.3304	2	2.5064-2.9710	1
100	10	5.3401-5.5473	3	8.1638-8.9105	2	3.2765-3.6409	2
100	20	6.4503-6.6214	1	9.6548-10.4686	2	4.1105-4.4486	2
100	50	8.2593-8.4461	2	12.4449-14.0268	3	5.0256-5.4645	1
100	70	8.8291-9.0081	2	13.7746-15.3293	2	5.5658-6.0474	1
200	0	2.3532-2.4236	2	4.0325-4.4659	2	1.2214-1.3413	2
200	10	7.2661-7.4614	2	10.8580-12.9156	1	4.0265-4.7015	1
300	0	2.9651-3.1248	1	5.1449-6.3903	1	1.6174-1.8495	1
300	2	6.4539-6.5348	4	10.2913-11.5347	2	3.8820-4.2937	2
300	5	7.5122-7.8032	1	11.9353-12.9979	3	4.5141-4.9976	2
300	10	9.0310-9.2363	2	13.7013-15.3326	2	5.3783-5.9109	2
300	30	12.0088-12.3872	2	20.0146-22.0593	2	7.1512-7.6963	2
500	0	4.3187-4.4998	1	7.2146-8.8799	1	2.4456-2.6467	2

*σ = weight used in regression analysis.

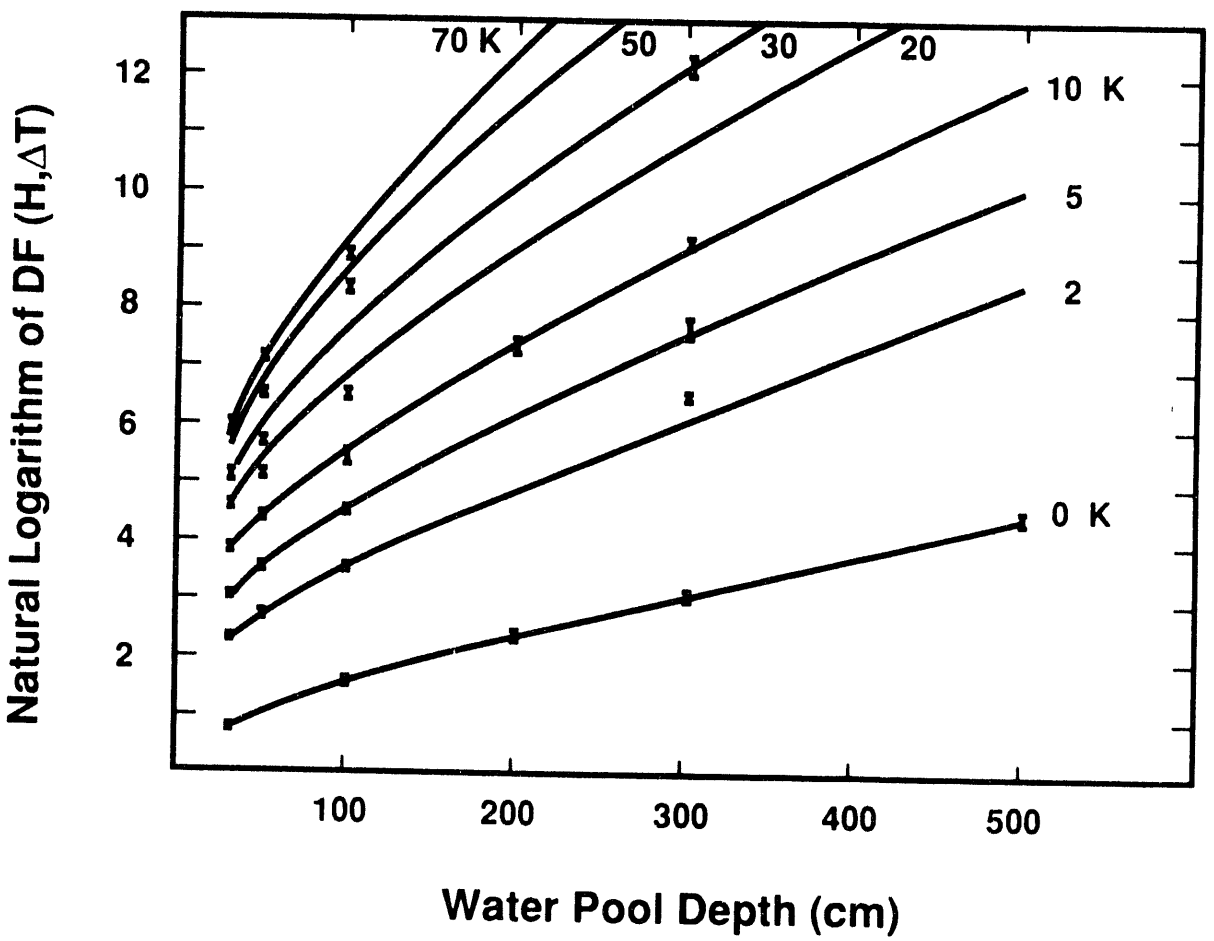

Figure 13. Natural Logarithm of the Decontamination Factor as a Function of Pool Depth for Various Levels of Subcooling. The bars denote the median values of the distribution at 50% confidence level. The solid lines were calculated from the regression equation.

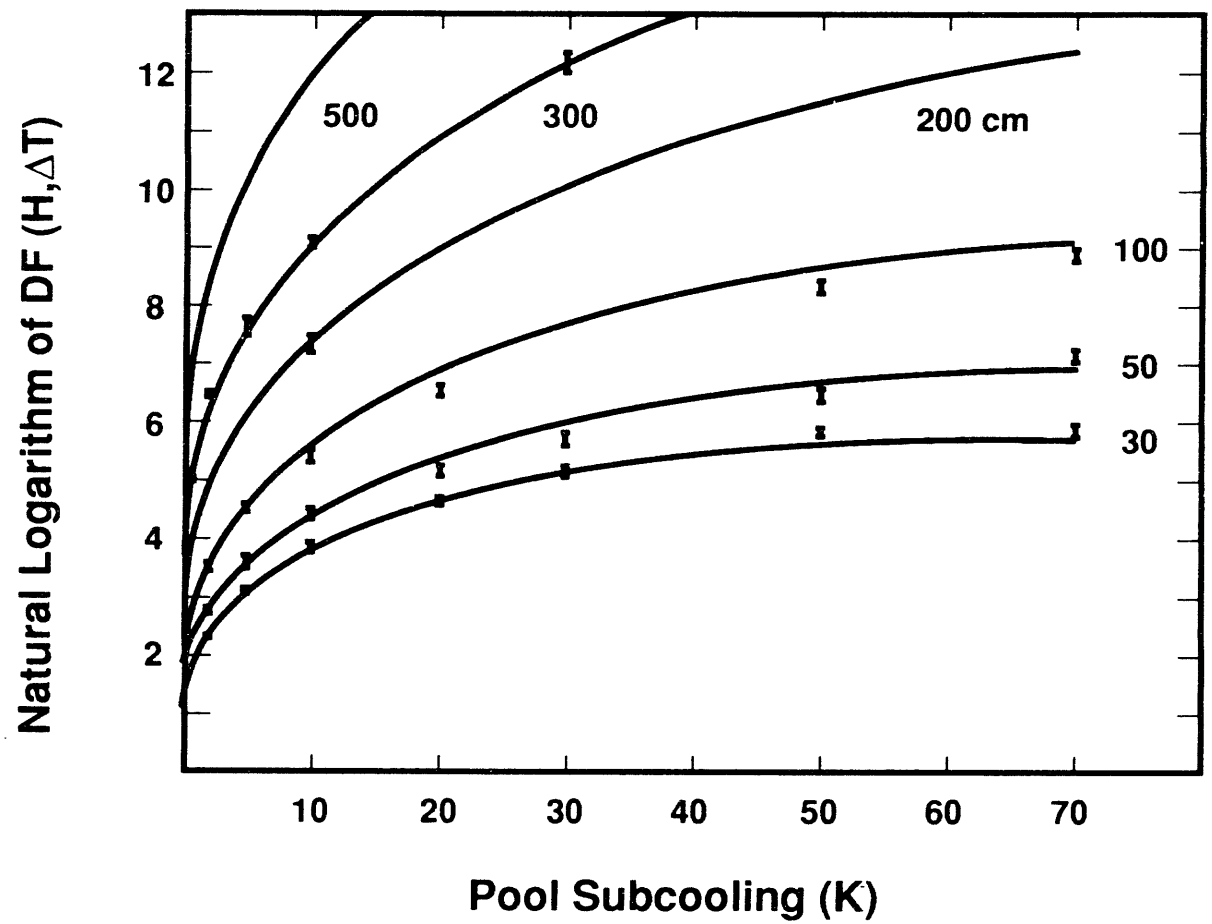

Figure 14. Natural Logarithm of the Decontamination Factor as a Function of Subcooling for Various Pool Depths. The bars denote the median values of the distribution at 50% confidence level. The solid lines were calculated from the regression equation.

IV. REGRESSION OF THE RESULTS

The results of the Monte Carlo uncertainty analysis are easily used to obtain simplified expressions for the decontamination of aerosol-laden gases by a water pool overlying core debris that is interacting with concrete. Simple polynomial regression of the results using as the independent variable a quantity the analyst will know or can assume provides the necessary expressions.

A. Saturated Results

For the cases in which the water pool was assumed to be saturated, pool depth was taken as the independent variable (see Section III.B.1). Conventional linear least squares regression was done. Transformed independent variables available for the regression were taken to be:

$$\sqrt{H},\ H,\ H^{3/2},\ H^2,\ H^{5/2},\ and\ H^3$$

where H is the water pool depth. The statistical 'F test' was used to determine how many terms to include in the polynomial regression equations.

The dependent variables were taken to be the mean values of the uncertainty ranges for particular quantiles of the distributions for the natural logarithms of the decontamination factors. These mean values were weighted in the regressions in proportion to the reciprocals of the widths of the uncertainty ranges.

Only selected quantiles of the distributions have been regressed against the independent variable and its transforms. Perhaps the most interest will be in the median values of the distribution (50% quantile). Interest focused on the median values will, it is presumed, not demand high confidence levels, so the median used in the fitting process were the values obtained at the 50% confidence level. The uncertainty ranges for the median of the ln(DF) at various pool depths are shown in Table 11 along with the weighting factor used in the regression process. The regression equation obtained for these results for the median values at 50% confidence is:

$$\ln(DF) = -0.195036 + (0.17976 \pm 0.00049)\sqrt{(H)}$$

$$+ (4.68319 \pm 0.084) x 10^{-9} H^3$$

Table 11
Results for 50% Quantile at the 50% Confidence Level
- Saturated Pool Case -

Pool Depth (cm)	Range for ln(DF)	Weight in Regression*
30	0.7854-0.8158	12
50	1.0511-1.0763	14
100	1.5948-1.6251	12
200	2.3532-2.4236	6
300	2.9651-3.1248	3
500	4.3187-4.4998	2

Regression Equation:

$$ln(DF) = -0.195036 + (0.17976 \pm 0.00049)\sqrt{H} + (4.68319 \pm 0.084) \times 10^{-9} H^3$$

Standard Error = 0.00935

Sum of Squares of Residuals = 0.00395

*Integral weights proportional to the reciprocals of the ranges for ln (DF)

Estimates of the median of the natural logarithm of the decontamination factor (at 50% confidence) are compared to the results of the Monte Carlo uncertainty analysis in Figure 15. The quality of the regression equation fit to the results of the Monte Carlo uncertainty analysis is indicated in Tables 11 to 13 by the sum of the squares of the residuals given by:

$$S^2 = \sum_{i=1}^{N} [x(i) - f(H(i))]^2 \; W(i) = 0.00395$$

where

S^2 = *sum of the squares of the residuals*

$x(i)$ = $\ln(DF)$ *for a pool depth* $H(i)$ *obtained in the Monte Carlo uncertainty analysis*

$H(i)$ = *pool depth used for the calculation of the* i^{th} *result*

$f(H(i))$ = *estimate of* $\ln(DF)$ *obtained from the regression equation*

$W(i)$ = *weighting factor for the results obtained in the case of pool depth* $H(i)$

It is important to remember that the regression equation developed here is a completely empirical fit to the results of the Monte Carlo uncertainty analysis done with a mechanistic model. No physical significance should be attached to the functional forms of the transformed independent variables that appear in the polynomial expression. Similarly, the coefficients in the polynomial expression ought not be physically interpreted.

It is also important that the regression equation be used only for interpolation for pool depths in the range $30 \leq H(i) \leq 500$ cm. Uncertainties in the estimates grow rapidly for pool depths greater than 500 cm. For pool depths less than 30 cm, transient effects associated with the formation of bubbles, which were neglected in the mechanistic modeling of the decontamination process, can affect decontamination significantly.

Conservative analysts interested in the amount of aerosol produced by core debris/concrete interactions that passes through the water pool into the containment atmosphere might find the 10% quantile results for ln(DF) of more interest than the median. For such conservative purposes, it must be assumed, much higher levels of confidence are required. The 10% quantile results for ln(DF) in the case of a saturated pool at 90% confidence were found to fit well the regression equation:

$$\ln(DF) = -0.1832417 + (0.0879653 \pm 0.00035558)\sqrt{(H)}$$

$$+ (8.192503 \pm 0.125763) \times 10^{-5} H^{3/2}$$

$$- (1.2281546 \pm 0.068840) \times 10^{-9} H^3$$

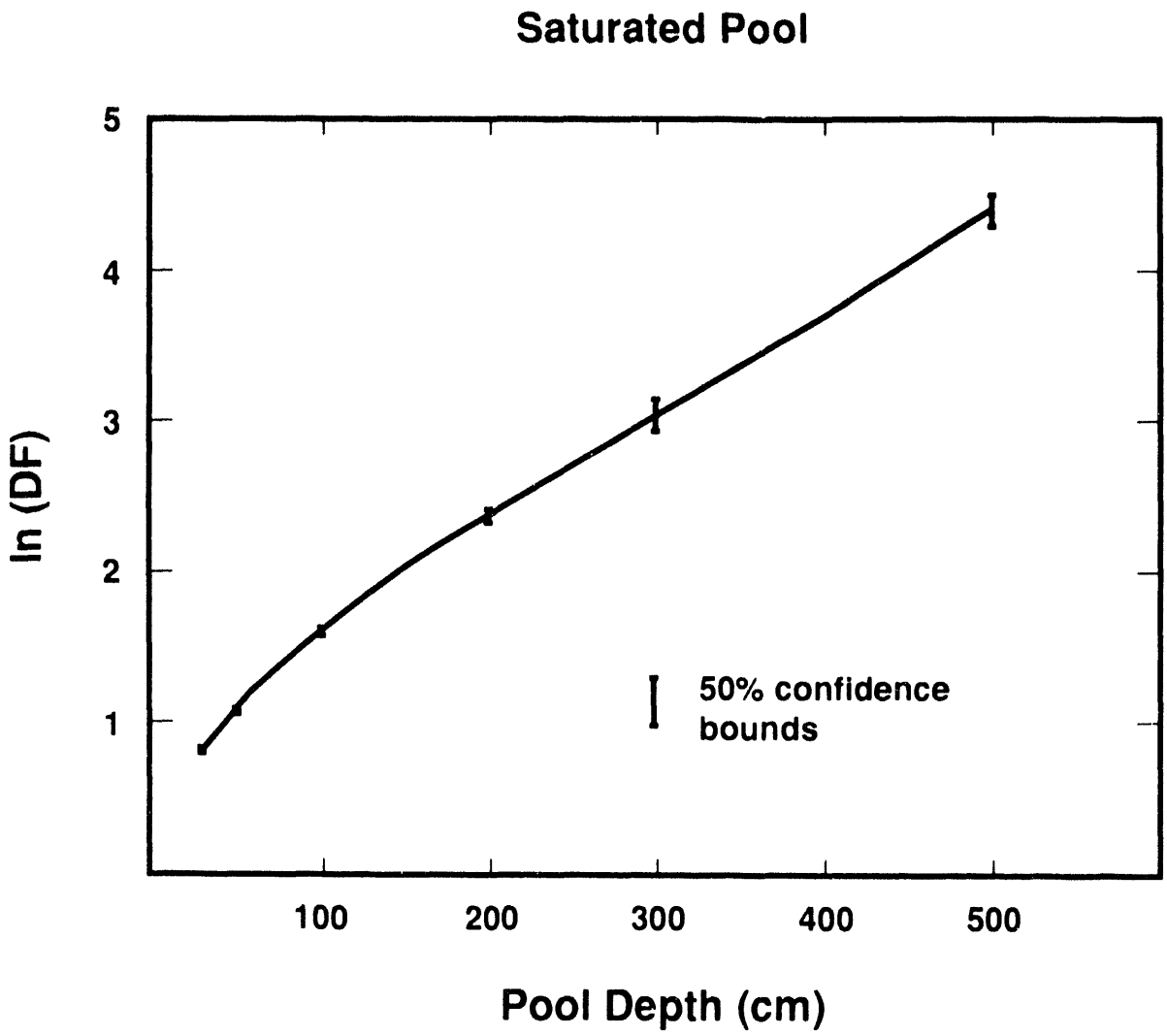

Figure 15. Comparison of Median ln(DF) Values Obtained in the Monte Carlo Uncertainty Analyses for Various Pool Depths (bars) with Estimates Obtained from the Regression Equation (continuous curve).

Table 12
Results for 10% Quantile at the 90% Confidence Level
- Saturated Pool Case -

Pool Depth (cm)	Range for ln(DF)	Weight in Regression*
30	0.2915-0.3348	16
50	0.4419-0.4885	15
100	0.7454-0.8135	10
200	1.2214-1.3413	6
300	1.6174-1.8495	3
500	2.4456-2.6467	3

Regression Equation:

$$ln(DF) = -0.1832417 + (0.0879653 \pm 0.00035558)\sqrt{H} + (8.192503 \pm 0.125763) \times 10^{-5} H^{3/2} - (1.2281546 \pm 0.068840) \times 10^{-9} H^{3}$$

Standard Error = 0.00188

Sum of Squares of Residuals = 0.00017

*Integer weights proportional to the reciprocals of the ranges for ln (DF)

Table 13
Results for 90% Quantile at the 90% Confidence Level
- Saturated Pool Case -

Pool Depth (cm)	Range for ln(DF)	Weight in Regression*
30	1.6267-1.8245	17
50	2.1050-2.3269	15
100	2.9863-3.2813	11
200	4.0325-4.4659	8
300	5.1449-6.3903	3
500	7.2146-8.8759	2

Regression Equation:

$$ln(DF) = 0.114994 + (0.295871 \pm 0.003738)\sqrt{(H)} + (1.087539 \pm 0.068814) \times 10^{-8} H^3$$

Standard Error = 0.08103

Sum of Squares of Residuals = 0.34796

*Integer weights proportional to the reciprocals of the ranges for ln (DF)

The additional term in this regression equation in comparison to that for the median ln(DF) was justified by an F test. Other details of the development of this regression equation are shown in Table 12.

On the other hand, an analyst interested in the radiation dose to the water pool might find most useful the 90% quantile results for ln(DF). Again, interests in the extremes of the distribution of the logarithm of the decontamination factor would indicate high confidence level demands. The regression equation developed for the 90% quantile at the 90% confidence level (see Table 13) is:

$$ln(DF) = 0.114994 + (0.29587 \pm 0.003738)\sqrt{(H)}$$

$$+ (1.087539 \pm 0.068814) \times 10^{-8} H^3$$

The estimates obtained with this regression equation are compared to results of the Monte Carlo uncertainty analysis in Figure 16.

Tabulated results of the Monte Carlo uncertainty analysis for saturated cases can be used to produce regression equations for other combinations of confidence levels and quantiles. Together, the results could be used to produce a response surface with either constant confidence level or correlated confidence levels.

B. Subcooled Results

A similar regression analysis was done for the cases in which the water pool was considered to be subcooled. For these cases, the variables assumed to be known to the analyst were pool depth, H, and subcooling, ΔT. Transformations of these variables considered in the regression analyses were:

$$H^{1/2}, H^{3/2}, H^3, \Delta T, \Delta T^{1/2}, \Delta T^{3/2}, \Delta T^2, \Delta T^3$$

$$H\Delta T, (H\Delta T)^{1/2}, H^3\Delta T, H^3(\Delta T)^{1/2}$$

Separate regressions were done for the median (50% quantile) results at 50% confidence, 10% quantile results at 90% confidence, and 90% quantile results at 90% confidence. Results of the Monte Carlo analyses were weighted in the regression by the reciprocals of the widths of the uncertainty ranges divided by the respective values of the logarithm of the decontamination factors. Results of the regressions for subcooled pool cases are:

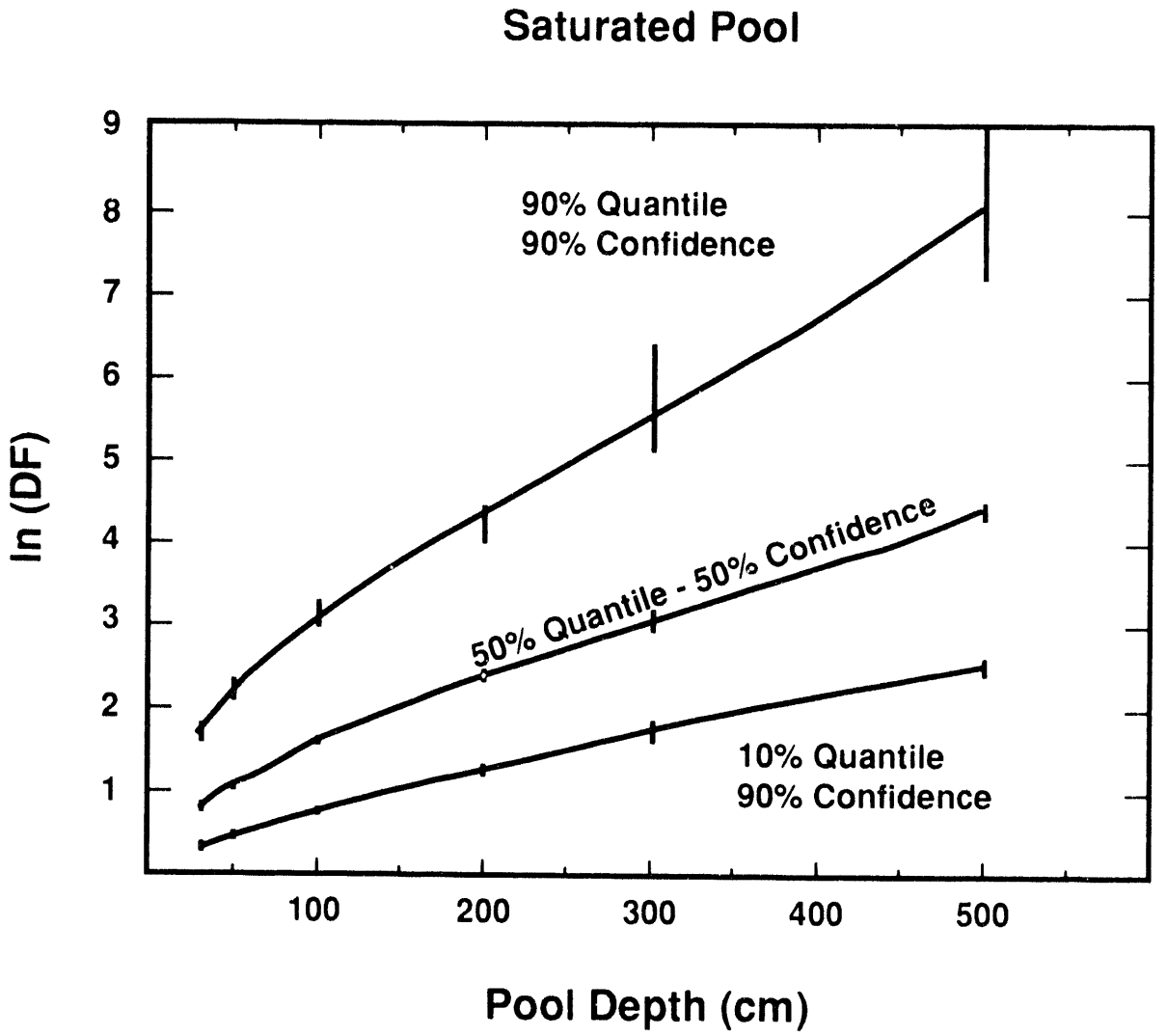

Figure 16. Comparison of Results of the Monte Carlo Uncertainty Analyses (bars) to Estimates Obtained with the Regression Equations (continuous curves).

1. Median Values at 50% Confidence Level:

$$\begin{aligned} lnDF(H,\Delta T) = {} & lnDF(H,0) - 0.084381550 \\ & - (0.07040774 \pm 0.0042757)\ \Delta T \\ & + (8.2346311 \pm 1.58412) \times 10^{-5}\ H^{3/2} \\ & + (0.8238286 \pm 0.0453165)\ \sqrt{\Delta T} \\ & + (0.0668004 \pm 0.0022341)\ \sqrt{H\Delta T} \end{aligned}$$

Standard error = 0.2274.

where ln DF (H,0) is the calculated value for the natural logarithm of the decontamination factor, at the same confidence level, for a saturated pool of the same depth.

2. 90% Quantile Results at 90% Confidence:

$$\begin{aligned} lnDF(H,\Delta T) = {} & lnDF(H,0) + 0.03437166 \\ & - (0.2333505 \pm 0.0346206)\ \Delta T \\ & + (1.4415216 \pm 0.140201)\sqrt{\Delta T} \\ & + (0.01234607 \pm 0.0027294)\ \Delta T^{3/2} \\ & + (3.92396212 \pm 0.650023) \times 10^{-4} H\Delta T \\ & + (0.075810892 \pm 0.00889012)\ \sqrt{H\Delta T} \\ & + (1.3850581 \pm 0.105336) \times 10^{-8}\ H^3\sqrt{\Delta T} \end{aligned}$$

Standard error = 0.33049.

3. 10% Quantile Results at 90% Confidence

$$lnDF(H,\Delta T) = lnDF(H,0) + 0.00993606$$
$$- 0.0474108\,(\pm 0.0021796)\Delta T$$
$$+ 0.5696997\,(\pm 0.019987)\sqrt{(\Delta T)}$$
$$+ 0.0433372\,(\pm 0.00139914)\sqrt{H\Delta T}$$

Standard error = 0.12447.

The regression equation predictions are compared to the results of the Monte Carlo analyses in Figures 13 and 14.

The regression equations have been used to develop plots of constant decontamination factor as functions of pool depth and subcooling. These plots are shown in Figures 17, 18 and 19. Decontamination factors in excess of 1000 were calculated in the Monte Carlo analyses and can be calculated with the simplified expressions using suitable values of pool depth and subcooling. It is, however, difficult to have confidence in such large decontamination factors. Phenomena that have not been considered here can prevent achieving decontamination factors in excess of about 1000 in real systems. One such phenomenon is the entrainment of contaminated liquid by sparging gases [6]. The authors recommend that predicted values of the decontamination factor in excess of 1000 be reduced to 1000.

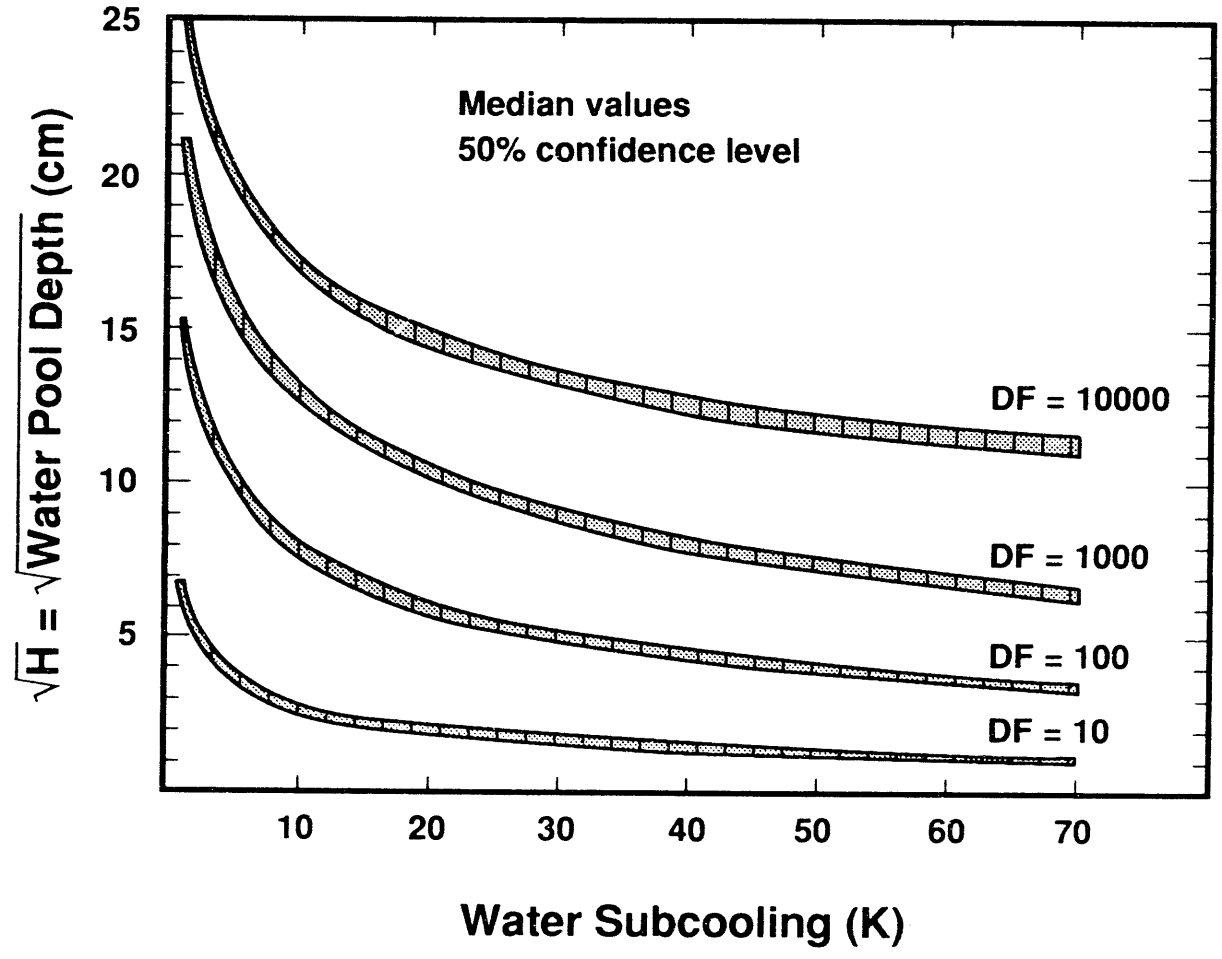

Figure 17. Map of Median Values of the Decontamination Factor of 10, 100, 1000 and 10000 as Functions of Pool Depth and Subcooling. Note that decontamination factors in excess of 1000 may not be realized in real systems because of unmodeled phenomena that can reverse decontamination by water pools.

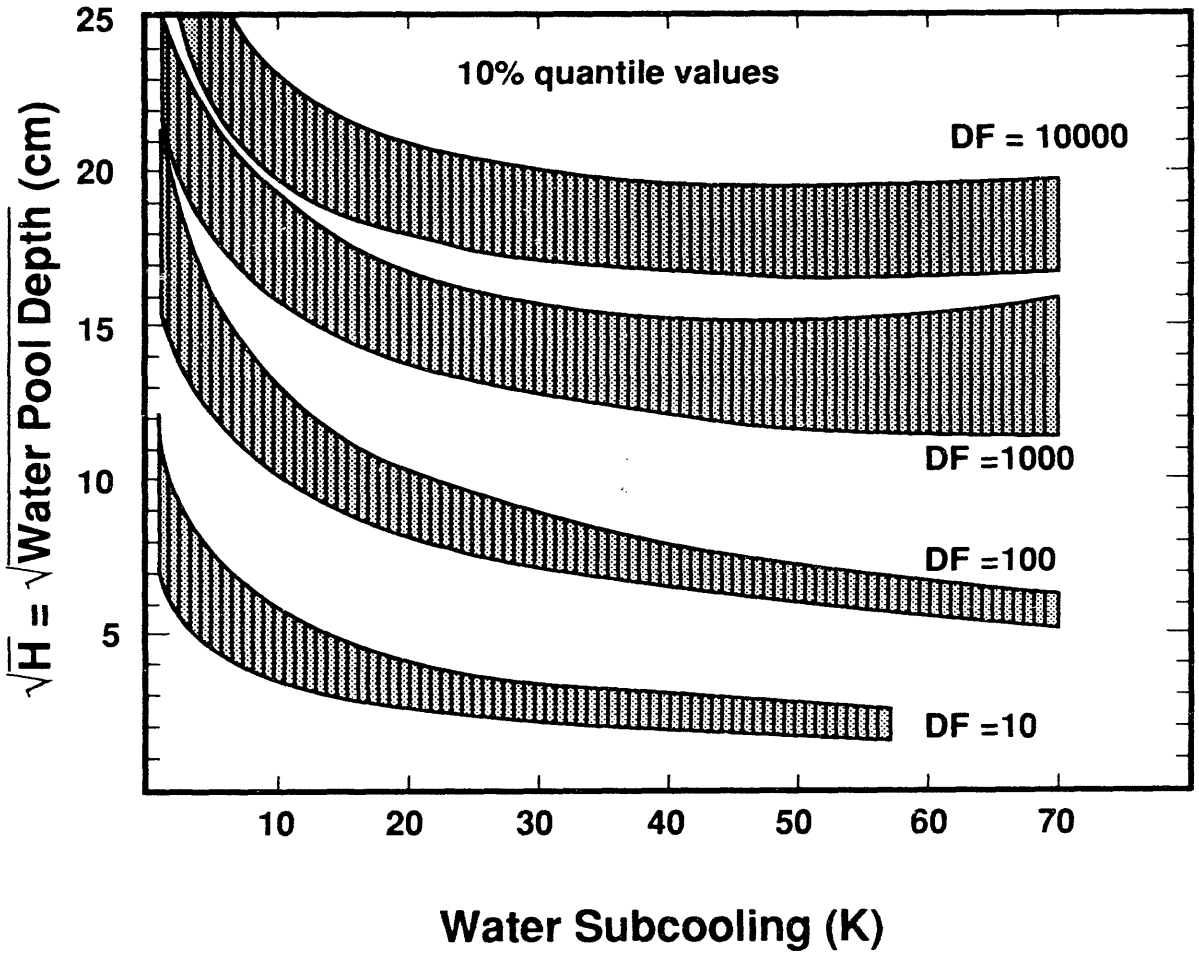

Figure 18. Map of 10% Quantile Values of the Decontamination Factor of 10, 100, and 1000 as Functions of Pool Depth and Subcooling.

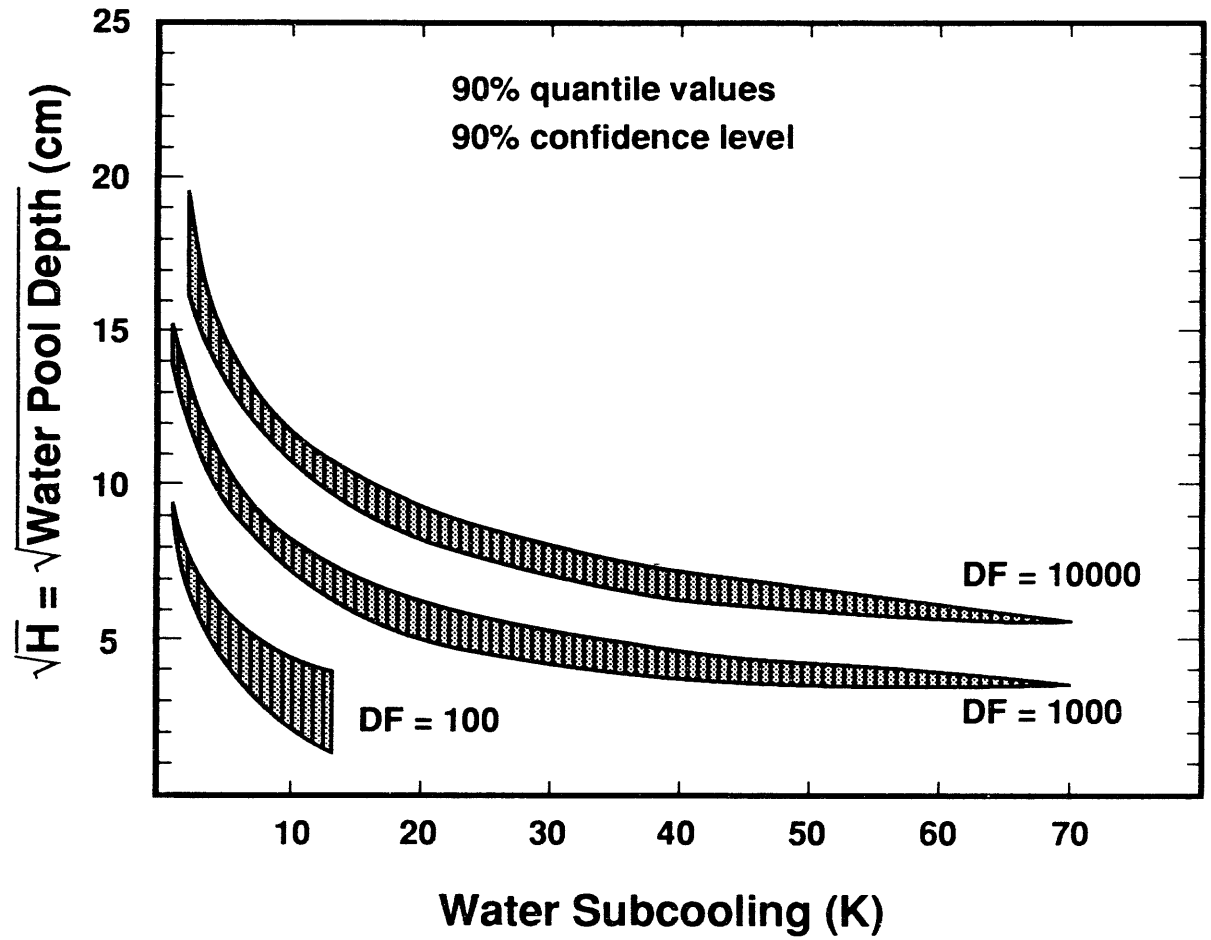

Figure 19. Map of 90% Quantile Values of the Decontamination Factor of 100, 1000 and 10000 as Functions of Pool Depth and Subcooling. Note that decontamination factors in excess of 1000 may not be realized in real situations because of unmodeled phenomena that reverse decontamination by water pools.

V. SUMMARY

A mechanistic model of the decontamination of aerosol-laden gases by a water pool overlying core debris interacting with concrete has been described. This model was used to conduct a Monte Carlo analysis of the uncertainty in the decontamination achieved by saturated water pools 30, 50, 100, 200, 300, and 500 cm deep. Cumulative probability distributions for the natural logarithms of the decontamination factors are developed based on nonparametric statistical analyses. Results of the uncertainty analyses are used to prepare simple polynomial regression equations for estimating the decontamination factors for saturated pools 30 to 500 cm deep. The median (50% quantile) decontamination factors (DF) for saturated cases can be estimated from:

$$ln(DF) = -0.195036 + 0.17976\sqrt{(H)} + 4.68319 \times 10^{-9} H^3$$

where H is the pool depth. The 10 percent quantile decontamination factor for saturated cases can be estimated from:

$$ln(DF) = -0.1832417 + 0.0879653\sqrt{(H)} + 8.192503 \times 10^{-5} H^{3/2} - 1.2281546 \times 10^{-9} H^3$$

The 90 percent quantile decontamination factor for saturated cases can be estimated with:

$$ln(DF) = 0.114994 + 0.29587\sqrt{(H)} + 1.087539 \times 10^{-8} H^3$$

Subcooling of the water pool dramatically increases the decontamination that can be achieved. The mechanistic model was used in Monte Carlo uncertainty analyses for pools 30, 50, 100, 200, and 300 cm deep and subcooled by 2, 5, 10, 20, 30, 50, and 70 degrees Kelvin. Cumulative probability distributions for the decontamination factors for these cases were developed using nonparametric statistical analysis techniques. Results were then correlated by linear regression to obtain simple polynomial expressions in terms of pool depth, H, and the amount of subcooling, ΔT, for the decontamination factor. The median decontamination factor can be estimated from:

$$lnDF(H,\Delta T) = lnDF(H,0) - 0.084381550 - 0.0704774\ \Delta T + 8.23463118 \times 10^{-5} H^{3/2} + 0.8238286\sqrt{\Delta T} + 0.0668004\sqrt{H\Delta T}$$

where ln DF (H,0) is the decontamination factor calculated for a saturated pool of the same depth. The 90% quantile for a subcooled case can be estimated from:

$$lnDF(H,\Delta T) = lnDF(H,0) + 0.03437166 - 0.2333505\ \Delta T + 1.4415216\sqrt{\Delta T} + 0.01234607\Delta T^{3/2} + 3.92396212\ x\ 10^{-4} H\Delta T + 0.075810892\sqrt{H\Delta T} + 1.3850581\ x\ 10^{-8}\ H^3\sqrt{\Delta T}$$

The 10% quantile for a subcooled case can be estimated from:

$$lnDF(H,\Delta T) = lnDF(H,0) + 0.00993606 - 0.0474108\ \Delta T + 0.5696997\sqrt{(\Delta T)} + 0.0433372\sqrt{H\Delta T}$$

VI. REFERENCES

1. R. J. Lipinski et al., Uncertainty in Radionuclide Release Under Specific LWR Accident Conditions Volumes I-IV, SAND84-0410, Sandia National Laboratories, Albuquerque, NM, May 1984.

2. E. R. Copus et al., Core-Concrete Interactions Using Molten Steel with Zirconium on a Basaltic Basemat: The SURC4 Experiment, NUREG/CR-4994, SAND87-2008, Sandia National Laboratories, Albuquerque, NM, April 1989.

3. E. R. Copus et al., Core-Concrete Interactions Using Molten Urania with Zirconium on a Limestone Basemat: The SURC-1 Experiment, NUREG/CR-5443, SAND90-0087, Sandia National Laboratories, Albuquerque, NM, December 1990.

4. J. F. Muir et al., CORCON-MOD 1: An Improved Model for Molten Core/Concrete Interactions, NUREG/CR-2142, SAND80-2415, Sandia National Laboratories, Albuquerque, NM, July 1981.

5. R. K. Cole, Jr., D. P. Kelly, and M. A. Ellis, CORCON MOD 2: A Computer Program for Analysis of Molten Core-Concrete Interactions, NUREG/CR-3920, SAND84-1246, Sandia National Laboratories, Albuquerque, NM, August 1984.

6. D. A. Powers, J. E. Brockmann, and A. W. Shiver, VANESA: A Mechanistic Model of Radionuclide Release and Aerosol Generation During Core Debris Interactions with Concrete, NUREG/CR-4308, SAND85-1370, Sandia National Laboratories, Albuquerque, NM, July 1986.

7. W. E. Kastenberg, Proceedings of a Workshop on Severe Accident Management for BWRs, University of California Los Angeles, Los Angeles, CA, May 21, 1991.

8. W. E. Kastenberg, Proceedings of a Workshop on Severe Accident Management for PWRs, University of California Los Angeles, Los Angeles, CA, May 15-17, 1990.

9. W. S. Yu and W. T. Pratt, "H_2 Production from the Steel-Water Reaction During a Postulated Core Meltdown Accident," Proceedings Second International Conference on the Impact of Hydrogen on Water Reactor Safety, page 317, SAND82-2456, Sandia National Laboratories, Albuquerque, NM, 1983.

10. R. E. Blose et al., SWISS 1 and 2: Sustained Interaction of Molten Stainless Steel and Concrete in the Presence of Water, NUREG/CR-4727, SAND85-1546, Sandia National Laboratories, Albuquerque, NM, July 1987.

11. P. C. Owczarski, A. K. Postman, and R. L. Schrek, Technical Bases and User's Manual for SPARC - A Suppression Pool Aerosol Removal Code, NUREG/CR-3317, PNL-4742, Pacific Northwest Laboratory, Richland, WA, 1983.

12. A. T. Wassel, A. F. Mills, D. C. Bugby and R. Oehlberg, Nuclear Engineering and Design 90 (1985) 87.

13. P. N. Clough, S. A. Ramsdale and P. N. Smith, "Aerosol Decontamination Factors in Pools Overlying Molten Core-Concrete-Code Modeling," Proceedings OECD (NEA) CSNI Specialists' Meeting on Core Debris/Concrete Interactions, EPRI-NP-5054-SR Electric Power Research Institute, Palo Alto, CA, February 1987.

14. D. A. Powers, An Analysis of Radionuclide Behavior in Water Pools During Accidents at the Annular Core Research Reactor, SAND91-1222, Sandia National Laboratories, Albuquerque, NM, August 1992.

15. N. A. Fuchs, The Mechanics of Aerosols, Pergamon Press, 1964.

16. T. Demitrack and F. J. Moody, "Planetary Ellipsoid Bubble Model for Fission Product Scrubbing" Transactions American Nuclear Society 45 (1983) 483.

17. P. R. Kry and R. List, Physics of Fluids 17 (1974) 1093.

18. S. Webb, Transactions of the American Nuclear Society 52 (1986) 525.

19. I. V. Vakhrushev and G. I. Efremov, Chem. Technol. Fuels Oils (USSR) 5/6 (1970) 376.

20. R. Clift, J. R. Grace, and M. E. Weber, Bubbles, Drops and Particles, Academic Press, 1978.

21. J. R. Grace, T. Wairegi and T. H. Nguyen, Trans. Inst. Chem. Eng. 54 (1976) 167.

22. W. Fritz, Physik 36 (1965) 379.

23. F. G. Blottner, Hydrodynamics and Heat Transfer Characteristics of Liquid Pools with Bubble Agitation, NUREG/CR-0944, SAND79-1132, Sandia National Laboratories, Albuquerque, NM, November 1979.

24. J. F. Davidson and B. O. G. Schuler, Trans. Inst. Chem. Eng. 38 (1960) 335.

25. V. G. Levich, Physicochemical Hydrodynamics, Prentice-Hall Publishing Co., 1962.

26. Y. S. Touloukian, S. C. Saxena, and P. Hestermans, Thermophysical Properties of Matter Volume II Viscosity IFI/Plenum.

27. Handbook of Chemistry and Physics, 55th Edition, R. C. Weast, editor, page F-41, CRC Press, Cleveland, OH, 1974.

28. Chemical Engineer's Handbook, R. H. Perry, editor, McGraw-Hill Book Co., 4th Edition, 1963 citing work by Ting and Luebbers, Am. Inst. Chem. Eng. J. 3 (1957) 111.

29. CRC Handbook of Chemistry and Physics, page D-257, 68th Edition, R. C. Weast, editor, CRC Press, Inc., Boca Raton, FL, 1987.

30. T. C. Powers and T. L. Brownyard, Proc. Am. Concrete Institute 43 (1947) 469.

31. D. A. Powers, D. A. Dahlgren, J. F. Muir, and W. B. Murfin, Exploratory Study of Molten Core Material/Concrete Interactions, SAND77-2042, Sandia National Laboratories, Albuquerque, NM, February 1978.

32. D. A. Powers and F. E. Arellano, Direct Observation of Melt Behavior During High Temperature Melt/Concrete Interactions, NUREG/CR-2283, SAND81-1754, Sandia National Laboratories, Albuquerque, NM, January 1982.

33. W. W. Tarbell et al., Sustained Concrete Attack by Low-Temperature, Fragmented Core Debris, NUREG/CR-3024, SAND82-2476, Sandia National Laboratories, Albuquerque, NM, July 1987.

34. E. R. Copus, et al., Core-Concrete Interactions With Overlying Water Pool, WETCOR-1. NUREG/CR-5907, SAND92-1563, Sandia National Laboratories, Albuquerque, NM, in press.

35. Fauske and Associates, Inc. MAAP - Modular Accident Analysis Program User's Manual, Atomic Industrial Form, Bethesda, MD, undated.

36. DOE/ARSAP, Technical Support for the Debris Coolability Requirements for Advanced Light Water Reactors in the Utility/EPRI Light Water Reactor Requirements Document, DOE/ID-10278, Fauske and Associates, Inc., June 1990.

37. M. Fischer et al., MACE Scoping Test Data Report, ACE-TR-D3, Argonne National Laboratory, Argonne, IL, March 1991.

38. J. E. Brockmann, "Ex-Vessel Releases: Aerosol Source Terms in Reactor Accidents," Progress in Nuclear Energy 19 (1987) 7.

39. D. A. Powers and R. C. Schmidt, "Analysis of Revaporization of Deposited Radionuclides," in Evaluation of Accident Risks Volume 2 Appendices, Part 5 Supporting Calculations, NUREG/CR-4551, Rev. 1, Sandia National Laboratories, Albuquerque, NM, draft available in the NRC Public Document Room.

40. D. A. Powers, "Uncertainty in Revolatization of Iodine from Water Pools," in Evaluation of Accident Risks Volume 2 Appendices, Part 5 Supporting Calculations, NUREG/CR-4551, Rev. 1, Sandia National Laboratories, Albuquerque, NM, draft available in the NRC Public Document Room.

41. D. A. Powers and J. E. Brockmann, "An Analysis of Aerosol Transport Through a Ruptured Steam Generator Tube," in Evaluation of Accident Risks Volume 2 Appendices, Part 6 Other Issues, NUREG/CR-4551, Rev. 1, Sandia National Laboratories, Albuquerque, NM, draft available in the NRC Public Document Room.

42. D. A. Powers, "A Probabilistic Method for the Evaluation of Severe Accident Source Term Uncertainties," Proceedings of the International Conference on Probabilistic Risk Assessment and Management, Beverly Hills, CA, February 4-7, 1991.

43. I. Cook and S. D. Unwin, Nuclear Science and Engineering 94 (1986) 107.

44. D. E. Knuth, Seminumerical Algorithms, Second Edition, Addison-Wesley Publ. Co., 1981.

45. R. Adams, "Behavior of U_3O_8, Fe_2O_3 and Concrete Aerosols in a Condensing Steam Environment," Proc. Eleventh Water Reactor Safety Research Meeting, Volume 3, page 129, NUREG/CR-0048, U.S. Nuclear Regulatory Commission, Washington, D.C., January 1984.

APPENDIX A

STATISTICS OF ORDER DISTRIBUTIONS

The statistical methods used to develop the probability distributions described in the text are derived in this appendix. The derivations used here follow directly from derivations presented by Hogg and Craig [1].

Consider a random variable X. Assume this random variable to have a continuous, positive probability density function f(x) over the interval from a to b such that a < b. The cumulative probability distribution function for X is F(X) and is given by:

$$F(X) = \int_{-\infty}^{X} f(x)dx = \int_{a}^{X} f(x)dx$$

such that

$$\int_{-\infty}^{+\infty} f(x)dx = 1 = \int_{a}^{b} f(x)dx$$

The probability density function, f(x) or equivalently the cumulative probability distribution function F(x), are unknown for the problems posed in the text. The objective of the Monte Carlo sampling is to obtain a sample of the random variable X from which some estimate of f(x) or F(X) can be made.

At the conclusion of the Monte Carlo sampling for a given problem, a set of n possible values of the random variable X is available:

$$\{X_1, X_2, X_3 \ldots X_{n-1}, X_n\}$$

These sampled values can be arranged in increasing order--say, for example, X_1, X_{n-1}, $X_2 \ldots X_n$, X_3. The values can then be relabelled Y_i such that $Y_i < Y_{i+1}$:

$$\{Y_1, Y_2, Y_3, \ldots Y_{n-1}, Y_n\}$$

This ordered set of the sampled values of the random variable is the "order statistic" for the sample of size n. The joint probability density function for this order statistic is labelled $g(Y_1, Y_2, Y_3 \ldots Y_{n-1}, Y_n)$ and is given by:

$$g(Y_1,Y_2,Y_3,\ldots Y_{n-1},Y_n) = \begin{cases} n!f(y_1)f(Y_2)f(Y_3)\ldots f(Y_{n-1})f(Y_n) \\ \quad for \quad Y_i < Y_{i+1} \quad and\, i=1\, to\, n-1 \\ \quad 0 \quad otherwise \end{cases}$$

This follows directly because there are n! ways that it might have been necessary to arrange the sampled values of X in order to formulate the statistic.

A new statistic Z can be formulated from:

$$Z_i = F(Y_i)$$

where $F(Y_i)$ is the cumulative probability distribution function for the random variable X. The Jacobian for this transformation of Y into Z is:

$$J = \begin{vmatrix} \frac{dY_1}{dZ_1} & 0 & \ldots & 0 \\ 0 & \frac{dY_2}{dZ_2} & \ldots & 0 \\ 0 & 0 & \frac{dY_3}{dZ_3} & \ldots 0 \\ 0 & 0 & 0 \ldots & \frac{dY_n}{dZ_n} \end{vmatrix} = \frac{dY_1}{dZ_1}\frac{dY_2}{dZ_2}\frac{dY_3}{dZ_3}\cdots\frac{dY_n}{dZ_n}$$

$$= \frac{1}{\frac{dZ_1}{dY_1}\frac{dZ_2}{dY_2}\frac{dZ_3}{dY_3}\cdots\frac{dZ_n}{dY_N}}$$

Since $Z = F(Y)$ and $dZ_i/dY_i = f(Y_i)$:

$$J = \frac{1}{f(Y_1)f(Y_2)f(Y_3)\cdots f(Y_n)}$$

Then, the joint probability density function for the Z statistic is:

$$h(Z_1, Z_2, Z_3 \ldots Z_n) = J\varphi(Y_1, Y_2, Y_3 \ldots Y_n)$$

$$= n!$$

The probability density function of a particular Z_K is

$$h(Z_K) =$$

$$= \int_0^{Z_2} \cdots \int_0^{Z_K} \left[\int_{Z_K}^{1} \cdots \left[\int_{Z_{n-2}}^{1} \left[\int_{Z_{n-1}}^{1} h(Z_1, Z_2, Z_3, \ldots Z_n) dZ_n \right] dZ_{n-1} \right] \cdots dZ_{K+1} \right] dZ_{K-1} \cdots dZ_1$$

$$= \int_0^{Z_2} \cdots \int_0^{Z_K} \left[\int_{Z_K}^{1} \cdots \left[\int_{Z_{n-2}}^{1} n!(1-Z_{n-1}) dZ_{n-1} \right] \cdots dZ_{K+1} \right] dZ_{K-1} \cdots dZ_1$$

$$= \int_0^{Z^2} \cdots \int_0^{Z_K} \frac{n!}{(n-K)!} (1-Z_K)^{n-K} dZ_{K-1} \cdots dZ_1$$

$$= \frac{n!}{(K-1)!(n-K)!} Z_K^K (1-Z_K)^{n-K}$$

Now for some probability p such that $0 < p < 1$, the solution for

$$F(x) = p$$

is $\xi_p = x$. ξ_p is the p^{th} quantile of the cumulative distribution function. The order statistic for the sample of size n of the random variable X can be characterized by the probability that $Y_K < \xi_p$ or

$$Pr(Y_K < \xi_p) = Pr(Z_K < p)$$

From the probability density function of Z_K:

$$Pr(Z_K<p) = \int_0^p h(Z_K)dZ_K = \int_0^p \frac{n!}{(K-1)!(n-K)!} Z_K^K(1-Z_K)^{n-K}dZ_K$$

$$= \frac{n!}{K!(n-K)!}p^K(1-p)^{n-K} + \frac{n!}{(K+1)!(n-K-1)!}p^{K+1}(1-p)^{n-K-1} + \ldots\ldots + p^n$$

$$= \sum_{i=K}^{n} \frac{n!}{i!(n-i)!} p^i(1-p)^{n-i} = Pr(Y_K<\xi_p)$$

This result is sufficient to provide a basis to bracket critical values of the unknown distribution function F(X) from the order statistic Y [2]. Note that

$$Pr(Y_i < \xi_p) = Pr(Y_j < \xi_p) + Pr(Y_i < \xi_p < Y_j)$$

and that

$$Pr(Y_i < \xi_p < Y_j) = Pr(Y_i < \xi_p) - Pr(Y_j < \xi_p)$$

The joint probability density function of $Z_i = F(Y_i)$ *and* $Z_j = F(Y_j)$ *for* $i < j$ is:

$$h_{ij}(Z_i, Z_j) =$$

$$= \int_0^{Z_i}\ldots\int_{0}^{Z_iZ_j}\ldots\int_{Z_{j-2}}^{Z_j}\int_{Z_j}^{1}\ldots\int_{Z_{n-1}}^{1} n!dZ_n\ldots dZ_{j+1}dZ_{j-1}\ldots dZ_{i+1}dZ_1\ldots dZ_{i-1}$$

$$= \frac{n!}{(i-1)!(j-i-1)!(n-j)!} Z_i^{i-1}(Z_j-Z_i)^{j-i-1}(1-Z_j)^{n-j}$$

$$for\ 0 < Z_i < Z_j < 1$$

The most interesting of the joint probabilities is that of Z_1 and Z_n. Then,

$$h_{1n}(Z_1, Z_n) = n(n-1)\ (Z_n - Z_1)^{n-2}\ \ for\ 0 < Z_1 < Z_n < 1$$

Then, the probability that the sample of X exceeds some fraction p of the range of values of X is given by:

$$Pr[F(Y_n) - F(Y_1) \geq p] = Pr[Z_n - Z_1 \geq p]$$

$$= \int_0^{1-p} \int_{p+Z_1}^{1} n(n-1)(Z_n - Z_1)^{n-2} dZ_n dZ_1$$

$$= 1 - np^{n-1} + (n-1)p^n = C$$

C is then the confidence level that a sample of n values spans a fraction of the distribution p.

Some values of the confidence level C for various values of n and p are shown in Table A-1.

An example helps to illuminate the features of the non-parametric analysis of the Monte Carlo sampling to characterize an unknown distribution. Suppose five expert opinions are solicited on the maximum ground acceleration of 5 Hz during an earthquake. These opinions are:

Expert #	Ground Acceleration = X(i)
1	0.24
2	0.05
3	0.33
4	0.25
5	0.68

The order statistic for this set of samples is:

j	Expert #	X(i)	Y(j)
1	2	0.05	0.05
2	1	0.24	0.24
3	4	0.25	0.25
4	3	0.33	0.33
5	5	0.68	0.68

Human opinions probably are not random samples of the true distribution of current uncertainty. Here, however, it is assumed that these experts are special and do provide random samples of the distribution. The first question to pose is "What is the probability that the five expert opinions span 90% of the range of the distribution of opinions?" This question is answered with:

$$\text{Probability} = 1\text{-}np^{n-1} + (n\text{-}1)p^n$$

with n = 5 and p = 0.9. Thus,

Table A-1 Sample Size Necessary to Span a Fraction of the Uncertainty Distribution, p, at a Confidence Level C				
Confidence Level	Sample Size to Span p =			
	0.9	0.95	0.99	0.999
90%	37	76	388	3888
95%	46	93	473	4742
99%	64	130	661	6635
99.9%	88	180	919	9228

$$\text{Probability} = 1\text{-}5(0.9)^4 + 4(0.9)^5$$

$$\approx 0.082$$

It is likely, then, that there are opinions much more extreme than those reflected in the sample of five opinions. Risk-adverse analysts would want to get a larger sample than just five random opinions. Note that the probability computed above is independent of the values provided by the experts. This independence is, at first examination, surprising. The independence comes about because it has been assumed that the opinions are random samples of the underlying distribution. This is an acceptable assumption for the mechanical treatment of uncertainties described in the main text of this report. Real expert panels, on the other hand, are capable of providing opinions that span 90% of the range of opinions if charged to do so.

The next question that might be asked is based on the values provided by the experts. Expert Number 5 has provided a value that appears to be substantially higher than values provided by the other experts. Pressure to delete this extreme opinion might develop. It is useful to have an objective assessment of the probability that the opinion comes from the extreme limits of the underlying distribution. Some indication of this can be obtained by asking what is the probability that the 90% quantile of the underlying distribution is between the third and fourth values in the order sample of opinions. This probability is found from:

$$Pr(Y(3) < \xi_{0.9} < Y(4)) =$$
$$= Pr(Y(3) < \xi_{0.9}) - Pr(Y(4) < \xi_{0.9})$$

where

$$Pr(Y(k) < \xi_p) = \sum_{i=k}^{n} \frac{n!}{i!(n-i)!} p^i(1-p)^{n-i}$$

$$n = 5$$

$$p = 0.9$$

Then,

$$Pr(Y(3) < \xi_{0.9}) = \sum_{i=3}^{5} \frac{5!}{i!(5-i)!} 0.9^i(0.1)^{5-i}$$

$$= \frac{5!}{3!2!}(0.9)^3(0.1)^2 + \frac{5!}{4!1!}(0.9^4(0.1) + (0.9)^5$$

$$\approx 0.9914$$

And,

$$Pr(Y(4) < \xi_{0.9}) = \sum_{i=4}^{5} \frac{5!}{i!(5-i)!} (0.9)^i(0.1)^{5-i}$$

$$= 5(0.9)^4(0.1) + (0.9)^5 \approx 0.9185$$

Thus,

$$Pr(Y(3) < \xi_{0.9} < Y(4)) \approx 0.073$$

The probability that the 90% quantile lies between the third and the fourth value of the ordered sample is not very high. With such a small sample there is not a strong statistical basis to exclude a value that might appear extreme in comparison to other values.

An example is used to illustrate how the characterization of the distribution improves with the sample size. For this example, samples of 100, 500, 1000, and 3000 values were taken from a lognormal distribution with a mean of 1.48 and a geometric standard deviation of 2.546. The samples were ordered and subjected to the non-parametric statistical analyses described above. Cumulative probability distributions derived from the samples at the 95% confidence level are shown in Figures A-1 to A-4. These are conventional cumulative probability plots. The known distribution is also shown in the figures for comparison purposes. These results show that median values are derived fairly accurately from samples of just 100 values if the distribution

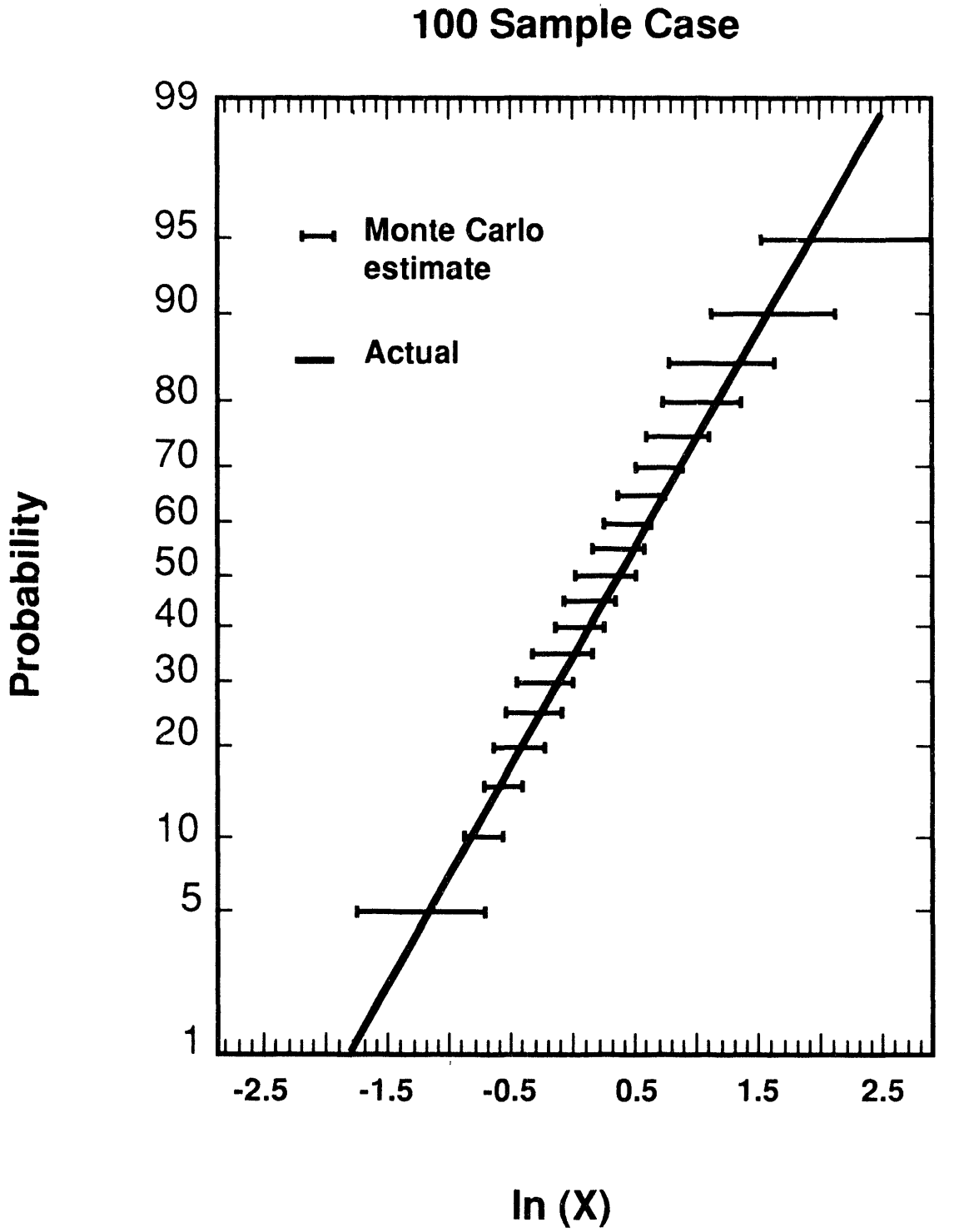

Figure A-1. 95% Confidence Intervals for Quantiles of the Example Distribution Derived from a 100 Value Sample. The actual underlying distribution is shown by the continuous line.

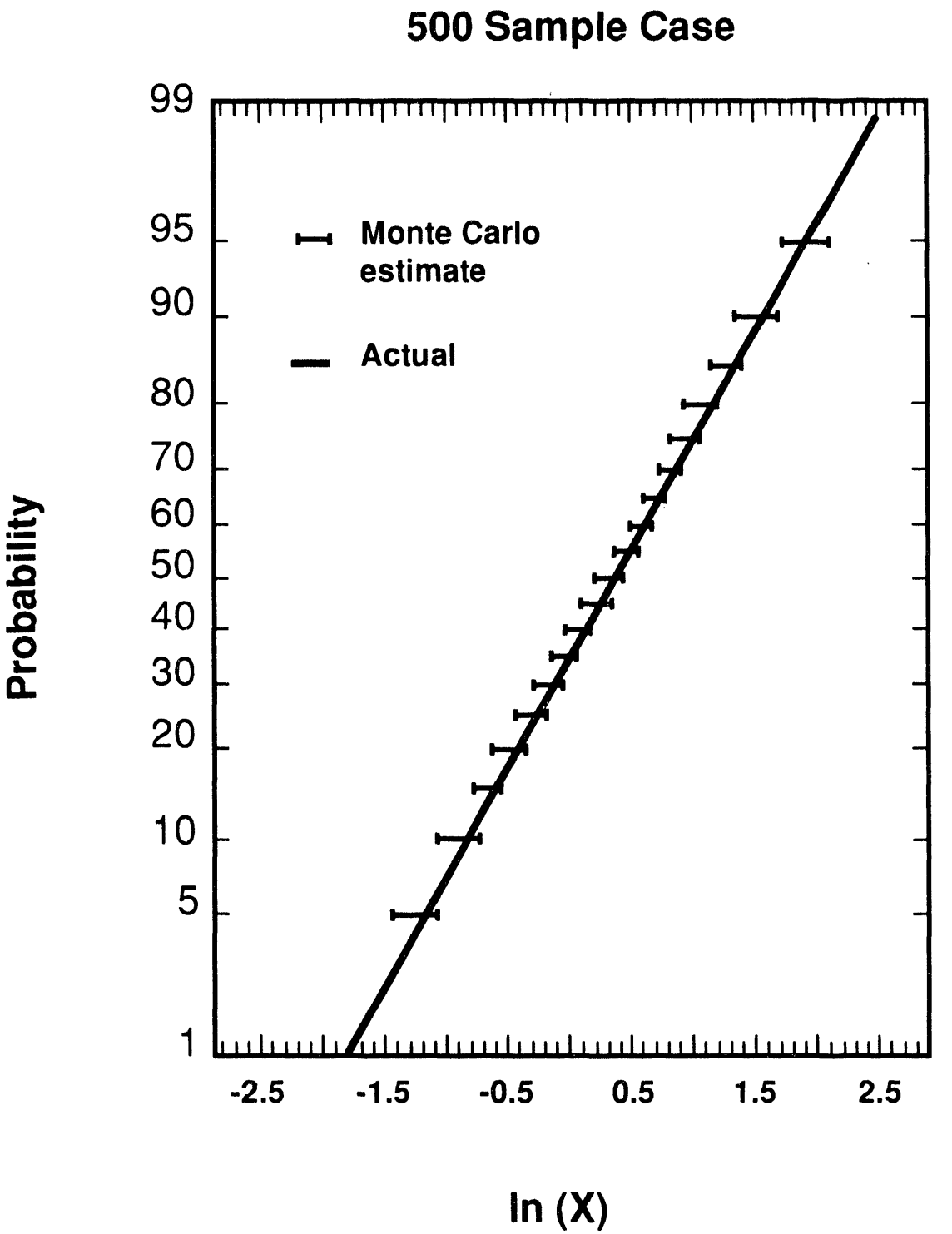

Figure A-2. 95% Confidence Intervals for Quantiles of the Example Distribution Derived from a 500 Value Sample. The actual underlying distribution is shown by the continuous curve.

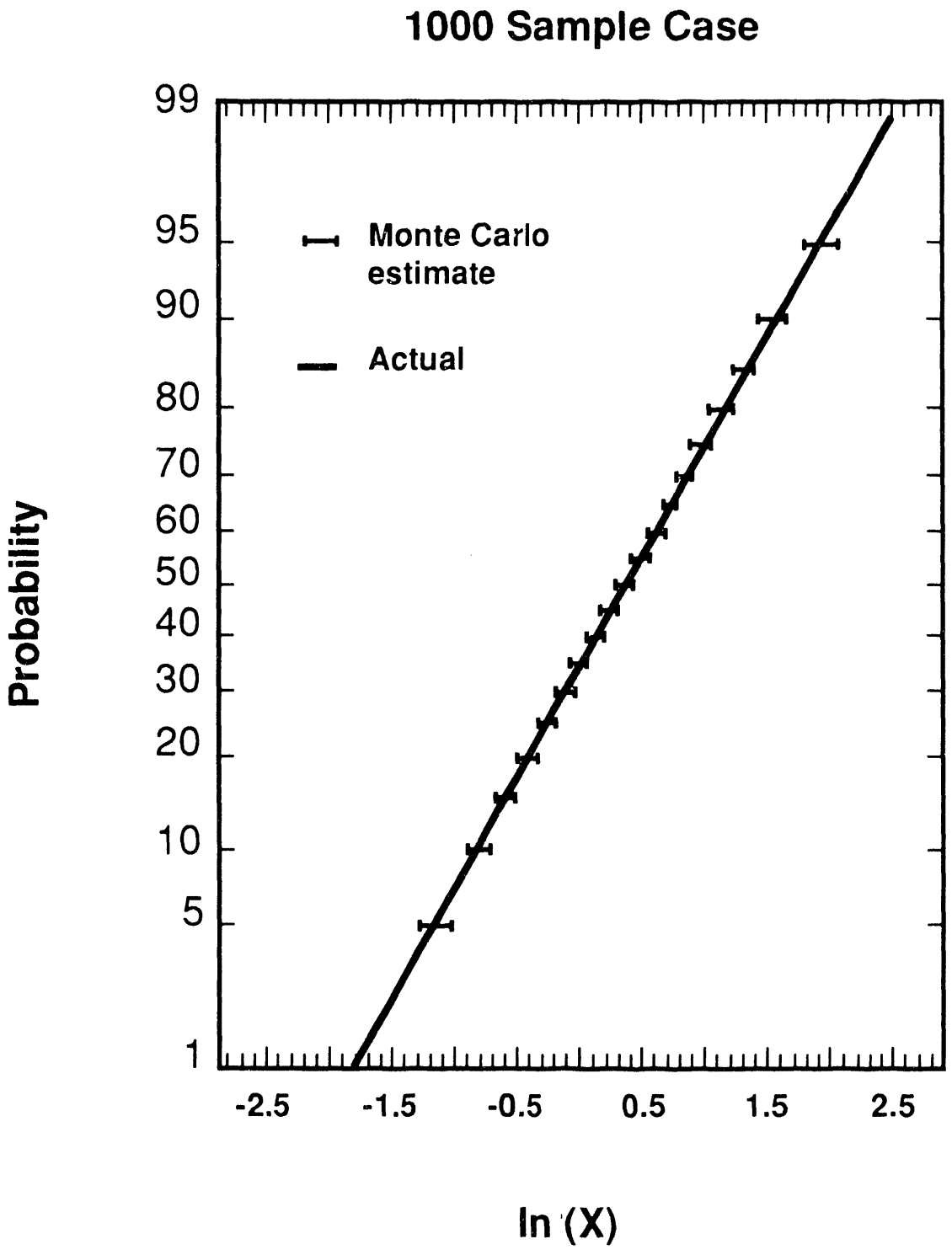

Figure A-3. 95% Confidence Intervals for Quantiles of the Example Distribution Derived from a 1000 Value Sample. The actual underlying distribution is shown by the continuous curve.

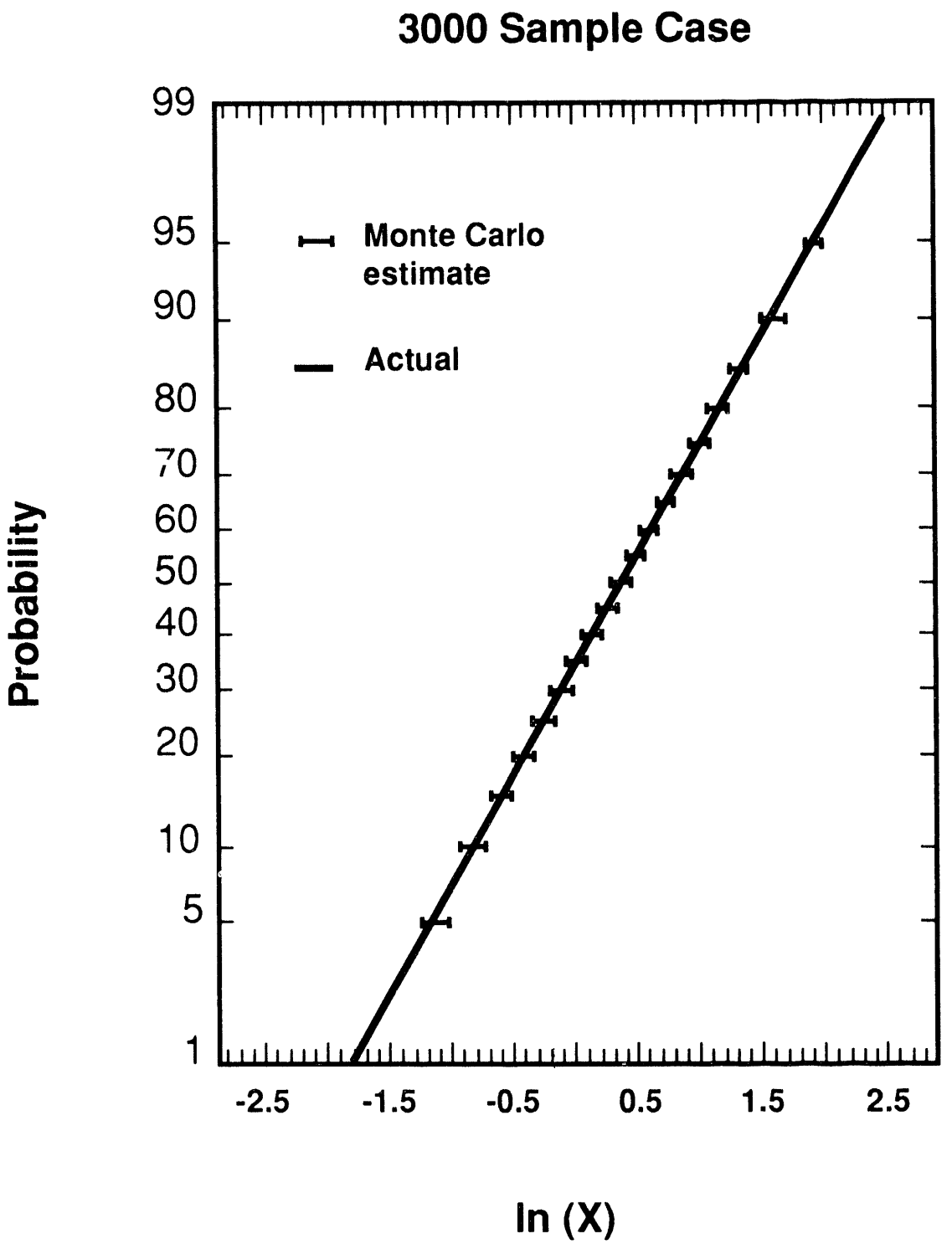

Figure A-4. 95% Confidence Intervals for Quantiles of the Example Distribution Derived from a 3000 Value Sample. The actual underlying distribution is shown by the continuous curve.

is not too complicated. Samples of about 1000 values are needed to get accurate values at the 5% and 95% quantiles.

The principal advantage of the Monte Carlo method and the non-parametric order statistic analysis adopted here is that the number of samples that must be taken to characterize a distribution is independent of the number of uncertain quantities that arise in calculations of the type described in the text. The values listed in Table A-1 can be compared to the number of calculations of values that would be required in a deterministic analysis. For instance, a simple two-level factorial analysis of a problem with 16 uncertain variables would require

$$2^{16} = 65536$$

calculations. A far more complete characterization of the distribution is obtained at fairly high confidence levels with only a few hundred calculations following the Monte Carlo method.

REFERENCES:

1. R. V. Hogg and A. T. Craig, Introduction to Mathematical Statistics, MacMillan Co.

2. The factorials found in these equations can be accurately calculated for values greater than 10 from:

$$\ln x! = (n+\frac{1}{2})\ln(n+1) - n - 1 + \frac{1}{2}\ln(2\pi) + \frac{1}{12(n+1)} - \frac{1}{360(n+1)^3} + \frac{1}{1260(n+1)^5} - \frac{1}{1680(n+1)^7}$$

See

M. Abramowitz and I. A. Stegan, Handbook of Mathematical Functions, Dover Publications, 1970.

APPENDIX B

CUMULATIVE DISTRIBUTIONS DERIVED FOR CASES WITH SUBCOOLED WATER POOLS

The detailed cumulative probability distributions for the natural logarithm of the decontamination factor for cases with subcooled water pools are listed in Tables B-1 to B-25. The tabulated results show quantiles of the distribution caused by phenomenological uncertainty at 5% intervals from 5% to 95%. These quantiles are shown for confidence levels of 50, 90 and 95% with respect to the stochastic uncertainty associated with finite sample size. Means and standard deviations for the samples are also shown in the tables. The entries in the tables can be used in regression analyses to construct simplified expressions for different quantiles and confidence levels than those developed in the main text of this report.

Table B-1
Results for a 30 cm Pool with 2 Degrees Subcooling

Pool Depth (cm)	Sub-Cooling (K)	Quantile (%)	Range for ln(DF) at a Confidence Level (%) of		
			50	90	95
30	2	5	1.0257-1.0852	0.9941-1.1612	0.9738-1.1811
		10	1.2581-1.3275	1.2111-1.3854	1.1994-1.3880
		15	1.4488-1.5122	1.3868-1.5770	1.3759-1.5992
		20	1.6158-1.6934	1.5693-1.7319	1.5505-1.7655
		25	1.7675-1.8252	1.7056-1.8673	1.6979-1.8712
Mean = = 2.5024		30	1.8689-1.9311	1.8302-2.0025	1.8185-2.0153
		35	2.0101-2.0562	1.9448-2.0994	1.9139-2.1102
		40	2.0992-2.1741	2.0555-2.2308	2.0426-2.2446
		45	2.2293-2.3129	2.1709-2.3715	2.1478-2.3918
		50	2.3629-2.4250	2.3093-2.4797	2.2841-2.5172
Std. Dev. = = 0.9867		55	2.4779-2.5960	2.4233-2.6368	2.4109-2.6471
		60	2.6315-2.6881	2.5940-2.7510	2.5615-2.7663
		65	2.7510-2.8230	2.6881-2.8827	2.6765-2.9000
		70	2.8852-2.9622	2.8255-3.0398	2.8125-3.0450
		75	3.0407-3.1082	2.9686-3.1780	2.9570-3.2204
Sample Size= = 500		80	3.2251-3.3533	3.1482-3.4288	3.1115-3.4364
		85	3.4903-3.5975	3.4207-3.6856	3.4014-3.6873
		90	3.7549-3.8952	3.6861-3.9945	3.6817-4.0237
		95	4.1755-4.4744	4.0739-4.5574	4.0475-4.6018

Table B-2
Results for a 30 cm Deep Pool with 5 Degrees Subcooling

Pool Depth (cm)	Sub-Cooling (K)	Quantile (%)	Range for ln(DF) at a Confidence Level (%) of		
			50	90	95
30	2	5	1.5373-1.6335	1.5210-1.6783	1.5129-1.7439
		10	1.8902-1.9810	1.7941-2.0150	1.7893-2.0250
		15	2.0492-2.1081	2.0168-2.1921	2.0050-2.2105
		20	2.2275-2.2749	2.1630-2.3547	2.1221-2.3657
		25	2.3753-2.4100	2.3141-2.4644	2.2766-2.4715
Mean = = 3.2797		30	2.4659-2.6034	2.4257-2.6611	2.4097-2.6723
		35	2.6636-2.7146	2.6071-2.7760	2.5490-2.7970
		40	2.7760-2.8648	2.7138-2.8991	2.6977-2.9266
		45	2.8928-3.0120	2.8637-3.0733	2.8463-3.0904
		50	3.0708-3.1175	3.0027-3.1798	2.9705-3.2119
Std. Dev. = = 1.2323		55	3.1757-3.2879	3.1147-3.3649	3.1071-3.3809
		60	3.3628-3.5007	3.2853-3.5632	3.2622-3.5739
		65	3.5622-3.6447	3.5006-3.7297	3.4503-3.7477
		70	3.7322-3.8668	3.6515-3.9180	3.6215-3.9511
		75	3.9321-4.0614	3.8796-4.0905	3.8620-4.0963
Sample Size = = 500		80	4.0981-4.1963	4.0774-4.2568	4.0630-4.2976
		85	4.3174-4.4735	4.2341-4.6745	4.2134-4.7341
		90	4.7935-4.9239	4.7041-5.1801	4.6312-5.1901
		95	5.3264-5.5741	5.2359-5.8275	5.2254-6.0112

Table B-3
Results for a 30 cm Deep Pool with 10 Degrees Subcooling

Pool Depth (cm)	Sub-Cooling (K)	Quantile (%)	Range for ln(DF) at a Confidence Level (%) of		
			50	90	95
30	10	5	2.0850-2.1362	2.0321-2.1696	1.9847-2.1887
		10	2.2844-2.3495	2.2236-2.4091	2.2033-2.4176
		15	2.4945-2.5830	2.4148-2.6741	2.3983-2.7137
		20	2.7177-2.8447	2.6495-2.8957	2.6253-2.9217
		25	2.9361-3.0377	2.8550-3.1085	2.8450-3.1215
Mean =		30	3.1168-3.1989	3.0591-3.2653	3.0329-3.2954
= 3.9776		35	3.2725-3.3724	3.2042-3.4207	3.1825-3.4521
		40	3.4195-3.5316	3.3711-3.6125	3.3416-3.6351
		45	3.6106-3.7186	3.5313-3.7957	3.5109-3.8224
		50	3.7884-3.8978	3.7083-3.9601	3.6953-3.9794
Std. Dev. =		55	3.9584-4.0543	3.8955-4.1354	3.8724-4.1496
= 1.3552		60	4.1300-4.2265	4.0504-4.2868	4.0364-4.3196
		65	4.2867-4.4153	4.2265-4.5534	4.2030-4.5801
		70	4.5607-4.6504	4.4380-4.7227	4.3733-4.7329
		75	4.7287-4.8177	4.6656-4.9203	4.6402-4.9981
Sample Size =		80	5.0109-5.1016	4.8387-5.2624	4.8182-5.3399
= 500		85	5.3728-5.5039	5.2001-5.5840	5.1462-5.5996
		90	5.6705-5.7915	5.5855-5.9541	5.5803-5.9787
		95	6.2587-6.5598	6.0905-6.7729	6.0132-6.9426

Table B-4
Results for a 30 cm Deep Pool with 20 Degrees Subcooling

Pool Depth (cm)	Sub-Cooling (K)	Quantile (%)	Range for ln(DF) at a Confidence Level (%) of		
			50	90	95
30	20	5	2.6347-2.7398	2.5383-2.8428	2.5068-2.8864
		10	3.0192-3.1206	2.9425-3.1907	2.9079-3.2034
		15	3.2568-3.3255	3.1940-3.4021	3.1721-3.4175
		20	3.4377-3.5874	3.3814-3.6365	3.3616-3.6514
		25	3.6521-3.7318	3.6013-3.7989	3.5886-3.8236
Mean = = 4.8443		30	3.8150-3.9267	3.7420-4.0208	3.7262-4.0315
		35	4.0269-4.0907	3.9364-4.2127	3.9109-4.2594
		40	4.2111-4.3187	4.0902-4.3639	4.0748-4.4023
		45	4.3575-4.5125	4.3180-4.5771	4.3083-4.5968
		50	4.5743-4.6779	4.5122-4.7774	4.4785-4.7851
Std. Dev. = = 1.6431		55	4.7740-4.8883	4.6670-4.9425	4.6285-4.9676
		60	4.9380-5.0416	4.8878-5.1318	4.8458-5.1495
		65	5.1313-5.2527	5.0408-5.3464	5.0133-5.3869
		70	5.3521-5.5278	5.2551-5.6537	5.2234-5.6630
		75	5.6575-5.8328	5.5420-5.9024	5.5237-5.9127
Sample Size = = 500		80	5.9134-6.0184	5.8602-6.1186	5.8349-6.1902
		85	6.2049-6.4617	6.0880-6.5898	6.0502-6.6331
		90	6.7291-6.9697	6.6050-7.1592	6.5446-7.1919
		95	7.5790-7.8508	7.3273-8.0699	7.2758-8.2959

Table B-5
Results for a 30 cm Deep Pool with 30 Degrees Subcooling

Pool Depth (cm)	Sub-Cooling (K)	Quantile (%)	Range for ln(DF) at a Confidence Level (%) of		
			50	90	95
30	30	5	2.9779-3.0352	2.9381-3.1484	2.9058-3.2035
		10	3.3771-3.5028	3.3269-3.5749	3.2715-3.6555
		15	3.7332-3.8961	3.5874-3.9572	3.5662-3.9717
		20	3.9941-4.0576	3.9275-4.1629	3.9069-4.1906
		25	4.1940-4.3134	4.0981-4.3932	4.0600-4.4062
Mean = = 5.4376		30	4.4022-4.5314	4.3306-4.6116	4.2922-4.6335
		35	4.6208-4.7124	4.5345-4.7563	4.5223-4.7851
		40	4.7560-4.8752	4.7106-4.9577	4.6914-4.9632
		45	4.9575-5.0272	4.8566-5.0995	4.8321-5.1384
		50	5.0977-5.2478	5.0240-5.3400	5.0062-5.3761
Std. Dev. = = 1.7468		55	5.3385-5.4562	5.2467-5.5309	5.2222-5.5743
		60	5.5298-5.6807	5.4524-5.7874	5.4064-5.8436
		65	5.7863-5.9235	5.6802-6.0494	5.6519-6.0771
		70	6.0515-6.1883	5.9298-6.2800	5.8964-6.3282
		75	6.3195-6.4185	6.1971-6.5623	6.1774-6.6045
Sample Size = = 500		80	6.6173-6.8605	6.4811-6.9937	6.4407-7.0165
		85	7.0453-7.1639	6.9697-7.2634	6.9370-7.3101
		90	7.4124-7.7175	7.2795-7.9798	7.2528-8.0105
		95	8.3130-8.6026	8.1195-8.7214	8.0512-8.7538

Table B-6
Results for a 30 cm Deep Pool with 50 Degrees Subcooling

Pool Depth (cm)	Sub-Cooling (K)	Quantile (%)	Range for ln(DF) at a Confidence Level (%) of		
			50	90	95
30	50	5	3.3845-3.4949	3.2113-3.7281	3.2023-3.7483
		10	3.9292-4.0371	3.8181-4.0992	3.8012-4.1233
		15	4.1895-4.3306	4.1074-4.4489	4.0898-4.4806
		20	4.5394-4.6987	4.4248-4.7990	4.3415-4.8269
		25	4.8318-4.9420	4.7443-5.0172	4.6994-5.0422
Mean =		30	5.0392-5.0979	4.9508-5.1337	4.9272-5.1559
= 6.1298		35	5.1356-5.2794	5.0983-5.3743	5.0942-5.3849
		40	5.3743-5.4952	5.2770-5.6030	5.2416-5.6413
		45	5.6009-5.7182	5.4912-5.7921	5.4563-5.8056
		50	5.7907-5.8814	5.7123-5.9605	5.6871-5.9889
Std. Dev. =		55	5.9489-6.0682	5.8780-6.1986	5.8580-6.2536
= 1.9380		60	6.1882-6.3343	6.0673-6.4419	6.0200-6.4851
		65	6.4392-6.6593	6.3341-6.7734	6.2758 6.8136
		70	6.7872-6.9641	6.6663-7.1096	6.6220-7.1250
		75	7.1219-7.1979	6.9931-7.3482	6.9330-7.4932
Sample Size =		80	7.4948-7.6300	7.2440-7.7231	7.2004-7.7953
= 500		85	7.8153-8.0135	7.6916-8.3703	7.6536-8.4072
		90	8.4943-8.6151	8.3760-8.7992	8.1916-8.9859
		95	9.3548-9.8350	9.1332-10.5710	9.0560-10.6971

Table B-7
Results for a 30 cm Deep Pool with 70 Degrees Subcooling

Pool Depth (cm)	Sub-Cooling (K)	Quantile (%)	Range for ln(DF) at a Confidence Level (%) of		
			50	90	95
30	70	5	3.3027-3.3830	3.2045-3.4768	3.1998-3.5083
		10	3.7114-3.8132	3.5725-3.9342	3.5353-3.9765
		15	4.0950-4.2563	3.9511-4.3468	3.9168-4.3890
		20	4.4233-4.5492	4.3352-4.6987	4.2830-4.7625
		25	4.7825-4.9973	4.6032-5.0504	4.5548-5.0754
Mean =		30	5.0548-5.1541	5.0050-5.2112	4.9818-5.2349
= 6.2685		35	5.2204-5.3896	5.1570-5.4512	5.1443-5.4702
		40	5.4511-5.5326	5.3889-5.6179	5.3721-5.6452
		45	5.6156-5.7374	5.5279-5.7946	5.4959-5.8645
		50	5.7892-5.9429	5.7356-6.0294	5.7062-6.0547
Std. Dev. =		55	6.0133-6.1635	5.9331-6.2253	5.9184-6.2597
= 2.3913		60	6.2221-6.3566	6.1630-6.5356	6.1396-6.5709
		65	6.5319-6.7318	6.3558-6.7987	6.3349-6.8278
		70	6.8022-6.9888	6.7390-7.1184	6.6929-7.1428
		75	7.1308-7.3062	7.0013-7.5420	6.9848-7.6333
Sample Size =		80	7.6359-7.9165	7.4235-8.0845	7.3269-8... 4
= 500		85	8.1484-8.3169	8.0539-8.5225	7.9710-8.5505
		90	8.7262-9.0258	8.5337-9.3989	8.5010-9.5258
		95	9.8988-10.2119	9.7265-10.6287	9.6539-10.7503

Table B-8
Results for a 50 cm Deep Pool with 2 Degrees Subcooling

Pool Depth (cm)	Sub-Cooling (K)	Quantile (%)	Range for ln(DF) at a Confidence Level (%) of		
			50	90	95
50	2	5	1.3659-1.3889	1.3350-1.4337	1.3156-1.4389
		10	1.5577-1.6100	1.4652-1.6618	1.4463-1.6838
		15	1.7519-1.8133	1.6671-1.8628	1.6551-1.8831
		20	1.8920-1.9600	1.8279-2.0160	1.8215-2.0690
		25	2.0819-2.1342	1.9909-2.1936	1.9610-2.2067
Mean =		30	2.2055-2.2676	2.1453-2.3246	2.1325-2.3464
= 2.9413		35	2.3333-2.3919	2.2695-2.4247	2.2553-2.4386
		40	2.4247-2.5097	2.3915-2.5814	2.3843-2.5955
		45	2.5801-2.6354	2.4905-2.7073	2.4784-2.7279
		50	2.7048-2.7805	2.6288-2.8377	2.6215-2.8508
Std. Dev. =		55	2.8341-2.8975	2.7781-2.9912	2.7565-3.0369
= 1.2085		60	2.9812-3.1059	2.8968-3.1549	2.8766-3.1750
		65	3.1521-3.2584	3.1056-3.3155	3.0919-3.3512
		70	3.3169-3.4360	3.2648-3.5164	3.2407-3.5517
		75	3.5341-3.6894	3.4660-3.7573	3.4216-3.7854
Sample Size =		80	3.7871-3.8553	3.7066-4.0302	3.6921-4.0435
= 500		85	4.0527-4.1490	3.9509-4.2475	3.8835-4.2826
		90	4.3327-4.4848	4.2535-4.5795	4.2347-4.6509
		95	4.9590-5.2124	4.8064-5.5113	4.7482-5.7450

Table B-9
Results for a 50 cm Deep Pool with 5 Degrees Subcooling

Pool Depth (cm)	Sub-Cooling (K)	Quantile (%)	Range for ln(DF) at a Confidence Level (%) of		
			50	90	95
50	5	5	1.8375-1.9170	1.7369-1.9426	1.7332-1.9566
		10	2.0554-2.1692	1.9907-2.2740	1.9766-2.2885
		15	2.3632-2.4497	2.2853-2.5103	2.2175-2.5417
		20	2.5760-2.6734	2.4896-2.7193	2.4705-2.7396
		25	2.7401-2.8545	2.6840-2.9037	2.6736-2.9320
Mean = = 3.7644		30	2.9206-2.9856	2.8619-3.0453	2.8301-3.0698
		35	3.0493-3.1560	2.9962-3.1970	2.9766-3.2210
		40	3.1967-3.2975	3.1552-3.3895	3.1214-3.4340
		45	3.3700-3.4962	3.2908-3.5328	3.2808-3.5466
		50	3.5281-3.6559	3.4957-3.7443	3.4758-3.7656
Std. Dev. = = 1.3447		55	3.7408-3.8356	3.6427-3.8898	3.6031-3.9090
		60	3.8883-3.9825	3.8271-4.0534	3.8070-4.0701
		65	4.0530-4.2045	3.9825-4.3215	3.9453-4.3732
		70	4.3366-4.4367	4.2088-4.5298	4.2000-4.5911
		75	4.5643-4.6775	4.4401-4.7370	4.4321-4.7553
Sample Size = = 500		80	4.7570-4.8597	4.6973-4.9217	4.6776-4.9328
		85	4.9969-5.2619	4.9088-5.3842	4.8810-5.4393
		90	5.5344-5.6614	5.4022-5.8733	5.3691-5.9016
		95	6.1494-6.3807	6.0455-6.5367	5.9789-6.5692

Table B-10
Results for a 50 cm Deep Pool with 10 Degrees Subcooling

Pool Depth (cm)	Sub-Cooling (K)	Quantile (%)	Range for ln(DF) at a Confidence Level (%) of		
			50	90	95
50	10	5	2.3539-2.4919	2.2108-2.5785	2.1557-2.5910
		10	2.7134-2.8351	2.6093-2.9217	2.5992-2.9428
		15	2.999-3.1200	2.9302-3.2129	2.9011-3.2471
		20	3.2612-3.3757	3.1588-3.4521	3.1350-3.4776
		25	3.4805-3.5738	3.4169-3.6180	3.3833-3.6368
Mean =		30	3.6246-3.7397	3.5852-3.8249	3.5698-3.8722
= 4.6346		35	3.8293-3.9660	3.7506-4.0281	3.7301-4.0439
		40	4.0277-4.1252	3.9658-4.1966	3.9530-4.2474
		45	4.1933-4.2944	4.1225-4.3839	4.1142-4.4087
		50	4.3825-4.4949	4.2929-4.5726	4.2769-4.5875
Std. Dev. =		55	4.5596-4.6625	4.4942-4.7690	4.4793-4.7944
= 1.6077		60	4.7619-4.8707	4.6603-4.9900	4.6321-5.0060
		65	4.9884-5.1080	4.8707-5.1621	4.8615-5.1812
		70	5.1674-5.2976	5.1193-5.4006	5.0810-5.4260
		75	5.4039-5.6399	5.3402-5.7857	5.2907-5.8469
Sample Size =		80	5.8566-5.9593	5.7161-5.9987	5.6463-6.0477
= 500		85	6.0748-6.2124	5.9880-6.4273	5.9769-6.4549
		90	6.5519-6.6764	6.4373-6.9502	6.3408-7.0046
		95	7.2270-7.6409	7.1663-7.9425	7.1024-7.9884

Table B-11
Results for a 50 cm Deep Pool with 20 Degrees Subcooling

Pool Depth (cm)	Sub-Cooling (K)	Quantile (%)	Range for ln(DF) at a Confidence Level (%) of		
			50	90	95
50	20	5	2.6821-2.8589	2.6265-2.9573	2.5903-2.9762
		10	3.1933-3.3115	3.0929-3.4076	3.0300-3.4445
		15	3.5537-3.7511	3.4235-3.7984	3.3922-3.8178
		20	3.8411-3.9427	3.7882-4.0153	3.7680-4.0374
		25	4.0414-4.1843	3.9727-4.2715	3.9466-4.2940
Mean = = 5.5245		30	4.2822-4.4249	4.2030-4.5547	4.1651-4.5951
		35	4.5746-4.6450	4.4293-4.7271	4.4026-4.7575
		40	4.7265-4.8574	4.6437-4.9356	4.6240-4.9627
		45	4.9339-5.0749	4.8548-5.0980	4.8386-5.1195
		50	5.0951-5.2448	5.0562-5.3978	5.0208-5.4725
Std. Dev. = = 2.0147		55	5.3887-5.6161	5.2430-5.6858	5.2255-5.7316
		60	5.6755-5.8010	5.5947-5.8801	5.5393-5.9264
		65	5.8781-6.0302	5.8002-6.1735	5.7762-6.1968
		70	6.1751-6.2983	6.0376-6.5530	6.0079-6.5842
		75	6.5445-6.8054	6.3185-6.9905	6.2830-7.0012
Sample Size = = 500		80	7.0019-7.1165	6.8716-7.3138	6.8068-7.3186
		85	7.3324-7.4754	7.2611-7.7264	7.2409-7.8019
		90	7.8994-8.1412	7.7528-8.2354	7.6376-8.3488
		95	8.6196-9.0436	8.5191-9.7546	8.4695-9.9856

Table B-12
Results for a 50 cm Deep Pool with 30 Degrees Subcooling

Pool Depth (cm)	Sub-Cooling (K)	Quantile (%)	Range for ln(DF) at a Confidence Level (%) of		
			50	90	95
50	30	5	3.1952-3.2875	3.1241-3.3776	3.1127-3.4077
		10	3.6486-3.8498	3.4996-3.9106	3.4312-3.9227
		15	4.0447-4.1304	3.9134-4.1723	3.9010-4.2068
		20	4.2683-4.3837	4.1526-4.4785	4.1472-4.5174
		25	4.5222-4.6568	4.4409-4.7591	4.3852-4.8221
Mean =		30	4.7933-4.9559	4.6929-5.0378	4.6531-5.0586
= 5.9125		35	5.0396-5.1507	4.9589-5.2356	4.9218-5.2615
		40	5.2354-5.3638	5.1501-5.4698	5.1388-5.4929
		45	5.4610-5.6025	5.3525-5.6575	5.3203-5.6845
		50	5.6469-5.7914	5.5588-5.8551	5.5321-5.8800
Std. Dev. =		55	5.8538-5.9509	5.7863-6.0039	5.7473-6.0389
= 1.9181		60	6.0034-6.1567	5.9475-6.2434	5.9263-6.2700
		65	6.2428-6.3659	6.1560-6.5450	6.0799-6.6080
		70	6.5482-6.7791	6.3736-6.8286	6.3497-6.8499
		75	6.8340-7.0403	6.7988-7.1326	6.7633-7.1757
Sample Size =		80	7.1766-7.4141	7.0594-7.5486	7.0412-7.6113
= 500		85	7.6568-7.8402	7.5167-8.0184	7.4584-8.0489
		90	8.1099-8.3041	8.0362-8.5868	8.0007-8.6305
		95	9.0330-9.4238	8.7304-9.5990	8.6665-9.6518

Table B-13
Results for a 50 cm Deep Pool with 50 Degrees Subcooling

Pool Depth (cm)	Sub-Cooling (K)	Quantile (%)	Range for ln(DF) at a Confidence Level (%) of		
			50	90	95
50	50	5	3.5955-3.7463	3.4620-3.8611	3.4008-3.8757
		10	4.0290-4.1873	3.9472-4.2385	3.8972-4.2506
		15	4.4203-4.5973	4.2452-4.7099	4.2263-4.7235
		20	4.7695-4.9482	4.6884-5.0877	4.6506-5.1087
		25	5.1095-5.2601	5.0145-5.3882	4.9486-5.4115
Mean = = 6.9015		30	5.4092-5.5023	5.2757-5.6100	5.2560-5.6615
		35	5.6308-5.7628	5.5115-5.8638	5.4880-5.9031
		40	5.8638-6.0270	5.7624-6.1575	5.7518-6.1873
		45	6.1561-6.2937	6.0159-6.4312	5.9820-6.4736
		50	6.4307-6.5659	6.2867-6.7004	6.2682-6.7163
Std. Dev. = = 2.7161		55	6.6930-6.7883	6.5609-6.9479	6.5370-7.0126
		60	6.9416-7.1590	6.7747-7.3125	6.7359-7.3266
		65	7.3114-7.4201	7.1566-7.5848	7.0955-7.6529
		70	7.5868-7.8314	7.4227-8.0317	7.4036-8.0648
		75	8.0500-8.2038	7.8774-8.3263	7.7748-8.3989
Sample Size = = 500		80	8.4019-8.6177	8.2476-8.7365	8.2116-8.7603
		85	8.8977-9.0595	8.7161-9.3008	8.6476-9.3544
		90	9.4390-10.1692	9.3374-10.4523	9.2363-10.6419
		95	11.1363-11.7915	10.7847-12.0537	10.7063-12.2857

Table B-14
Results for a 50 cm Deep Pool with 70 Degrees Subcooling

Pool Depth (cm)	Sub-Cooling (K)	Quantile (%)	Range for ln(DF) at a Confidence Level (%) of		
			50	90	95
50	70	5	3.8315-4.0895	3.6110-4.2238	3.5782-4.3633
		10	4.5572-4.8263	4.3884-4.9852	4.2368-5.0320
		15	5.0411-5.1829	4.9309-5.3146	4.8410-5.3832
		20	5.3427-5.5712	5.2240-5.6406	5.1558-5.6593
		25	5.6381-5.7291	5.5604-5.9033	5.5244-5.9209
Mean =		30	5.8943-6.1627	5.7250-6.2422	5.6955-6.3451
= 7.7924		35	6.2155-6.5148	6.0860-6.6834	5.9778-6.7047
		40	6.6387-6.7932	6.4203-6.9270	6.3663-6.9729
		45	6.8950-7.0522	6.7469-7.1433	6.7027-7.2037
		50	7.1014-7.2417	6.9867-7.3856	6.9395-7.4254
Std. Dev. =		55	7.3402-7.5045	7.2171-7.6119	7.1856-7.6659
= 3.5256		60	7.5512-7.8159	7.4665-8.0150	7.4155-8.0574
		65	7.9304-8.2269	7.6843-8.3344	7.6659-8.4080
		70	8.2603-8.6093	8.1902-8.7249	8.0720-8.7860
		75	8.7077-9.0308	8.5621-9.2267	8.4891-9.3086
Sample Size =		80	9.2093-9.4807	9.0217-9.6231	8.9516-9.7032
= 360		85	9.6563-9.9369	9.4994-10.2462	9.4567-10.2803
		90	10.2879-11.2271	10.0721-12.4243	10.0132-12.7523
		95	13.2847-14.1425	12.7569-15.6067	12.5553-16.6816

Table B-15
Results for a 100 cm Deep Pool with 2 Degrees Subcooling

Pool Depth (cm)	Sub-Cooling (K)	Quantile (%)	Range for ln(DF) at a Confidence Level (%) of		
			50	90	95
100	2	5	1.7927-1.9251	1.7112-1.9823	1.6744-1.9939
		10	2.1189-2.1669	2.0625-2.2355	2.0106-2.2683
		15	2.3594-2.4656	2.2395-2.5067	2.2225-2.5134
		20	2.5516-2.6143	2.4972-2.6839	2.4827-2.6939
		25	2.6920-2.7715	2.6272-2.8284	2.6175-2.8592
Mean = = 3.8077		30	2.8550-2.9483	2.7755-2.9930	2.7674-3.0265
		35	3.0011-3.0967	2.9497-3.1354	2.9239-3.1522
		40	3.1353-3.2512	3.0953-3.3068	3.0824-3.3232
		45	3.3042-3.4013	3.2408-3.4848	3.1931-3.5120
		50	3.4795-3.5774	3.3937-3.6883	3.3758-3.7130
Std. Dev. = = 1.4598		55	3.6659-3.7880	3.5760-3.9520	3.5512-4.0054
		60	3.9516-4.1035	3.7846-4.1943	3.7560-4.2211
		65	4.1934-4.2717	4.1032-4.3402	4.0555-4.4128
		70	4.3513-4.5281	4.2776-4.6441	4.2601-4.6873
		75	4.6573-4.7798	4.5490-4.8771	4.5192-4.9436
Sample Size = = 500		80	4.9454-5.0698	4.8016-5.1766	4.7851-5.2008
		85	5.2279-5.3092	5.1393-5.4282	5.1162-5.4488
		90	5.5653-5.6976	5.4399-5.9751	5.4027-6.0525
		95	6.2781-6.3759	6.1722-6.6805	6.1115-6.8114

Table B-16
Results for a 100 cm Deep Pool with 5 Degrees Subcooling

Pool Depth (cm)	Sub-Cooling (K)	Quantile (%)	Range for ln(DF) at a Confidence Level (%) of		
			50	90	95
100	5	5	2.2899-2.3479	2.1337-2.4495	2.1269-2.4695
		10	2.6316-2.8324	2.5064-2.9710	2.4779-3.0070
		15	3.0670-3.1999	2.9815-3.2641	2.9547-3.3217
		20	3.3457-3.4339	3.2496-3.5354	3.2361-3.5511
		25	3.5527-3.6822	3.4429-3.7767	3.4340-3.7977
Mean = = 4.8364		30	3.7904-3.8733	3.6870-3.9630	3.6629-3.9747
		35	3.9665-4.1043	3.8829-4.1409	3.8407-4.1601
		40	4.1406-4.2298	4.1030-4.3050	4.0462-4.3247
		45	4.2991-4.4118	4.2246-4.4891	4.2070-4.5090
		50	4.4869-4.5630	4.3980-4.7396	4.3689-4.8048
Std. Dev. = = 1.8178		55	4.7362-4.8986	4.5541-4.9572	4.5437-5.0087
		60	4.9562-5.1445	4.8934-5.2390	4.8505-5.2704
		65	5.2386-5.3814	5.1442-5.5289	5.0913-5.5819
		70	5.5473-5.6999	5.4041-5.8272	5.3545-5.8451
		75	5.8430-5.9125	5.7097-6.0209	5.6759-6.1113
Sample Size = = 500		80	6.1148-6.2508	5.9432-6.3089	5.9166-6.3544
		85	6.3883-6.4992	6.2805-6.6743	6.2700-6.6937
		90	6.7625-7.0593	6.6838-7.3304	6.5778-7.4016
		95	7.7128-8.1128	7.5571-8.6866	7.5228-9.1066

Table B-17
Results for a 100 cm Deep Pool with 10 Degrees Subcooling

Pool Depth (cm)	Sub-Cooling (K)	Quantile (%)	Range for ln(DF) at a Confidence Level (%) of		
			50	90	95
100	10	5	2.9708-3.1347	2.7223-3.2202	2.6951-3.2327
		10	3.4210-3.5795	3.2765-3.6409	3.2450-3.6535
		15	3.6992-3.7925	3.6451-3.8766	3.6233-3.8977
		20	3.9234-4.0238	3.8409-4.1263	3.8178-4.1378
		25	4.1443-4.2520	4.0509-4.2988	4.0254-4.3373
Mean = = 5.7409		30	4.3200-4.4800	4.2586-4.5603	4.2384-4.6103
		35	4.5736-4.7677	4.4833-4.9015	4.4733-4.9270
		40	4.9014-5.0298	4.7659-5.0868	4.7126-5.1237
		45	5.0845-5.2094	5.0255-5.3450	5.0034-5.4070
		50	5.8401-5.5473	5.1909-5.7076	5.1689-5.7257
Std. Dev. = = 2.0804		55	5.7061-5.8363	5.5467-5.8997	5.4620-5.9473
		60	5.8942-6.0162	5.8270-6.1523	5.7893-6.1961
		65	6.1510-6.3536	6.0160-6.4678	6.0007-6.4935
		70	6.4724-6.6317	6.3591-6.7165	6.3263-6.7538
		75	6.7437-6.9594	6.6390-7.0658	6.6183-7.1364
Sample Size = = 500		80	7.1423-7.3818	6.9845-7.5519	6.9635-7.5766
		85	7.6014-7.9873	7.4566-8.1545	7.4319-8.2179
		90	8.3057-8.4287	8.1638-8.9105	8.1364-9.0591
		95	9.2659-9.8746	9.1602-10.4412	9.1250-10.4569

Table B-18
Results for a 100 cm Deep Pool with 20 Degrees Subcooling

Pool Depth (cm)	Sub-Cooling (K)	Quantile (%)	Range for ln(DF) at a Confidence Level (%) of		
			50	90	95
100	20	5	3.6095-3.8192	3.4742-3.9675	3.4644-4.0518
		10	4.2335-4.3607	4.1105-4.4486	4.0849-4.4682
		15	4.5742-4.6873	4.4610-4.7819	4.4202-4.7964
		20	4.8414-4.9526	4.7371-5.0990	4.7001-5.1066
		25	5.1107-5.2969	5.0226-5.3880	4.9577-5.4122
Mean =		30	5.4007-5.5328	5.3273-5.6008	5.2813-5.6138
= 6.9541		35	5.6027-5.7211	5.5339-5.8575	5.5260-5.8959
		40	5.8566-6.0217	5.7191-6.1500	5.6919-6.1792
		45	6.1480-6.3513	6.0116-6.4647	5.9681-6.5107
		50	6.4503-6.6214	6.3422-6.7222	6.2990-6.7727
Std. Dev. =		55	6.7084-6.8690	6.6190-7.0468	6.5968-7.1203
= 2.5041		60	7.0467-7.2615	6.8639-7.3847	6.8096-7.4027
		65	7.3847-7.5636	7.2614-7.7112	7.1968-7.7674
		70	7.7202-8.0348	7.5842-8.2166	7.5379-8.2851
		75	8.2707-8.4281	8.0924-8.5396	8.0159-8.5767
Sample Size =		80	8.5805-8.7761	8.4892-8.9849	8.4298-9.0697
= 500		85	9.1206-9.4115	8.9687-9.6164	8.8963-9.7317
		90	9.8588-10.2102	9.6548-10.4686	9.5529-10.5547
		95	11.2287-11.5825	10.9431-11.9483	10.6687-12.0597

Table B-19
Results for a 100 cm Deep Pool with 50 Degrees Subcooling

Pool Depth (cm)	Sub-Cooling (K)	Quantile (%)	Range for ln(DF) at a Confidence Level (%) of		
			50	90	95
100	50	5	4.7726-4.8614	4.5009-4.9575	4.3755-4.9697
		10	5.1372-5.3550	5.0256-5.4645	5.0092-5.5352
		15	5.6546-5.8608	5.4852-5.9759	5.4425-6.0644
		20	6.0852-6.2705	5.9604-6.3983	5.9135-6.4622
		25	6.4643-6.7137	6.3153-6.9252	6.2734-6.9714
Mean = = 9.0289		30	6.9481-7.1495	6.7295-7.3335	6.6779-7.3655
		35	7.3450-7.5070	7.1703-7.5764	7.1210-7.6445
		40	7.5755-7.7227	7.5059-7.8513	7.4394-7.8971
		45	7.8462-8.1481	7.7198-8.2662	7.7075-8.3517
		50	8.2593-8.4461	8.1465-8.5975	8.0439-8.6474
Std. Dev. = = 3.6621		55	8.5960-8.7781	8.4443-9.0021	8.4157-9.0344
		60	8.9953-9.3113	8.7765-9.4143	8.7535-9.5176
		65	9.4129-9.6311	9.3111-9.7778	9.2778-9.8417
		70	9.7945-10.0856	9.6388-10.2787	9.5917-10.3325
		75	10.3221-10.6899	10.1065-10.8596	10.0674-10.9152
Sample Size = = 500		80	10.9381-11.4698	10.7631-11.6492	10.6987-11.7231
		85	11.8047-12.0824	11.6002-12.4191	11.5602-12.4904
		90	12.9160-13.5053	12.4449-14.0268	12.3881-14.3653
		95	15.6413-16.8060	15.1249-17.4116	14.9593-17.6362

Table B-20
Results for a 100 cm Deep Pool with 70 Degrees Subcooling

Pool Depth (cm)	Sub-Cooling (K)	Quantile (%)	Range for ln(DF) at a Confidence Level (%) of		
			50	90	95
100	70	5	5.1645-5.2518	5.0053-5.3942	4.9971-5.3996
		10	5.7566-5.9317	5.5658-6.0474	5.5097-6.0528
		15	6.1193-6.2888	6.0522-6.4825	6.0010-6.5735
		20	6.6163-6.8196	6.3813-6.9103	6.3619-6.9546
		25	6.9600-7.2096	6.8590-7.2921	6.8220-7.3292
Mean =		30	7.3080-7.5730	7.2139-7.7713	7.1821-7.8368
= 9.8510		35	7.7728-7.9555	7.5762-8.1786	7.5090-8.2079
		40	8.1785-8.3756	7.9534-8.5042	7.9054-8.5357
		45	8.4997-8.7084	8.3369-8.8303	8.3009-8.9041
		50	8.8291-9.0081	8.6997-9.2010	8.6537-9.2555
Std. Dev. =		55	9.1642-9.6367	8.9937-9.8061	8.9820-9.8576
= 4.1113		60	9.8049-10.0923	9.6302-10.2359	9.4924-10.3531
		65	10.2352-10.5874	10.0921-10.9488	10.0116-11.0237
		70	10.9693-11.3249	10.6021-11.4665	10.5487-11.4851
		75	11.4753-11.7491	11.3321-11.9149	11.2806-11.9811
Sample Size =		80	11.9891-12.3028	11.8598-12.5991	11.7695-12.6843
= 500		85	12.7822-13.0620	12.4738-13.7495	12.3842-13.9517
		90	14.5184-15.0637	13.7746-15.3293	13.6707-15.5513
		95	17.1182-18.4318	16.2910-19.4881	15.9303-20.7024

Table B-21
Results for a 200 cm Deep Pool with 10 Degrees Subcooling

Pool Depth (cm)	Sub-Cooling (K)	Quantile (%)	Range for ln(DF) at a Confidence Level (%) of		
			50	90	95
200	10	5	3.6681-3.8299	3.4005-4.0055	3.3147-4.0164
		10	4.2680-4.5216	4.0265-4.7015	4.0122-4.7296
		15	4.7610-4.9467	4.6727-5.0713	4.5884-5.1212
		20	5.1233-5.3316	4.9747-5.6073	4.9447-5.6515
		25	5.6161-5 8491	5.3571-6.0175	5.2090-6.0841
Mean = = 7.8476		30	6.0011-6.2197	5.8491-6.3393	5.7540-6.3671
		35	6.3284-6.4975	6.1946-6.5735	6.1331-6.6029
		40	6.5483-6.7322	6.4406-6.8871	6.3814-6.9356
		45	6.8101-7.1249	6.6751-7.2793	6.6080-7.3082
		50	7.2661-7.4614	7.0700-7.5318	6.9634-7.5765
Std. Dev. = = 3.5157		55	7.5157-7.7229	7.3542-7.8121	7.3225-7.8448
		60	7.7675-7.9766	7.6407-8.1796	7.5863-8.1993
		65	8.1459-8.3149	7.9474-8.4779	7.8644-8.5272
		70	8.4536-8.7275	8.2515-8.8419	8.2209-8.8782
		75	8.8291-9.0579	8.7251-9.2862	8.6591-9.4533
Sample Size = = 402		80	9.3183-9.7908	9.0758-10.0484	9.0288-10.2212
		85	10.2156-10.6476	9.8708-11.0576	9.7938-11.1459
		90	11.2708-11.8634	10.8580-12.9156	10.7347-13.2522
		95	13.8248-14.5412	13.5048-15.5666	13.1992-15.9748

Table B-22
Results for a 300 cm Deep Pool with 2 Degrees Subcooling

Pool Depth (cm)	Sub-Cooling (K)	Quantile (%)	Range for ln(DF) at a Confidence Level (%) of		
			50	90	95
300	2	5	3.6443-3.7633	3.4842-3.8283	3.3462-3.8335
		10	3.9929-4.1775	3.8820-4.2937	3.8392-4.3039
		15	4.3421-4.5412	4.2944-4.6057	4.2437-4.6323
		20	4.6727-4.7975	4.5837-4.9139	4.5553-4.9479
		25	4.9464-5.2079	4.8364-5.2965	4.7897-5.3173
Mean =		30	5.2985-5.4794	5.2252-5.6243	5.1807-5.6466
= 7.1248		35	5.6266-5.7987	5.4788-5.8952	5.4600-5.9213
		40	5.8872-6.0320	5.7929-6.1856	5.7576-6.2320
		45	6.1671-6.3368	5.9975-6.4784	5.9658-6.4975
		50	6.4529-6.5348	6.3002-6.6383	6.2761-6.7039
Std. Dev. =		55	6.6094-6.8458	6.5340-6.9716	6.5314-6.9837
= 3.1029		60	6.9655-7.1255	6.8322-7.3295	6.7959-7.3658
		65	7.3163-7.4910	7.1108-7.6237	7.0510-7.6816
		70	7.6235-7.8709	7.4932-8.0575	7.4539-8.2832
		75	8.1876-8.5362	7.8732-8.7251	7.8521-8.8145
Sample Size =		80	8.8111-9.0761	8.5976-9.3605	8.5346-9.4070
= 472		85	9.4265-9.8400	9.2286-10.2825	9.1810-10.3913
		90	10.5650-10.9403	10.2913-11.5347	10.2266-11.6748
		95	12.5010-13.1552	11.8902-13.7969	11.7191-13.8568

Table B-23
Results for a 300 cm Deep Pool with 5 Degrees Subcooling

Pool Depth (cm)	Sub-Cooling (K)	Quantile (%)	Range for ln(DF) at a Confidence Level (%) of		
			50	90	95
300	5	5	4.2330-4.3344	4.1712-4.4445	4.1275-4.4637
		10	4.6516-4.8320	4.5141-4.9976	4.4912-5.0254
		15	5.1266-5.3018	5.0165-5.4542	4.9499-5.4912
		20	5.5044-5.6470	5.4014-5.7776	5.3606-5.7813
		25	5.7818-5.9572	5.6869-6.1351	5.6495-6.2146
Mean =		30	6.1851-6.3492	6.0244-6.5053	5.9487-6.5138
= 8.2769		35	6.5076-6.6091	6.3636-6.7785	6.3082-6.9303
		40	6.7766-7.0842	6.6082-7.1604	6.5794-7.2161
		45	7.1578-7.4290	7.0821-7.5635	7.0433-7.5813
		50	7.5122-7.8032	7.4015-7.9818	7.3045-8.0071
Std. Dev. =		55	7.9602-8.1526	7.7994-8.2632	7.7436-8.3112
= 3.4529		60	8.2549-8.4535	8.1522-8.6021	8.0740-8.6426
		65	8.5997-8.8499	8.4533-9.0115	8.3924-9.0937
		70	9.0285-9.4048	8.8589-9.6080	8.8344-9.6787
		75	9.6292-9.9172	9.4552-10.0775	9.3719-10.1831
Sample Size =		80	10.1848-10.5440	9.9560-10.7668	9.9281-10.8889
= 500		85	11.0402-11.6220	10.6791-11.8800	10.6222-11.9674
		90	12.1001-12.6239	11.9353-12.9979	11.7624-13.0883
		95	14.0972-14.5055	13.4663-16.0356	13.1336-16.2842

Table B-24
Results for a 300 cm Deep Pool with 10 Degrees Subcooling

Pool Depth (cm)	Sub-Cooling (K)	Quantile (%)	Range for ln(DF) at a Confidence Level (%) of		
			50	90	95
300	10	5	4.9688-5.1729	4.7563-5.3608	4.6893-5.3792
		10	5.5186-5.8537	5.3783-5.9109	5.3533-5.9398
		15	5.9539-6.2783	5.8874-6.6978	5.8549-6.7295
		20	6.7100-6.9561	6.3056-7.0641	6.1864-7.1724
		25	7.0326-7.2776	6.8978-7.5190	6.8524-7.5441
Mean =		30	7.4802-7.6745	7.2521-7.8099	7.2119-7.8688
= 9.7677		35	7.7454-7.9913	7.5735-8.1083	7.5515-8.1469
		40	8.0520-8.3313	7.9632-8.5008	7.8670-8.5597
		45	8.4507-8.8466	8.1956-9.1039	8.1206-9.1520
		50	9.0310-9.2363	8.5756-9.4188	8.5155-9.4265
Std. Dev. =		55	9.2929-9.5332	9.1691-9.6792	9.1078-9.7203
= 4.0360		60	9.6370-9.8971	9.4312-10.1130	9.4211-10.1676
		65	10.0561-10.2758	9.7922-10.6048	9.6945-10.7587
		70	10.5697-10.9479	10.2167-11.2115	10.1640-11.3217
		75	11.1493-11.7747	10.8814-12.0560	10.7665-12.0861
Sample Size =		80	12.0491-12.2551	11.6708-12.5308	11.5673-12.5474
= 333		85	12.5342-12.9475	12.2842-13.8620	12.2235-14.0249
		90	14.0847-14.6774	13.7013-15.3326	13.0656-16.3180
		95	17.2297-18.5623	16.0529-20.2029	15.2753-20.8188

Table B-25
Results for a 300 cm Deep Pool with 30 Degrees Subcooling

Pool Depth (cm)	Sub-Cooling (K)	Quantile (%)	Range for ln(DF) at a Confidence Level (%) of		
			50	90	95
300	30	5	6.3864-6.7122	6.1488-6.8646	6.0837-6.9421
		10	7.2244-7.4976	7.1512-7.6963	7.0186-7.7828
		15	8.1421-8.5044	7.7380-8.7365	7.6529-8.8282
		20	8.8695-9.0740	8.5864-9.1967	8.5495-9.3108
		25	9.3228-9.5465	9.0864-9.6870	9.0750-9.7463
Mean =		30	9.7183-9.9271	9.5826-10.2573	9.5401-10.3870
= 13.3052		35	10.3086-10.6075	9.9301-10.8658	9.8964-10.8866
		40	10.8655-11.1869	10.6048-11.3963	10.5306-11.4852
		45	11.3414-11.6652	11.1500-12.0117	11.0529-12.0747
		50	12.0088-12.3872	11.6573-12.6266	11.5998-12.7166
Std. Dev. =		55	12.6121-12.9944	12.3603-13.3740	12.2485-13.4263
= 5.5663		60	13.3693-13.5290	12.9922-13.7929	12.9505-13.9812
		65	13.7845-14.4523	13.5274-14.7629	13.4806-14.7864
		70	14.7718-14.9722	14.4620-15.4354	14.3385-15.4984
		75	15.4735-16.0348	15.0428-16.3242	14.9266-16.4215
Sample Size =		80	16.4246-16.8708	16.1113-17.5521	16.0357-17.7363
= 500		85	18.0308-19.2504	17.0819-19.9762	16.9703-20.1467
		90	20.5216-21.1332	20.0146-22.0593	19.8737-22.2381
		95	23.8324-27.6241	22.7318-28.6891	22.5645-29.2342

DISTRIBUTION:

U.S. Nuclear Regulatory Commission (19)
Office of Nuclear Regulatory Research
Attn: E. Beckjord, NLS-007
T. Speis, NLS-007
W. Minners, NLS-360
J. Murphy, NLS-358
C. Ader, NLS-324
L. Soffer, NLS-324
S. B. Burson, NLS-324
C. M. Ferrell, NLS-324
J. N. Ridgely, NLS-324
J. H. Schaperow, NLS-324
B. Sheron, NLS-344
F. Eltawila, NLN-344
R. Y. Lee, NLN-344
A. Reuben, NLN-344
A. Behbahani, NLN-344
M. A. Cunningham, NLS-372
J. C. Glynn, NLS-372
J. C. Ryder, NLS-372
R. O. Meyer, NLS-013
Washington, D.C. 20555

U.S. Nuclear Regulatory Commission (4)
Office of Nuclear Reactor Regulation
Attn: R. Palla, 10E4
R. Barrett, 10E4
W. Lyon, 8E23
J. Lee, 10D4
Washington, DC 20555

U.S. Department of Energy (1)
Office of Nuclear Safety
Attn: S. Blush
1000 Independence Ave., S.W.
Washington, DC 20585

U.S. Department of Energy (1)
NE-42
Attn: W. F. Pasedag
19901 Germantown Rd.
Germantown, MD 20585

U.S. Department of Energy (2)
Albuquerque Operations Office
Attn: C. E. Garcia, Director
For: C. B. Quinn
R. L. Holton
P.O. Box 5400
Albuquerque, NM 87185

Electric Power Research Institute (3)
Attn: John Trotten
D. Leaver
J. C. DeVine, Jr.
3412 Hillview Avenue
Palo Alto, CA 94303

Brookhaven National Laboratory (5)
Attn: V. Mubayi
R. Davis
G. A. Greene
H. Nourbakhsh
T. Ginsberg
Upton, NY 11973

U.S. Department of Energy (1)
Office of Nuclear Safety Coordination
Attn: R. W. Barber
Washington, DC 20545

Los Alamos National Laboratories (1)
Attn: M. Stevenson
P.O. Box 1663
Los Alamos, NM 87545

University of California Los Angeles (4)
Nuclear Energy Laboratory
Attn: I. Catton
D. Okrent
W. Kastenberg
G. Apostolakis
405 Hilgaard Avenue
Los Angeles, CA 90024

Wang Lu
TVA
400 Commerce, WGC157-CK
Knoxville, TN 37902

W. Stratton
2 Acoma Lane
Los Alamos, NM 87544

EG&G Idaho
Willow Creek Building, W-3
Attn: R. Hobbins
P.O. Box 1625
Idaho Falls, ID 83415

Battelle Pacific Northwest Laboratory
Attn: M. Freshley
P.O. Box 999
Richland, WA 99352

Professor R. Seale
Department of Nuclear Engineering
University of Arizona
Tucson, Arizona 85721

Oak Ridge National Laboratory (2)
Attn: T. S. Kress
S. Hodge
P.O. Box Y
Oak Ridge, TN 37830

Battelle Columbus Laboratory (3)
Attn: C. Alexander
K. Lee
R. Denning
505 King Avenue
Columbus, OH 43201

D. Osetek
Los Alamos Technical Associates
Building 1, Suite 400
2400 Louisiana NE
Albuquerque, NM 87110

David Leaver
TENERA
1340 Saratoga-Sunnyvale Rd.
Suite 206
San Jose, CA 95129

S. Rosen
Nuclear Fuel Engineering
ABB Combustion Engineering
Nuclear Power
1000 Prospect Hill Road
P.O. Box 500
Windsor, CT 06095-0500

Alan Nelson
NUMARC
1776 I Street NW
Suite 300
Washington, DC 20006

Professor T. G. Theofanous
University of California-Santa Barbara
Chemical and Nuclear Engineering Dept.
UC-Santa Barbara
Santa Barbara, CA 93106

FOREIGN DISTRIBUTION

Alan Jones
ISPRA
CEC Joint Research Center
21020 Varese
ITALY

Japan Atomic Energy Research Institute
Tokai Research Establishment
Attn: Dr. S. Matsuura, Deputy Director General
Tokai-mura, Naka-gun, Ibaraki-ken
319-11
JAPAN

Japan Atomic Energy Research Institute (4)
Severe Accident Research Laboratory
Attn: K. Soda
J. Sugimoto
N. Yamano
Y. Maruyama
Tokai-mura, Naka-gun, Ibaraki-ken
319-11
JAPAN

Japan Atomic Energy Research Institute
Reactor Accident Laboratory
Attn: Dr. T. Fujishiro, Head
Tokai-mura, Naka-gun, Ibaraki-ken
319-11
JAPAN

Technische Universitat Munchen
Attn: Professor H. Karwat
8046 Garching, Forschungagelande
Munich
GERMANY

Kernforschungszentrum Karlsruhe
Attn: H. Alsmeyer
Postfach 3640
75 Karlsruhe
GERMANY

Nucleare e delle Protezione Sanitaria (DISP) (2)
Attn: Mr. Manilia
Mr. G. Petrangeli
Ente Nazionnle Energie Alternative (ENEA)
Viale Regina Margherita, 125
Caselle Postale M. 2358
I-00100 Roma A. D.
ITALY

Dr. K. J. Brinkman
Reactor Centrum Nederland
1755 ZG Petten
THE NETHERLANDS

M. Jankowski
International Atomic Energy Agency
Division of Nuclear Reactor Safety
Wagranerstrasse 5
P.O. Box 100
A/1400 Vienna
AUSTRIA

Stratens Karnfraftinspektion (2)
Attn: L. Hammer
W. Frid
P.O. Box 27106
S-10252 Stockholm
SWEDEN

Studvik Energiteknik AB
Attn: K. Johansson
5-611 82 Nykoping
SWEDEN

Institute of Nuclear Energy Research
Attn: Sen-I Chang
P.O. Box 3
Lungtan
Taiwan 325
REPUBLIC OF CHINA

P. Fehrenbach
Atomic Energy Canada, Ltd.
Chalk River, Ontario
CANADA KOJ IJO

Korea Advanced Energy Research Institute
Attn: H. R. Jun
P.O. Box 7
Daeduk-Danji
Choong-Nam
KOREA

POSTECH
Dept. of Mechanical Eng.
Attn: Moo Hwan Kim
P.O. Box 125
Kyungbuk 790-600
KOREA

Md. C. Lecomte
CEN FAR
60-68 Av. du G. Leclerc-B.P.6
92265 Fontenay aux Roses Cedex
FRANCE

Dr. A. Meyer-Heine
CEN Cadarache
13108 Saint Paul Lez Durance
FRANCE

H. Bairiot, Chief
Department LWR Fuel
Belgonucleair
Rue de Champde Mars. 25
B-1050 Brussels
BELGIUM

J. E. Antill
Berkeley Nuclear Laboratory
Berkeley GL 139 PB
Gloucestershire, England
UNITED KINGDOM

W. G. Cunliffe
Bldg. 396
British Nuclear Fuels, Ltd.
Springfield Works
Salwick, Preston
Lancashire, England
UNITED KINGDOM

AEA Technology (7)
Attn: A. Nichols, 102/A50
T. Butland
B. Bowsher, 105A/A50
J. Mitchell, 01/A50
P. Smith, 215,A23
D. Sweet, 210/A32
D. Williams, 210/A32
Winfrith, Dorchester
Dorset DT2 8DH, England
UNITED KINGDOM

Itaru Kaneko
Chemical Techology Group
Nuclear Engineering Laboratory
Toshiba Corporation
4-1 Ukishima Cho, Kawasaki Ku
Kawasaki 210
JAPAN

Japan Atomic Energy Research Institute
Attn: K. Sato
Fukoku Seime Building
2-2-2, Uchisaiwai-cho, Chiyoda-ku, Tokyo
JAPAN

SANDIA DISTRIBUTION

6400 N. R. Ortiz
6403 W. A. von Riesemann
6404 D. A. Powers (5)
6413 F. T. Harper
6413 T. D. Brown
6413 J. C. Helton
6413 L. A. Miller
6413 J. L. Sprung
6415 K. D. Bergeron
6418 S. L. Thompson
6422 M. D. Allen
6422 N. Bixler
6422 J. E. Brockmann
6422 T. K. Blanchat
6422 T. Y. Chu
6422 R. M. Elrick
6422 T. J. Heames
6429 K. E. Washington
6429 D. C. Williams
6429 K. K. Murata
6501 J. V. Walker
7141 Technical Library (5)
7151 Technical Publications
8523 Central Technical Files

END

DATE
FILMED
2/10/94